AD NUMBER

ADB024249

LIMITATION CHANGES

TO:

Approved for public release; distribution is unlimited.

FROM:

Distribution authorized to U.S. Gov't. agencies only; Test and Evaluation; AUG 1977. Other requests shall be referred to Air Force Weapons Lab., Kirtland AFB, NM 87117.

AUTHORITY

AFWL ltr 29 Apr 1985

AD B024249

AUTHORITY: AFWL ltr, 29 Apr 85

AFWL-TR-77-90

AFWL-TR-
77-90

(2)

(6)

DEVELOPMENT AND EVALUATION OF A TRIAXIAL INTERFACE STRESS TRANSDUCER.

(10) Stephen F. Pickett
University of New Mexico
Albuquerque, NM 87131

(18) AFWL, SBIE

(19) TR-77-90, AD-E 200 072

(11) Aug 77

(12) 104 p.

(9) Final Report,

(15) F29601-76-C-0015

This research was sponsored by the Defense Nuclear Agency under Subtask L11CAX5X352, Work Unit 52, Work Unit Title: "Development of Field Instrumentation."

15

(16)

(17)

Prepared for
Director
DEFENSE NUCLEAR AGENCY
Washington, DC 20305

AIR FORCE WEAPONS LABORATORY
Air Force Systems Command
Kirtland Air Force Base, NM 87117

256 050

AFWL-TR-77-90

This final report was prepared by the University of New Mexico, Albuquerque, New Mexico, under Contract F29601-76-C-0015, Job Order WDNS0318 with the Air Force Weapons Laboratory, Kirtland Air Force Base, New Mexico. Santos J. Ayala, (DED-I) is the Project Officer-in-Charge.

When US Government drawings, specifications, or other data are used for any purpose other than a definitely related Government procurement operation, the Government thereby incurs no responsibility nor any obligation whatsoever, the fact that the Government may have formulated, furnished, or in any way supplied the said drawings, specifications, or other data is not to be regarded by implication or otherwise as in any manner licensing the holder or any other person or corporation or conveying any rights or permission to manufacture or sell any patented invention that may in any way be related thereto.

This technical report has been reviewed and is approved for publication.

Santos J. Ayala

SANTOS J. AYALA,
Project Officer

FOR THE COMMANDER

Rudolph V. Matalucci

RUDOLPH V. MATALUCCI, Lt Col, USAF
Chief, Development Branch

Frank J. Leech

FRANK J. LEECH, Lt Col, USAF
Chief, Civil Engrg Rsch Division

DO NOT RETURN THIS COPY. RETAIN OR DESTROY.

UNCLASSIFIED

SECURITY CLASSIFICATION OF THIS PAGE *(When Data Entered)*

REPORT DOCUMENTATION PAGE		READ INSTRUCTIONS BEFORE COMPLETING FORM
1. REPORT NUMBER AFWL-TR-77-90	2. GOVT ACCESSION NO.	3. RECIPIENT'S CATALOG NUMBER
4. TITLE *(and Subtitle)* DEVELOPMENT AND EVALUATION OF A TRIAXIAL INTERFACE STRESS TRANSDUCER		5. TYPE OF REPORT & PERIOD COVERED Final Report 6. PERFORMING ORG. REPORT NUMBER
7. AUTHOR(s) Stephen F. Pickett		8. CONTRACT OR GRANT NUMBER(s) F29601-76-C-0015
9. PERFORMING ORGANIZATION NAME AND ADDRESS University of New Mexico Albuquerque, NM 87117		10. PROGRAM ELEMENT, PROJECT, TASK AREA & WORK UNIT NUMBERS Program Element: 62710H JON: WDNS0318
11. CONTROLLING OFFICE NAME AND ADDRESS Director Defense Nuclear Agency Washington, D. C. 20305		12. REPORT DATE August 1977 13. NUMBER OF PAGES 106
14. MONITORING AGENCY NAME & ADDRESS *(if different from Controlling Office)* Air Force Weapons Laboratory Kirtland Air Force Base, NM 87117		15. SECURITY CLASS. *(of this report)* UNCLASSIFIED 15a. DECLASSIFICATION/DOWNGRADING SCHEDULE

16. DISTRIBUTION STATEMENT *(of this Report)*

Distribution limited to US Government agencies only because of test and evaluation of military systems/equipment (Aug 77). Other requests for this document must be referred to AFWL (DED-I), Kirtland AFB, NM 87117.

17. DISTRIBUTION STATEMENT *(of the abstract entered in Block 20, if different from Report)*

18. SUPPLEMENTARY NOTES

This research was sponsored by the Defense Nuclear Agency under Subtask L11CAXSX353, Work Unit 52, Work Unit Title: "Development of Field Instrumentation."

19. KEY WORDS *(Continue on reverse side if necessary and identify by block number)*

Stress
Shear Stress
Transducers
Interface Stress
Structure/Media Interface Stress

20. ABSTRACT *(Continue on reverse side if necessary and identify by block number)*

A dual bending beam dynamic triaxial interface stress transducer was designed and built. Cross-axis sensitivities and unwanted input sensitivities were quite low. Both static and dynamic testing were performed to determine transducer response in an actual sand/concrete interface environment. Results showed that the shear-gage response followed the inferred shear response in trend, with outputs typically 65 percent of the inferred shear.

DD FORM 1 JAN 73 1473 EDITION OF 1 NOV 65 IS OBSOLETE

UNCLASSIFIED

SECURITY CLASSIFICATION OF THIS PAGE *(When Data Entered)*

CONTENTS

ILLUSTRATIONS

TABLES

SECTION 1
INTRODUCTION

BACKGROUND

Shear-stress loading on certain types of structures is a very important contribution to structural response and ultimate structural failure. In turn, structural response to shear loading is an important design factor in new designs for certain Air Force structures, as well as a useful analytical variable to predict the response of existing strategic structures with regard to structure and internally housed equipment survivability.

In the past, simple Coulomb friction models were used in structural response codes which yielded or inferred predictions for structure/media interface shear loading based on interface friction coefficients, normal stress, and structure/media relative motions. Simple static tests were used to determine friction coefficients for structure/media interfaces of interest; however, actual dynamic testing indicated that the model was entirely inadequate. Typical friction coefficients were found to be in the neighborhood of 0.5, based on static laboratory testing; however, results from actual testing indicated that friction coefficients of about 0.05 were required to bring the Coulomb friction model into the realm of actual loading. Because of this discrepancy a new, extremely complex, shear-loading code was developed to better predict the interface shear-loading contribution to structural response (ref. 1).

In order to determine the adequacy of the new code and to find what code changes were necessary in analytical predictions, an actual measurement of dynamic shear stress was needed and thus the requirement for a shear-stress transducer was established. Although transducers for static shear stress were available, there appeared to be none with dynamic capabilities--in particular, insensitivity to

---

1. Huck, Peter J., et al., *Dynamic Response of Soil/Concrete Interfaces at High Pressure*, AFWL-TR-73-264, Air Force Weapons Laboratory, Kirtland Air Force Base, New Mexico, April 1974.

acceleration. With such a device, electrical analogs of shear stress at selected points of interest on structure/media interfaces could be obtained. As with other types of measurements, i.e., velocity, acceleration, displacement, blast pressure, soil stress, and interface normal stress, data from actual testing of numerous structure/media interface configurations could be used to refine and perfect the analytical prediction codes.

An interface shear gage was developed and partially evaluated. The gage was fielded in the HARD PAN I Test Series* with apparent success and evaluated in the laboratory to check case sensitivity, axis interaction, dynamic acceleration sensitivity, and ring frequency. A static calibration fixture was developed and is in use, but to insure confidence in the data obtained, a dynamic calibration fixture and method were developed and used for evaluation.

OBJECTIVE

The objective of this research effort was to continue the evaluation of the interface shear gage developed previously. This transducer was originally designed to measure two orthogonal shear-stress vectors in the structure/media interface plane; however, a later modification allowed the basic primary element to be used for normal stress; thus, the transducer provides a measurement of three mutually orthogonal dynamic stress vector time histories. Target objectives included the following:

(1)	Range	2000-psi shear stress (two axes) 3000-psi normal stress (one axis)
(2)	Useable Frequency Range	dc to 500 Hz or higher
(3)	Mounting Requirements	3-in. thick wall or greater (gage may protrude into interior structure)
(4)	Shear-Axis Sensitivity to Normal Stress	No greater than 5 percent apparent shear stress at 1000-psi normal stress
(5)	Normal-Axis Sensitivity to Shear Stress	No greater than 5 percent apparent normal stress at 1000-psi shear stress
(6)	Acceleration Sensitivity (all axes)	Shear: 0.02 psi/g or better Normal: 0.03 psi/g or better

*The Hard Pan Test Series was composed of structure/media interaction test events conducted by the Air Force Weapons Laboratory (AFWL) at Trading Post, Kansas.

(7) The force-collecting surface of the transducer shall be 1 in. in diameter and shall be textured to match as nearly as possible the coefficient of friction of the structure.

In addition to these design and specification objectives, the following experimental and analytical objectives were undertaken:

(1) Determine stress sensitivities and develop a calibration procedure.
(2) Determine unwanted input sensitivities experimentally.
(3) Conduct both static and dynamic shear tests in a true structure/sand interface condition.
(4) Provide manufacturing drawings, performance data, calibration and installation instructions and data interpretation instructions to AFWL for production and utilization of the transducer.
(5) Investigate data-processing methods to provide for frequency response and cross-axis sensitivity corrections.

SCOPE

After initial conception of a bending-beam, shear-stress transducer, dynamic requirements were studied and a design for a modified dual bending-beam stress transducer was modeled to determine transducer shear-stress response, as well as sensitivities to unwanted inputs. Although the model was highly idealized, it did appear that unwanted sensitivities would be low enough to make the design practical. A prototype transducer was then built.

A calibration device was built, and the transducer was tested for scale factor, linearity, and unwanted sensitivities.

A shear test fixture, as well as an alternate shear measuring technique, was designed, developed, and modified to allow both static and dynamic shear tests to be performed, and comparisons were made between the transducer output and the inferred shear output.

SECTION 2
PRINCIPLE OF OPERATION

To meet the initial requirements of a single axis of shear measurement, it was determined that a bending beam properly strain-gaged with a force-collecting surface flush with the structure would respond linearly to applied shear stress.

When a vertical shear stress, σ_s, is applied to the effective force-collecting area, A, a load, $\sigma_s A$, is applied to the free end of the cantilever beam. The resulting bending moment at points a and a' (fig. 1) is (assuming simplified beam theory)

$$M_x = \sigma_s A(\ell - x)$$

where

M_x = bending moment

ℓ = total length of beam

x = distance from fixed end of beam to points a and a'

and the strain at points a and a' is

$$\xi_{a,a'} = \frac{\pm\sigma_s A(\ell - x)c}{EI}$$

where c is the distance from the neutral axis to the surface of the beam at points a and a'. Thus, $\xi_{a,a'}$ is linearly proportional to σ_s when σ_s is the only applied force on the transducer. Unfortunately, for this simple design, vertical shear stress will not be the only force input in field situations in which a vertical shear stress analog is required; the following inputs will also contribute to the strain at points a and a':

(1) normal (axial) stress

(2) horizontal shear stress*

(3) horizontal acceleration*

(4) vertical acceleration

(5) axial acceleration

(6) angular acceleration

*Ideally, horizontal shear stress and acceleration will not affect $\xi_{a,a'}$ if a and a' are on the horizontal bending neutral axis.

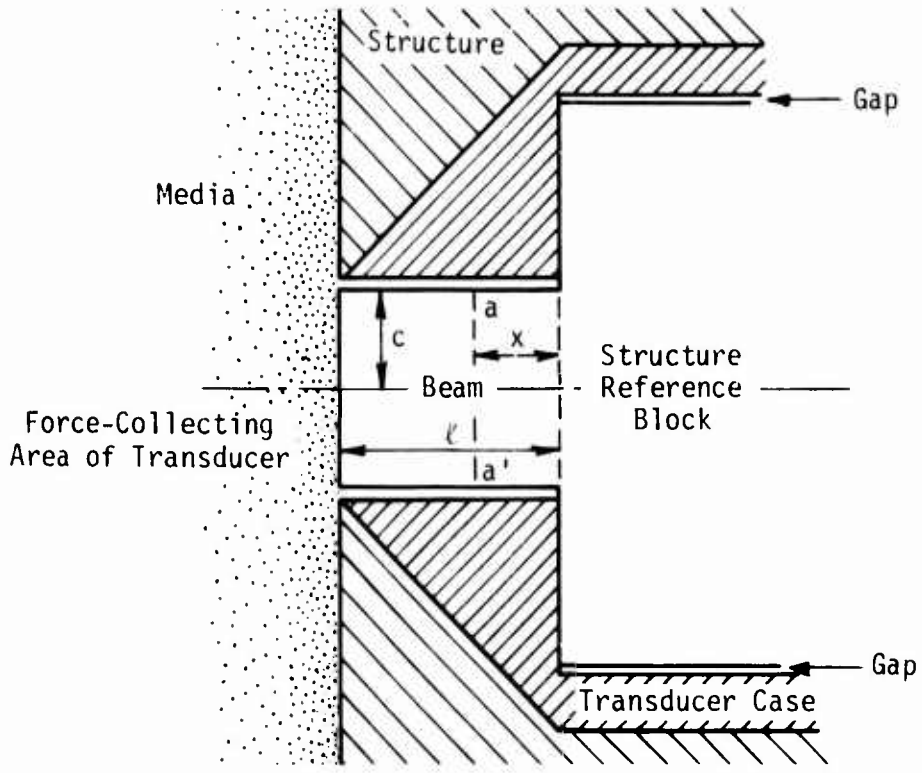

Figure 1. Basic Shear-Stress Transducer Beam

By adding a dummy beam as shown in figure 2 and properly interconnecting strain gages, these effects, except angular acceleration, can be effectively cancelled. With P-type piezoresistive strain gages located at points a, a', b, and b', a voltage analog of shear stress is produced by the circuit shown in figure 3.

When the primary element experiences downward vertical acceleration, R_a, and $R_{b'}$, increase the resistance equally, while R_b and $R_{a'}$ decrease the resistance equally; thus, bridge balance is maintained. When horizontal acceleration is experienced in the major axis of the primary element, R_a and $R_{a'}$, increase the resistance equally, while R_b and $R_{b'}$, decrease the resistance equally, and again bridge balance is maintained. If normal stress is experienced, R_b and $R_{b'}$, do not change, while R_a and $R_{a'}$, decrease equally and thus cause no bridge upset. Horizontal shear stress and acceleration in the horizontal shear-stress axis cause little or no change in any of the gage resistances if the gages are properly located on the neutral axis of the beam. The horizontal shear axis is gaged in the same manner as the vertical axis, and it performs in the same manner. The normal-stress axis presently uses only the active beam gaged as

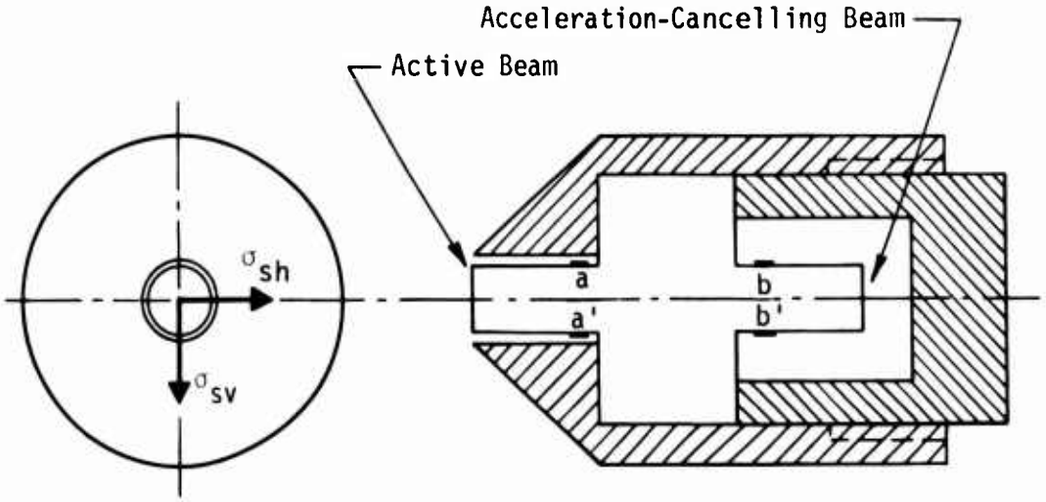

Figure 2. Total Primary Element Showing Active and Acceleration-Cancelling Beams

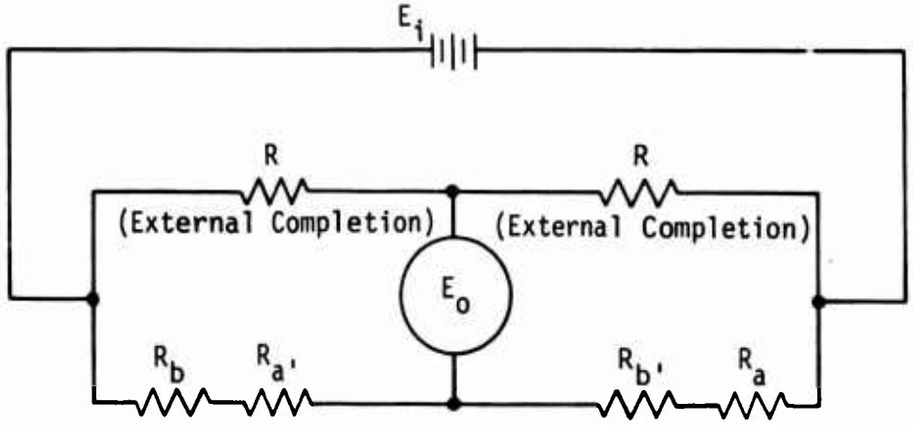

Figure 3. Electrical Circuit for Shear-Axis Bridge

a load cell much like the WAM gage (ref. 2). (Although this normal-stress bridge appears to perform well, it is felt that substantial improvement can be made by using both beams to eliminate acceleration sensitivity.) With these three independent bridges, the primary element of the dual beam is capable of providing voltage analogs of three mutually orthogonal interface stress vectors.

---

2. Pickett, Stephen F., *Development and Evaluation of Measurement Systems for Blast-Induced Motions in Buried Structures*, AFWL-TR-73-230, Air Force Weapons Laboratory, Kirtland Air Force Base, New Mexico, April 1974.

SECTION 3
DEVELOPMENT

INITIAL DESIGN

Three initial design triaxial stress transducers (fig. 4) were built. These transducers demonstrated that the shear-stress axes outputs were indeed linear with beam bending moment equivalent to 2000 psi shear on the force-collecting area and that cross-axis sensitivity was low. However, this transducer exhibited an extremely low tympanic resonance of 1100 to 1200 Hz because of the disk-like collecting elements which were used to match the overall beam stiffness with concrete stiffness.

INTERMEDIATE DESIGN

The second triaxial stress transducer of which six were built is shown in figure 5. This design incorporated a significant size reduction and the elimination of the disk collectors; the latter change provided a uniform cross-sectional area along the full length of the beams.

Initial testing of this transducer established that all three axes were linear with very little cross-axis sensitivity. In addition acceleration sensitivities were very low. Because of its size, this transducer was easy to handle and install compared to the initial transducer. While this transducer was being evaluated for unwanted sensitivity, careful attention was focused on the size of the force-collecting area. Although it was agreed by the Civil Engineering Research Facility (CERF), AFWL, and AFWL consultants that the small size and the maneuverability in field installation were desirable features, it was felt by some that the force-collecting area should be increased in order to minimize anomalies caused by large particles of media. Although not all were in agreement on this, the concensus opinion was that it would be better to have a 1-in. diameter beam to increase the force-collecting area by 300 percent. All agreed that the 1-in. diameter would not be harmful, and thus the requirement for a third design was established.

Figure 4. Initial Triaxial Stress Transducer

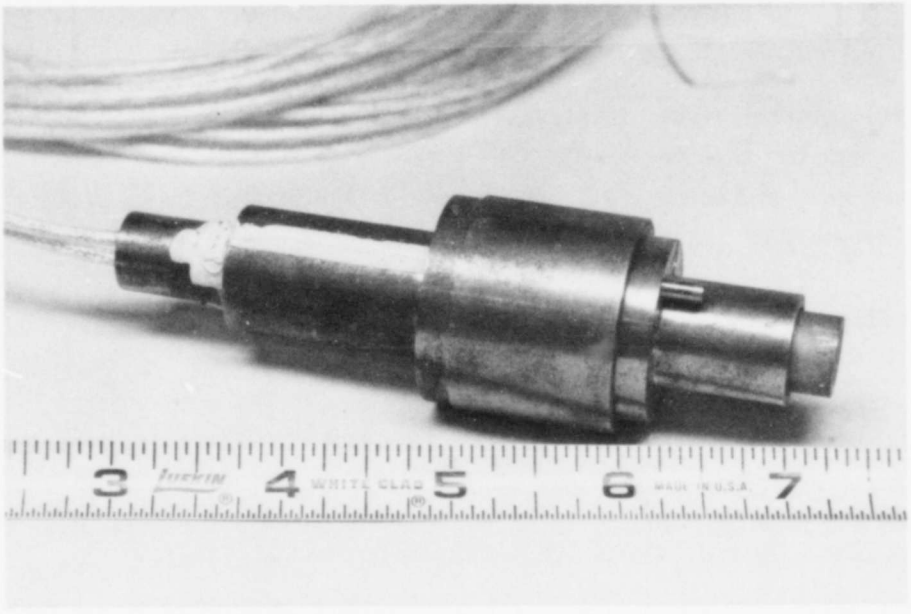

Figure 5. Intermediate Triaxial Stress Transducer

Figure 6. Final Triaxial Stress Transducer (Primary Element)

FINAL DESIGN

The final triaxial stress transducer developed is shown in figure 6. Engineering drawings for this transducer are contained in appendix A. All transducer parts are made of Ledloy 130, although any suitable steel could probably be used. Assembly of the transducer is covered in detail in appendix B.

Description

The primary element is made from a single piece of cylindrical stock. The two opposing beams are separated by a 2-in. diameter, 1.5-in. thick structure reference block, which has a dowel pin on the active beam side for axial alignment purposes and four threaded holes on the dummy beam side for attachment of the protection sleeve. Two holes through the reference block allow passage for the interconnecting wires between the active- and dummy-side strain gages.

The normal-axis gages are Kulite Type M(9) E-GP350-500 with a gage factor of 265 ± 5 percent and a resistance of 350 Ω ± 2 percent at 75°F. These gages are centered 0.650 in. from the end of the beam. The shear-axes gages are Kulite Type PEP350-090 with a gage factor of 130 ± 5 percent and a resistance of 350 Ω ± 2 percent at 75°F and are centered 1 in. from the end of the beam.

The sleeve provides a protective housing for the dummy beam as well as a termination point for internal circuitry attachment to external cables. It is attached to the primary element by four 4-40 screws.

The lock is used to secure the primary element in the case. (See appendix C.) Lead wires exit through a hole in the center of the lock and into the inside of the structure.

The case is a hollow cylinder tapered at the end and it must be placed in the structure form before the concrete is poured. (See appendix C.) Three 1/2-in. diameter 20 UNF tapped holes are located around the base for insertion of bolt-type concrete anchors. A dowel pin hole in the case mates with the dowel pin on the primary element to ensure desired case/sensitive-axis alignment.

Strain Gage Location

Since strain-gage location is important in order to achieve the desired balancing effect, a special device for correctly locating the gages was built (appendix B). From the equation in section 2 it is easy to see the effects of errors in locating the strain gages. The ℓ-x term by design should be 1.00 in.; this leaves 0.250 in. between the center of the strain gage and the supported end of the beam. This was felt to be necessary in order to avoid the unpredictable boundary strain effects near the supported end of the beam. If ℓ-x varies between the active and dummy beams, an undesired strain differential occurs and acceleration cancellation is jeopardized. Variation of the nominal resistance of the strain gage and of the gage factor also affects acceleration cancellation, but there is no way to control these variations.

Material Geometry

As indicated in the engineering drawings (appendix A) there is a number of tight tolerances on the primary element. This is to insure a good match between beam deflections (active and dummy) during shear-axes accelerations.

Calculated Sensitivities

With a simplified mathematical model of the primary element, various combinations of wanted and unwanted sensitivities were evaluated for unwanted sensitivity output contributions. These effects were found to be less than 1 percent of the true applied shear at combined unwanted input levels of 2000g acceleration, 2000-psi normal stress, and 2000-psi cross-axis shear stress. Based on this, it was felt that this design would have an excellent chance of meeting the unwanted sensitivity specification requirements.

The unwanted sensitivities appeared to be low for both a full-bridge and a half-bridge arrangement for shear, but the half bridge was slightly favored. The only possible problem with the half-bridge system is that the higher transducer source impedance could reduce the upper frequency response limits of the total system to an unacceptably low level when long lines are used.

Surface Texture Matching

Rather than determine static and dynamic coefficients of friction for both a Ledloy 130/sand interface and a typical structure/sand interface, a texturing scheme was devised to make the transducer active surface of concrete, except for a necessary small retaining annulus.

Several texture-retaining designs were tested with applied soil-stress (20-40 dry Ottawa sand) levels to 8000 psi and applied beam g-levels to 10,000g to determine which design would maintain the best surface integrity under these conditions. All designs appeared to work very well; however, the design chosen exhibited virtually no texture shrinkage (permanent compression) with the 8000-psi, soil-stress load.

A cup was cut in each end of the beam and four threaded holes were made in the bottom of each cup to allow 6-32 screws to be used as reinforcement for an epoxy/grout mix which was placed in the cups. (See primary element drawing in appendix A and texturing procedures in appendix B.)

The concrete insert material was Embeco 630 nonshrink grout with Epocast 530 epoxy and 9816 hardener. This was placed on both the active and dummy beam in an effort to maintain beam balance.

SECTION 4
CALIBRATION

A modified case mounted on pillow blocks (fig. 7) was used to calibrate the transducer. With this device, a known bending moment could be applied to each of the shear axes by a calibrated kip machine. To calibrate the normal axis, the encased primary element was removed and repositioned for kip machine loading in the normal axis only.

Although the calibration device worked well and showed that the shear axes outputs were linear with applied moment and that the normal axis output was linear with applied load, it was decided to test the load sensitivity of the case by applying a kip machine load to the case; i.e., the case was squeezed. At load levels up to 50 kips, the transducer outputs were 154 psi equivalent shear stress (worst case) and 187 psi equivalent normal stress (worst case). These were considered to be unreasonably high; the cause was not determined. However, after increasing the clearance between the structure reference block and the case (fig. 1), the problem cleared up (21 psi equivalent shear stress, worst case; 47 psi equivalent normal stress, worst case). Three separate primary elements were tested in each of three cases both before and after this modification.

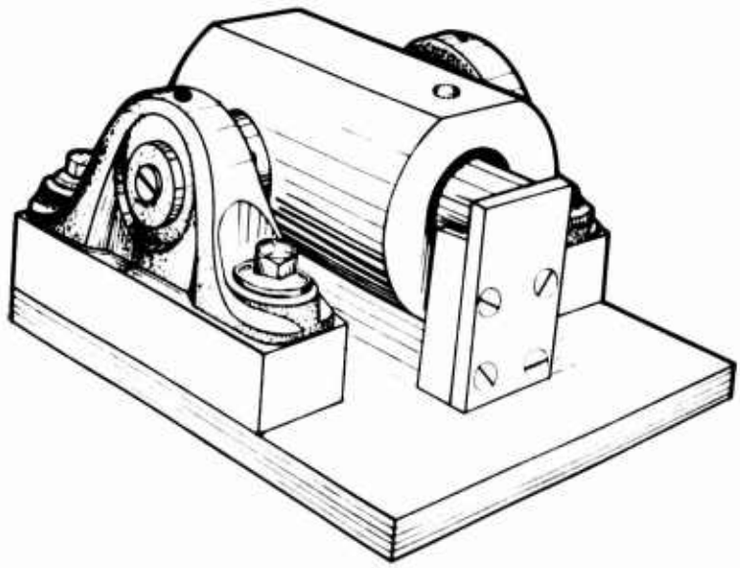

Figure 7. Calibration Fixture

SECTION 5
LABORATORY TESTING

CROSS-AXIS STRESS SENSITIVITY

Cross-axis stress sensitivities were evaluated in the calibration fixture (fig. 7). Three transducers were used in this test series, and the following tests were performed on each unit:

(1) A bending moment equivalent to a 2000-psi shear stress was applied to the vertical shear-stress axis and the outputs of the two remaining stress axes were monitored.

(2) A bending moment equivalent to a 2000-psi shear stress was applied to the horizontal shear-stress axis and the outputs of the two remaining stress axes were monitored.

(3) A normal load equivalent to a 2000-psi normal stress was applied to the normal axis, and the outputs of the two remaining stress axes were monitored.

Cross-axis normal loading resulted in 31.6- to 62.15-psi equivalent shear stress (1.5 to 3.1 percent of cross-axis loading). Cross-axis shear loading resulted in 14.7- to 57.6-psi equivalent shear stress on the unloaded shear axis (0.7 to 2.88 percent of cross-axis loading) and 200- to 320-psi equivalent normal stress (10 to 16 percent of cross-axis loading).

Shear-axis sensitivities were well within the desired specifications; however, the normal-axis sensitivities were extremely high. Before speculating on the cause of this, it should be pointed out that a number of the triaxial transducers built for the HARD PAN Events were tested in this same manner and the results from these tests showed that the normal axis was consistently less cross-axis stress sensitive than the shear axes. These data were not logged or recorded nor was it required for the HARD PAN Events. The tests were performed merely from curiosity and were easy to do during the normal calibration procedure; i.e., while the axis calibrated was being plotted on an X-Y recorder, millivolt outputs of the other two conditioned axes were monitored. Of eight transducers monitored in this fashion, all but one exhibited about the

same shear-axis response to cross-axis loading as found during cross-axis testing of the three experimental transducers. The remaining transducer exhibited virtually no cross-axis sensitivity on one shear axis with applied normal loading. For all eight transducers, normal-axis sensitivity to shear loading was in the range of 30 to 70 percent of the shear-axis sensitivity to cross-axis shear loading.

After the transducers were built for HARD PAN, it was decided jointly by CERF and AFWL to build and test three new prototypes employing the same features used on the HARD PAN transducers (primarily changes in the glass backing used on the shear-axis strain gages to reduce hysteresis). Three older prototypes had previously been tested for unwanted input sensitivities only.

There was an adequate supply of shear-axis strain gages left after satisfying HARD PAN requirements; however, the available normal-axis strain gages were not considered to be of high quality, primarily because of matrix skew (fig. 8). These gages were used anyway, and this could well be the reason for the poor normal-axis performance in cross-axis stress and acceleration sensitivity, linearity, and repeatability.

Figure 8. Typical Normal-Axis Strain Gages Used in Prototype Transducers

ACCELERATION SENSITIVITY

The three prototype transducers were evaluated for stress-axis acceleration sensitivity. In this experiment, the CERF drop tower was used to impart inputs of 225 to 3300 g to all three transducer axes. The transducer case, containing the transducer, was placed on top of two layers of blotter pad which rested on the dropping mass platform. The case was fastened in place with bookbinder's tape and the entire drop platform was raised approximately 30 in. for 2200g to 3000g drops. After being released and dropping the 30 in., the drop platform was arrested by the drop table. Four 4 by 4 in. precompressed styrofoam pads were used to cushion the drop and tailor the acceleration pulse. The conditioned stress outputs, as well as an acceleration output from an Endevco 2264-5000 accelerometer (used to sense vertical acceleration), were amplified through Astrodata 141 amplifiers and recorded on an Ampex CP100 tape deck running at 60 in/sec. Wideband FM recording was used (108 kHz center frequency ± 40 percent deviation with 20 kHz response). Results are shown in table 1.

The wide variance in g drop levels occurred because of difficulties in restraining angular acceleration and because many of the acceleration inputs contained significant energy at and above the transducer resonant frequency (12 kHz). In an effort to minimize these effects numerous drops at various g-levels were made. In spite of these efforts there were still some sensitivity contributions from ringing and angular acceleration.

STATIC-SHEAR SENSITIVITY

In order to check the shear response of the transducer in an actual shear environment a special fixture which allowed the transducer to be subjected to both static and dynamic vertical shear-stress inputs was built (fig. 9). Included in this fixture was a means of inferring vertical shear stresses. This inferred shear was necessary to evaluate the shear response of the transducer. The central part of this fixture is cylindrical with a 6-in. diameter and consists of the cased transducer embedded in a 6-in. diameter by 6-in. long concrete cylinder. Load cells at the top and bottom of the concrete cylinder separate the sample cylinder from the metal cylinder extensions. A surgical rubber tubular bladder

Table 1. Acceleration Sensitivity Test Data

	Vertical Shear-Axis Drop	Horizontal Shear-Axis Drop	Normal-Axis Drop
Transducer SN 07			
g-Level, g	528	3300*	1221
Vertical Shear Sensitivity, psi/g	0.01388	0.085	0.030
Horizontal Shear Sensitivity, psi/g	0.01440	0.0809	0.0417
Normal Sensitivity, psi/g	0.120	0.2033	0.2444
Transducer SN 08			
g-Level, g	226	265	396
Vertical Shear Sensitivity, psi/g	0.0196	0.010	0.0089
Horizontal Shear Sensitivity, psi/g	0.00787	0.02518	0.01123
Normal Sensitivity, psi/g	0.01962	0.150	0.02239
Transducer SN 16			
g-Level, g	3080**	396	409
Vertical Shear Sensitivity, psi/g	0.098	0.000	0.0223
Horizontal Shear Sensitivity, psi/g	0.032	0.0059	0.0113
Normal Sensitivity, psi/g	0.119	0.0297	0.0793

*Discontinuities in output noted.

**Acceleration had extremely fast rise time and a large level of high-frequency ringing.

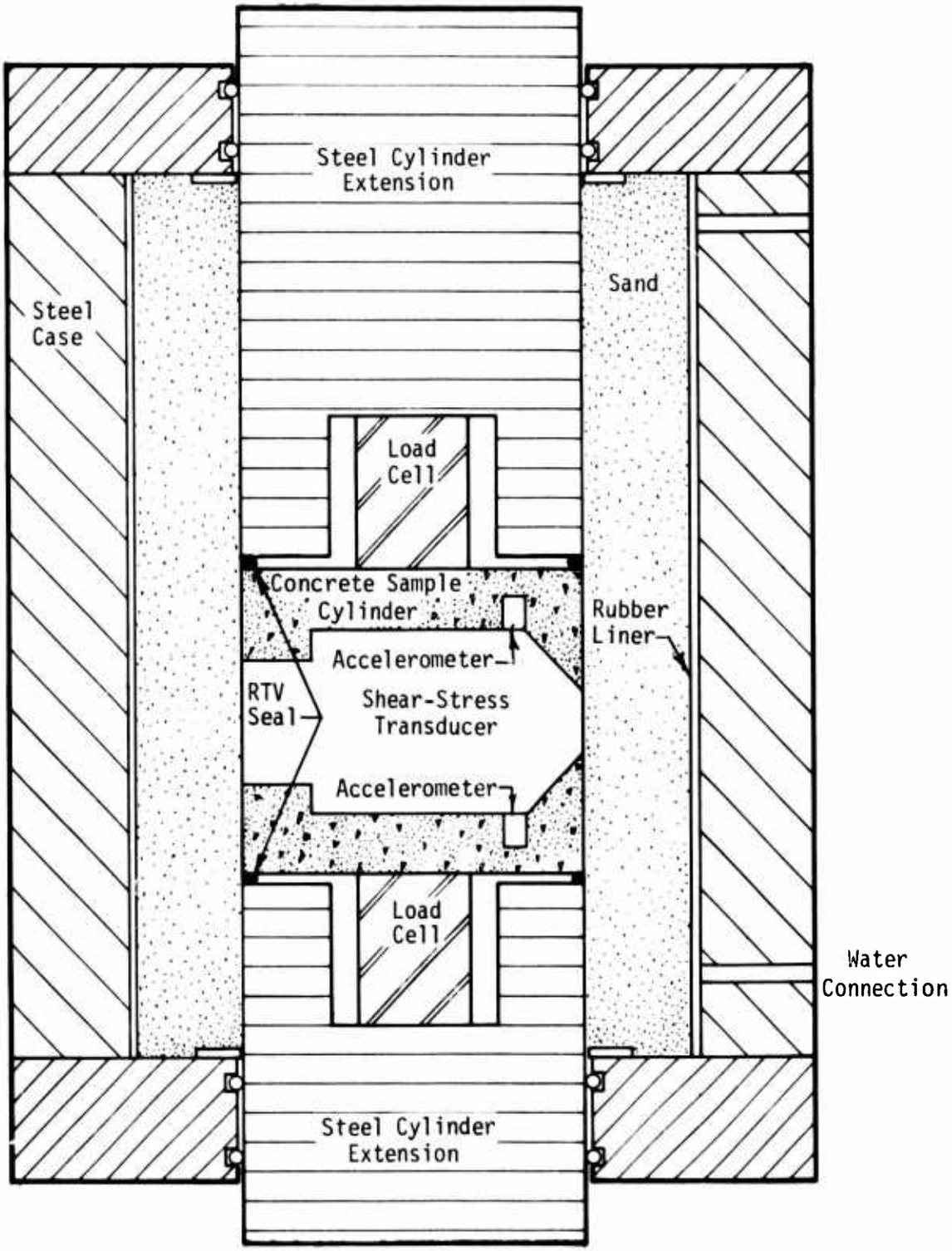

Figure 9. Shear-Stress Test Fixture

is used in conjunction with a hydraulic pump to establish a normal stress through 20-40 Ottawa sand against the central cylinder. Vertical load may then be placed on the upper portion of the central cylinder to create vertical shear stress on the sample interface surface.

This fixture is similar to the shear fixture used by Leonards (ref. 3) except that external pressure is applied to the outside of the bladder as opposed to evacuating the inside of the bladder. This allows higher normal interface stresses to be imparted to the sample. Two accelerometers are mounted--one above and one redundant accelerometer below the transducer case (fig. 10) in the concrete sample section (fig. 11). The acceleration measurement when scaled and summed properly with the load cell measurements are used to infer average shear stress on the sample. The following force-balance equations are employed:

$$F = ma$$

$$ma = F_u - F_L - F_s$$

or

$$F_s = F_u - F_L - ma$$

where

F_s = total shear force on concrete sample
F_u = upper load cell force
F_L = lower load cell force
m = mass of sample
a = acceleration of sample

Dividing both sides of the latter equation by the interface surface area of the sample, A, gives

$$\frac{F_s}{A} = \sigma_s = \frac{F_u - F_L - ma}{A}$$

Thus, the average shear stress on the sample is inferred by the algebraic weighted sum of the upper and lower load cell forces and sample acceleration.

---

3. Leonards, G. A., *Experimental Study of Static and Dynamic Friction Between Soil and Typical Construction Materials*, AFWL-TR-65-161, Air Force Weapons Laboratory, Kirtland Air Force Base, New Mexico, December 1965.

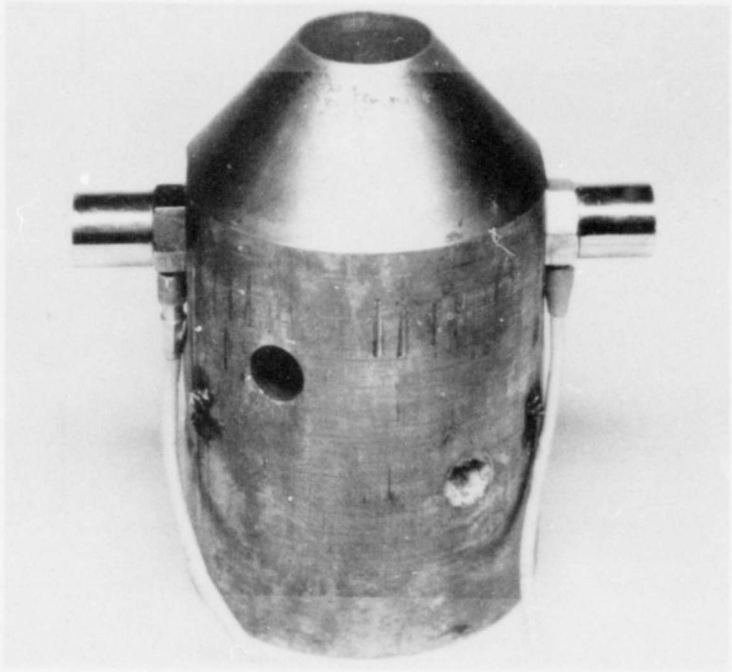

Figure 10. Transducer Case with Mounted Accelerometers

The following assumption must be made in order to use these data to evaluate shear-stress performance: the σ_s inferred by the three fixture transducers is the same as the σ_s encountered on the active surface of the transducer. There are a number of reasons why this may not be true:

(1) Differential load cell readings are subject to large common mode errors unless the lower load cell output is very nearly zero. For example, if the upper load is actually only 5 percent higher than the lower load and both cells are accurate to ± 5 percent of the reading, measured load differential is

$$F_u - F_L = [1.05(1 \pm 0.05) - (1 \pm 0.05)]F_L$$

This could yield implied load differentials with errors in the range of -105 to +305 percent. Fortunately this example represents a drastic case which was not encountered during testing. Typically, the lower load cell readings were about one-third to one-half the upper load cell readings; however, there is room for common mode errors.

Figure 11. Concrete Sample Assembly

(2) If sand penetrates the RTV seal between either load cell and the sample, load bridging can occur; i.e., the load cell will not see the total applied load since the sand will transmit some of the load. This obviously occurred on one series of static tests at the lower load cell junction. Extremely high shear stress was inferred because of pulverized sand in the lower portion of the fixture.*

(3) Although the sample surface appears to have a relatively uniform texture, the transducer force-collecting surface represents a plane of osculation on the cylindrical surface, i.e., a surface aberration which may cause a normal stress and shear stress planar gradient at and around the shear-stress, force-collecting surface (fig. 11).

The test specimen (shear transducer) was mounted in its steel housing and then placed in a mold, into which concrete was poured. The transducer was placed so that the sensing surface was even with the outside surface of the cylindrical mold and the normal sensing axis was perpendicular to the longitudinal axis of the concrete cylinder. After curing (approximately 7 days), the concrete cylinder was removed from the mold, and the upper and lower load cells were attached with the steel load-bearing cylinders. This test cylinder was then placed inside the steel test fixture. The test fixture has a rubber bladder inside so that water pressure may be applied to the sand surrounding the test cylinder without saturating the sand. After placing the test cylinder inside the test fixture, 20-40 Ottawa sand was rained around the test cylinder until the fixture was filled to the top (fig. 12). The top plate was then installed and torqued to 80 ft-lb on each of the eight bolts. The bottom plate had previously been installed in the same manner.

The test fixture was placed into a 300,000-lb capability Reihle Machine. All instrumentation was hooked up and balanced, and outputs were connected to

*In this test series the RTV seal was not used; only a small gap was used to retard sand bridging. The RTV seal was used in subsequent testing and appeared, upon post-test inspection, to eliminate load bridging.

Figure 12. Shear-Stress Test Fixture Before Placement of Lid

assigned tape recorder channels and the X-Y plotter. Water pressure applied to the test fixture compacted the sand around the inside of the test cylinder and against the face of the shear transducer. Various loads were applied to the top of the test cylinder; this caused a shear load on the face of the shear transducer. Water pressure, as well as the load into the test cylinder, was varied from test to test. Outputs from the shear-transducer sensors, as well as the two load cells and the water-pressure sensor, were recorded on magnetic tape. The outputs from the load cells were also recorded on an X-Y plotter so that slippage occurring inside the test fixture could be seen.

Results of the static testing are shown in appendix D. Various pressure loading and kip machine loading patterns were used. The normal-stress transducer, which was not expected to perform properly, did agree in trend with the hydraulic-pressure transducer but was typically about 30 percent higher. The vertical shear-stress transducer outputs had the same pattern as the inferred vertical shear stress with peaks about 70 percent of the inferred shear. During the last of this test series, peak outputs agreed more favorably, with

those from the vertical shear-stress transducer being slightly higher than those of the inferred shear stress. No explanation can be offered for this. Both the transducer vertical shear and the inferred vertical shear showed residuals when the kip load was dropped, with the transducer vertical shear-stress residual in excess of the inferred vertical shear stress. When the hydraulic load was removed, however, both residuals disappeared. Apparent horizontal shear-stress output was low; it ranged from 2 to 5 percent of the vertical shear stress.

DYNAMIC-SHEAR SENSITIVITY

Fixture preparation for the dynamic testing was identical to that for the static testing, except the CERF drop tower was used to impart dynamic loads to the sample column. The test fixture was placed under the impact machine so that the weight would drop on top of the test cylinder load-bearing cylinder. Styrofoam discs and rubber pads were placed on top of the test cylinder to reduce ringing in the test fixture and also to tailor the input shock waveform. The instrumentation was hooked up and checked out, and water pressure was applied to the test fixture as in static testing. The weight was then dropped on top of the test cylinder from various heights; this caused a shear load to be applied to the shear transducer. A total of 21 tests were made with different drop heights and water pressure combinations. Outputs from all instrumentation were recorded on magnetic tape.

The dynamic test results are shown in appendix E. In the nine tests shown, the initial normal stress is 14 to 26 percent higher than the hydraulic pressure; vertical shear peak outputs are 42 to 77 percent of the inferred shear peaks (average = 65 percent). The vertical shear and the inferred shear trends are the same, with closer agreement toward the end of the transient interval. Also, as in the static testing, apparent residuals appeared to be higher in the vertical shear than in the inferred shear. Peak horizontal shear-stress outputs averaged about 5.9 percent of the peak vertical shear-stress outputs. Peak accelerations to peak vertical shear ratios were 1.6 to 4.8 (g/psi) with peak g-inputs of 300g to 600g. Some obvious ring was apparent in both the vertical and horizontal shear transducer outputs, but this ringing was not seen in the normal-stress transducer output. This would indicate a bending ring mode

rather than an axial ring mode. Because of the ring, it is somewhat difficult to appraise the acceleration sensitivity of the shear transducers, although it appears that acceleration sensitivity may be contributing to transducer outputs, especially in the early part of the shear transient. Peak data from the shear transducer outputs were taken by fairing through the high-frequency ringing.

SECTION 6
SUMMARY OF TEST DATA

Test data findings and target objectives (requirements) are compared in the following summary:

(1) Range

Required: 2000-psi shear stress (two axes)
3000-psi normal stress (one axis)

Test Findings: Peak predicted stresses of 200 to 5000 psi can be handled on all axes.

(2) Useable Frequency Range

Required: dc to 500 Hz

Test Findings: dc to at least 2000 Hz

(3) Mounting Requirements

Required: 3-in. thick wall or greater

Test Findings: This requirement was met.

(4) Shear-Axis Sensitivity to Normal Stress

Required: No greater than 5 percent apparent shear stress at 1000-psi normal stress

Test Findings: Worst case was 3.1 percent.

(5) Normal-Axis Sensitivity

Required: No greater than 5 percent apparent normal stress at 1000-psi shear stress

Test Findings: Worst case was 16 percent. This requirement was met when data from HARD PAN transducers were taken into account.

(6) Acceleration Sensitivity (All Axes)

Required: Shear--0.02 psi/g or better
Normal--0.03 psi/g or better

Test Findings: Shear--0.0417 psi/g (worst case)
Normal--0.244 psi/g (worst case)

Note: The target objective is not met when worst-case test sensitivities are used; however, sensitivities other than worst case indicate satisfactory performance. The tests in which high-frequency ringing and output discontinuities occurred were not used for worst-case sensitivities.

(7) Shear-Axis Sensitivity to Cross-Axis Shear

Required: No target objective established

Test Findings: Worst case was 2.88 percent.

(8) Force-Collecting Surface

Required: The force-collecting surface of the transducer shall be 1 in. in diameter and textured to match as nearly as possible the coefficient of friction of the structure.

Test Findings: This requirement was met.

The vertical axis of the shear transducer in both static and dynamic testing exhibited a shear/time history quite similar in pattern and trend to the inferred shear.

During both dynamic and static testing, the peak vertical shear-stress output from the transducer was typically 65 to 70 percent of the inferred-shear peaks.

Residual (post-test) shear on the transducer appeared to be consistently higher than the inferred residuals, although both residuals dissappear when normal stress is relieved. The fact that a residual shear stress is indicated by both is not alarming and is probably due to locking of the test column against the upper and/or lower plate.

Cross-axis and acceleration sensitivities were adequately low and in most cases exceeded the target specifications.

Although the normal-stress gage did not perform well on the three test transducers, it does not mean that the normal-stress measurement cannot be made successfully. Indeed, during limited transducer testing for the HARD PAN Event, cross-axis and acceleration sensitivities were as good as, or better than, the shear-axis sensitivities.

SECTION 7
CONCLUSIONS AND RECOMMENDATIONS

CONCLUSIONS

During development and testing, the triaxial stress transducer met and exceeded nearly all target objectives. The triaxial transducer in its present configuration is recommended for field use, even though some improvements and additional experimental work would be beneficial.

Based on Ottowa sand test results and data from the HARD PAN Events, it appears that the device is capable of making good triaxial stress measurements in high g and high cross-axis stress environments. The bending moment calibration method can be employed along with the 0.65 registration factor to provide scale factors without an actual structure/media environment calibration if the structural surfaces have no pits, pockets, or other unusual surface anomalies. Calibration without actual interface shear stress input is roughly equivalent to 1g and 2g fallthrough calibrations, without actual velocity, performed on oil-damped pendulous velocity gages (ref. 4).

Since there was no established dynamic interface shear-stress standard before or during the development of the triaxial stress transducer, an actual structure/media inferred shear-stress method and apparatus were developed. These were used as a dynamic shear-stress standard for the triaxial stress transducer. Other methods were considered by both AFWL and CERF; but because of the requirement to evaluate the transducer in an actual structure/media environment, this method was considered superior to the others and a good dynamic shear-stress standard. The inferred shear measurement provides the average vertical shear stress seen by the entire sample area (100 $in.^2$); the transducer provides average shear seen by its force-collecting surface (less than 1 $in.^2$). This accounts for the differences seen in the two measurements.

---

4. Sonnenburg, Paul N., and Schulz, George, *Response Properties of an Orthogonal System of Pendulum-Type Velocity Gages*, AFWL-TR-73-31, Air Force Weapons Laboratory, Kirtland Air Force Base, New Mexico, June 1973.

RECOMMENDATIONS

Calibration Fixture

Although the dynamic shear-stress calibration fixture worked well, the following improvements can be made:

(1) Stiffer load cells should be made to allow higher shear-stress levels to be obtained and to decrease gap variation between the sample cylinder and cylinder extensions.

(2) The sample surface area should be decreased as much as possible to minimize shear gradient effects.

(3) The transducer force-collecting surface should be machined (for laboratory testing purposes only) to match the sample surface contour. This would provide a more uniform cylindrical sample surface and eliminate local shear gradients around the transducer force-collecting area. The same contouring procedure should be applied to both transducer beams to minimize beam imbalance.

(4) It would probably be beneficial if the steel cylinder extensions had concrete surfaces to further reduce shear gradients at the upper and lower boundaries of the sample. This could be accomplished by decreasing the diameter of the steel cylinders adjacent to the load cells and casting with concrete back up to the original diameter. A concrete anchoring system similar to the one used in the transducer beams should be employed.

Triaxial Stress Transducer

(1) Ledloy was chosen for the transducer material because it is not attacked by concrete. Stainless steel (416 annealed) would probably have been a better choice. This material is easily machined, not attacked by concrete, and not oxidized like Ledloy. It is thus recommended that future transducers be made of this material. Although the oxide coat on the transducers presented no real problem, better bonding of the RTV seal could be achieved on stainless steel.

(2) The acceleration-cancelling beam used to reduce acceleration sensitivity on the shear-stress axes could also be used in a half-bridge configuration to reduce acceleration sensitivity on the normal-stress axis. It is recommended that this be evaluated for effectiveness.

(3) The necessary steel retaining annulus around the concrete force-collecting surface makes up over 30 percent of the total beam surface, and this is responsible in part for the shear underregistration. However, this area cannot be substantially reduced without jeopardizing beam integrity. It would be adviseable to test a transducer without the concrete textured surface to determine the shear-force contribution from the steel force-collecting area. This information could be used to provide the effective force-collecting area for the shear axes of the transducer.

(4) The medium used in this investigation was Ottowa sand; however, tests should be performed in the calibration fixture with other media of interest to determine if transducer shear performance and shear scale factor are media biased.

(5) In field use, significant input components above 3 kHz should be avoided to eliminate the possibility of ringing. It is recommended that future studies include either vibration testing or transient-generated transfer functions to establish actual upper-frequency limitations.

(6) With the usable frequency range of the transducer being at least three times higher than the 500 Hz required, it is anticipated that data reconstruction techniques need not be employed. However, if obvious output components above 3 kHz are seen in the data and if these are attributable to shear inputs, methods are available to extend the effective gage frequency passband. By characterizing the gage in the laboratory with known inputs of adequate high-frequency content, relatively

simple reconstruction procedures can be used to correct the voltage data analogs. In particular, the ratio of the known input sample set fast Fourier transform to the input response sample set fast Fourier transform multiplied appropriately by the fast Fourier transform of the field data sample set in question can be brought back corrected in the time domain with an inverse fast Fourier transform operation. Time-domain methods are also available for data reconstruction. For step-input-related time-domain deconvolution, a laboratory-generated, step-response sample set is required along with the field data sample set to determine the corrected or reconstructed sample set. With arbitrary input-related, time-domain deconvolution, sample sets of any sufficiently known arbitrary input, gage response to this input, and field data are used to generate a reconstructed field data sample set. Other time-domain data-reconstruction methods include impulse-invariant, step-invariant, and ramp-invariant Z transform methods, which require a system mathematical model (refs. 5, 6, 7).

(7) Cross-axis response correction can also be easily made if cross-axis sensitivity scale factors are constant (which appears to be the case for the triaxial stress transducers tested). Correction then becomes a matter of solving three simultaneous equations with three unknowns.

$$E_{ov} = \alpha\sigma_{sv} + \beta\sigma_{sh} + \gamma\sigma_{n}$$

$$E_{oh} = \alpha'\sigma_{sv} + \beta'\sigma_{sh} + \gamma'\sigma_{n}$$

$$E_{on} = \alpha''\sigma_{sv} + \beta''\sigma_{sh} + \gamma''\sigma_{n}$$

---

5. Schulz, George L., *Method of Transfer Function Calculation and Distorted Data Correction*, AFWL-TR-73-300, Air Force Weapons Laboratory, Kirtland Air Force Base, New Mexico, March 1975.

6. Pickett, Stephen F., *An Evaluation of Four Data Reconstruction Techniques Applied to Seismometer Data*, Masters Thesis, University of New Mexico, Albuquerque, New Mexico, December 1974.

7. Stearns, Samuel D., *Digital Signal Analysis*, Hayden Book Co., Inc., Rochelle Park, New Jersey, 1975.

where

E_{ov} = vertical-axis output voltage
E_{oh} = horizontal-axis output voltage
E_{on} = normal-axis output voltage
σ_{sv} = vertical shear stress
σ_{sh} = horizontal shear stress
σ_n = normal stress

$$\left.\begin{aligned} \alpha &= E_{ov}/\sigma_{sv} \\ \alpha' &= E_{oh}/\sigma_{sv} \\ \alpha'' &= E_{on}/\sigma_{sv} \end{aligned}\right\} \quad \text{when } \sigma_{sh} = \sigma_n = 0$$

$$\left.\begin{aligned} \beta &= E_{ov}/\sigma_{sh} \\ \beta' &= E_{oh}/\sigma_{sh} \\ \beta'' &= E_{on}/\sigma_{sh} \end{aligned}\right\} \quad \text{when } \sigma_{sv} = \sigma_n = 0$$

$$\left.\begin{aligned} \gamma &= E_{ov}/\sigma_n \\ \gamma' &= E_{oh}/\sigma_n \\ \gamma'' &= E_{on}/\sigma_n \end{aligned}\right\} \quad \text{when } \sigma_{sv} = \sigma_{sh} = 0$$

$$\begin{bmatrix} \alpha & \beta & \gamma \\ \alpha' & \beta' & \gamma' \\ \alpha'' & \beta'' & \gamma'' \end{bmatrix} \begin{bmatrix} \sigma_{sv} \\ \sigma_{sh} \\ \sigma_n \end{bmatrix} = \begin{bmatrix} E_{ov} \\ E_{oh} \\ E_{on} \end{bmatrix}$$

$$\begin{bmatrix} \sigma_{sv} \\ \sigma_{sh} \\ \sigma_n \end{bmatrix} = \begin{bmatrix} \alpha & \beta & \gamma \\ \alpha' & \beta' & \gamma' \\ \alpha'' & \beta'' & \gamma'' \end{bmatrix}^{-1} \begin{bmatrix} E_{ov} \\ E_{oh} \\ E_{on} \end{bmatrix}$$

The solution becomes more complicated when cross-axis sensitivity scale factors are not constant, i.e., if cross-axis output is a nonlinear function of cross-axis input, and virtually impossible if the input/output relationship is multi-valued. Sonnenburg and Schulz addressed similar cross-axis sensitivity problems of an orthogonal system of pendulous velocity gages and developed a computer code for the solution of cross-axis sensitivities (ref. 4). Since cross-axis sensitivities are extremely low on the shear axes and can be made extremely low on the normal axis, it should not be necessary to employ cross-axis correction schemes on most field data.

REFERENCES

1. Huck, Peter J., et al., *Dynamic Response of Soil/Concrete Interfaces at High Pressure*, AFWL-TR-73-264, Air Force Weapons Laboratory, Kirtland Air Force Base, New Mexico, April 1974.

2. Pickett, Stephen F., *Development and Evaluation of Measurement Systems for Blast-Induced Motions in Buried Structures*, AFWL-TR-73-230, Air Force Weapons Laboratory, Kirtland Air Force Base, New Mexico, April 1974.

3. Leonards, G. A., *Experimental Study of Static and Dynamic Friction Between Soil and Typical Construction Materials*, AFWL-TR-65-161, Air Force Weapons Laboratory, Kirtland Air Force Base, New Mexico, December 1965.

4. Sonnenburg, Paul N., and Schulz, George, *Response Properties of an Orthogonal System of Pendulum-Type Velocity Gages*, AFWL-TR-73-31, Air Force Weapons Laboratory, Kirtland Air Force Base, New Mexico, June 1973.

5. Schulz, George L., *Method of Transfer Function Calculation and Distorted Data Correction*, AFWL-TR-73-300, Air Force Weapons Laboratory, Kirtland Air Force Base, New Mexico, March 1975.

6. Pickett, Stephen F., *An Evaluation of Four Data Reconstruction Techniques Applied to Seismometer Data*, Masters Thesis, University of New Mexico, Albuquerque, New Mexico, December 1974.

7. Stearns, Samuel D., *Digital Signal Analysis*, Hayden Book Co., Inc., Rochelle Park, New Jersey, 1975.

APPENDIX A

ENGINEERING DRAWINGS

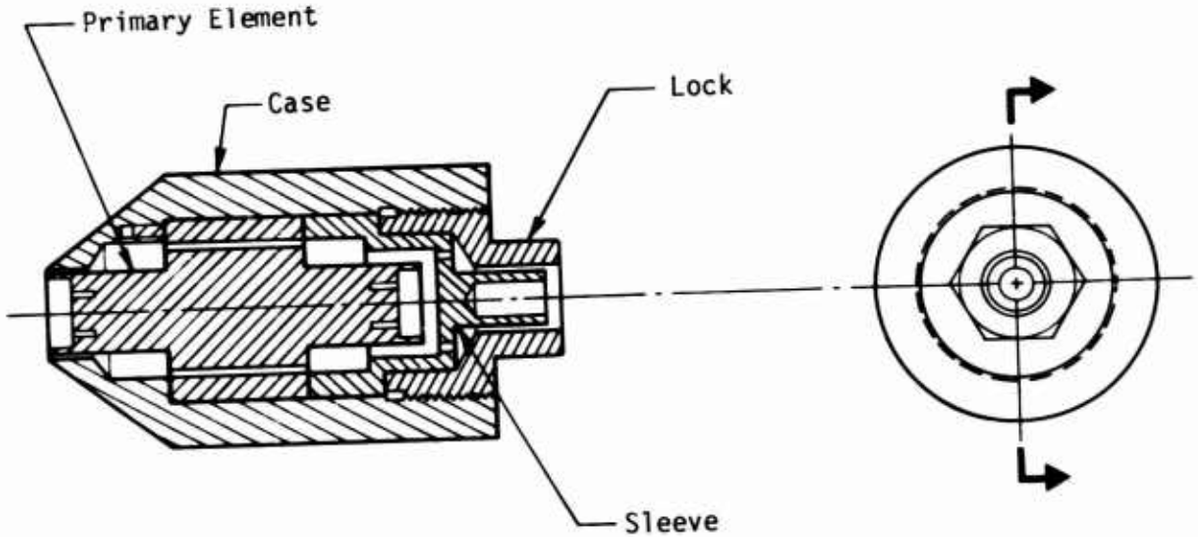

TRANSDUCER ASSEMBLY

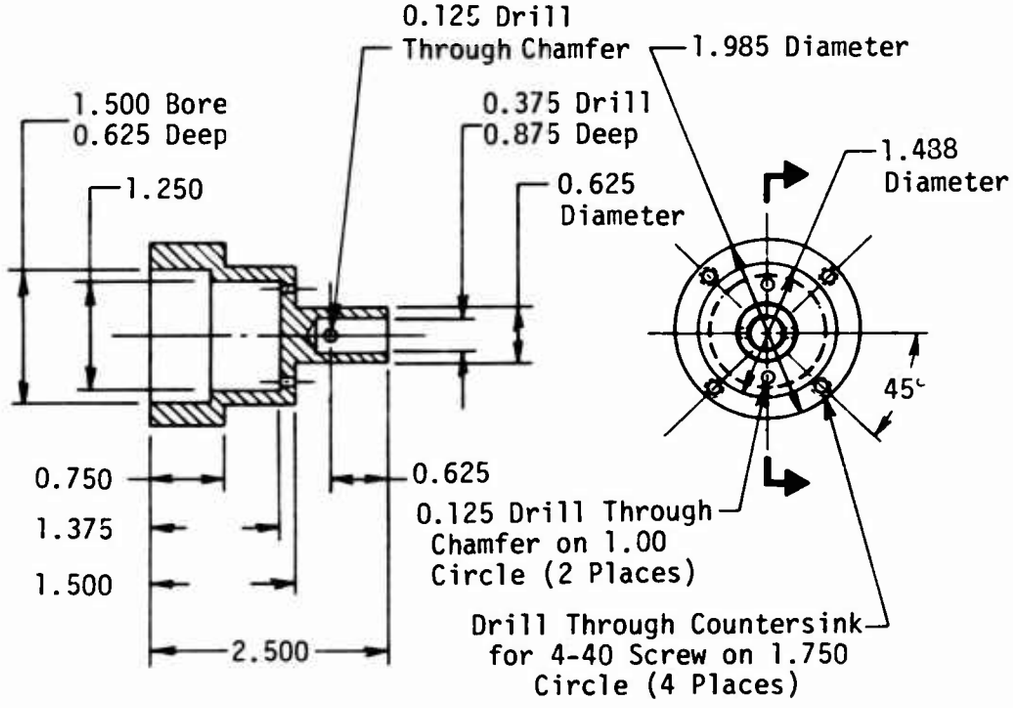

Note: All dimensions are in inches.

SLEEVE

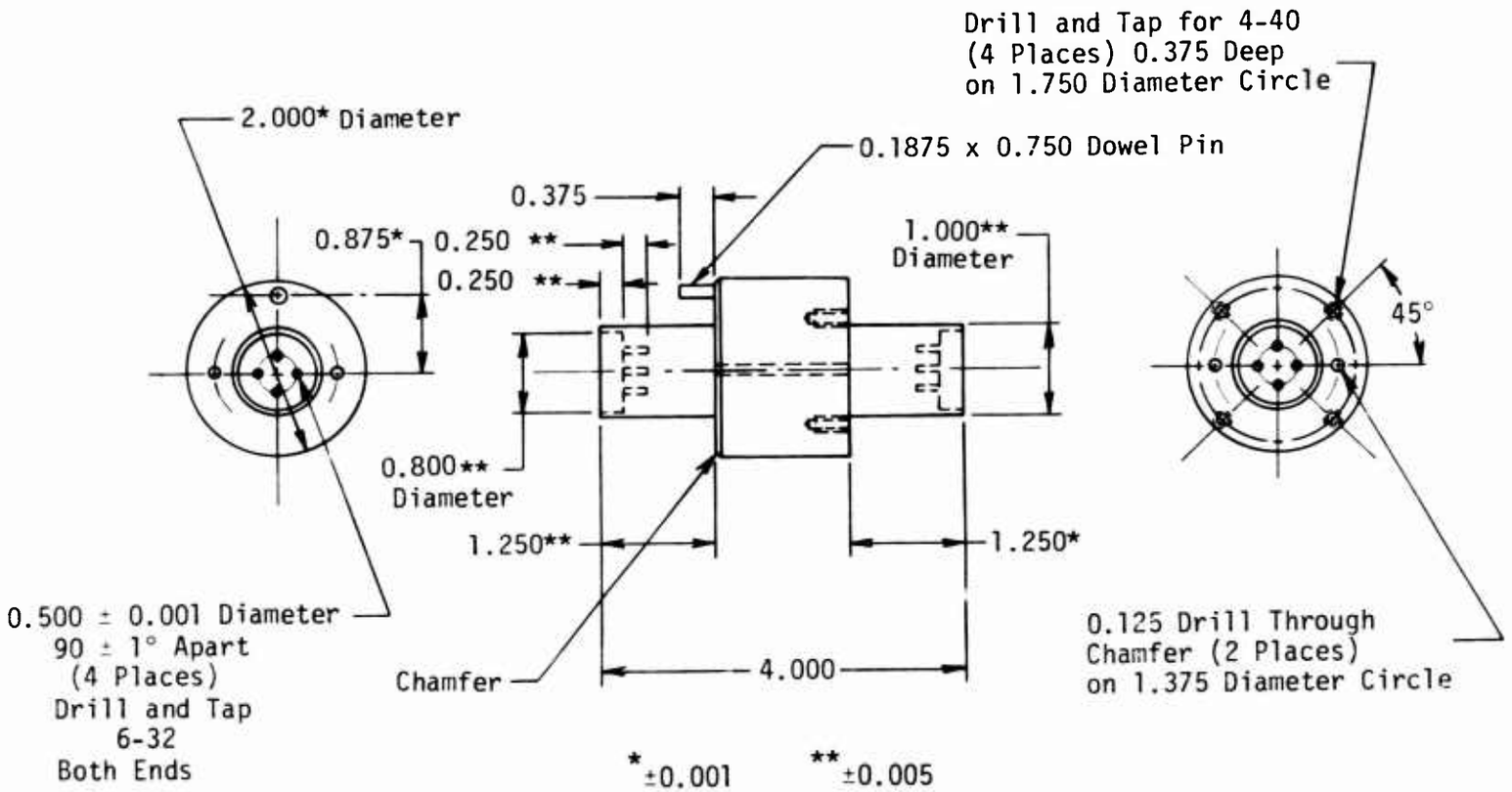

Note: All dimensions are in inches.

PRIMARY ELEMENT

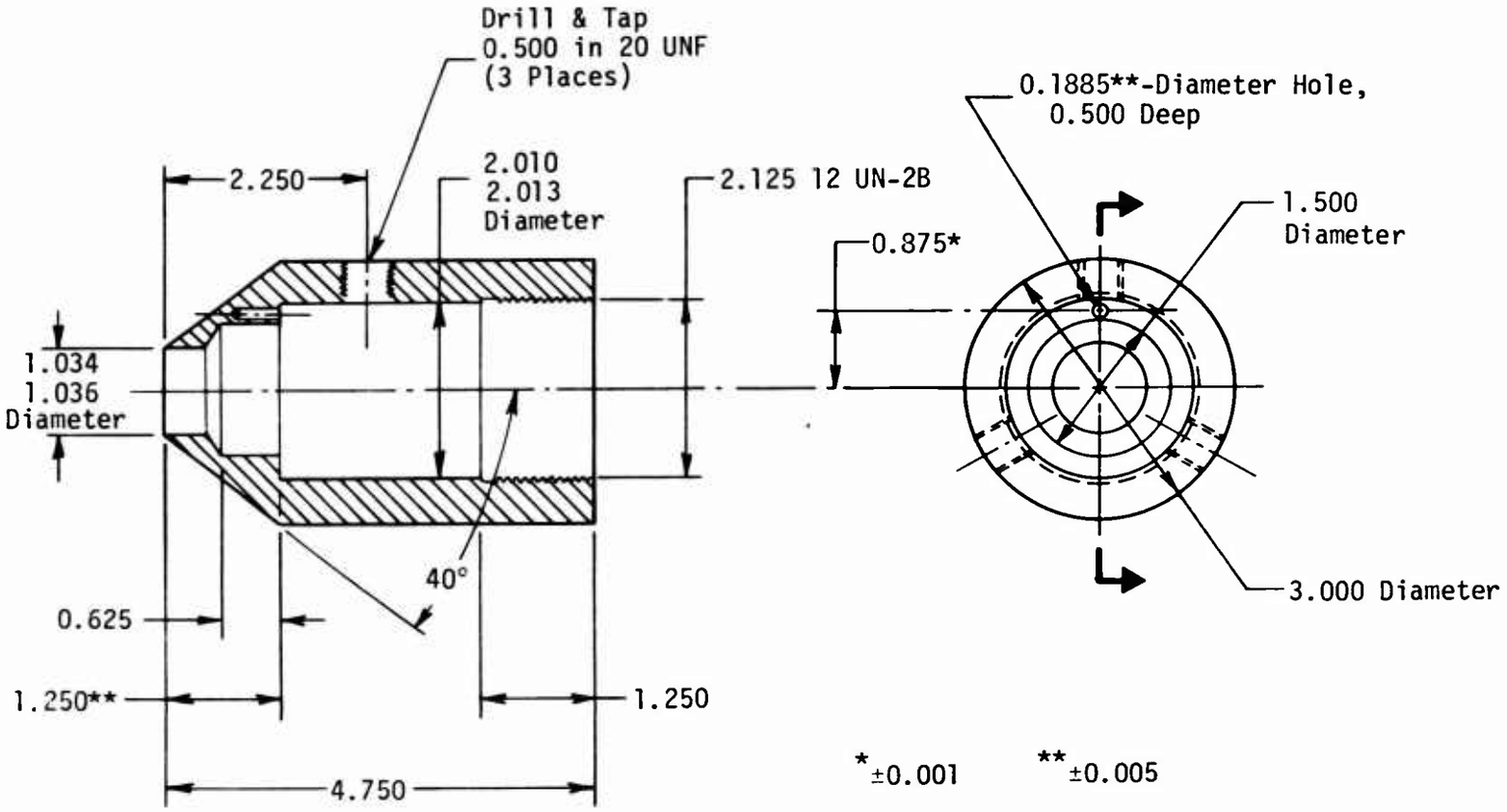

Note: All dimensions are in inches.

CASE

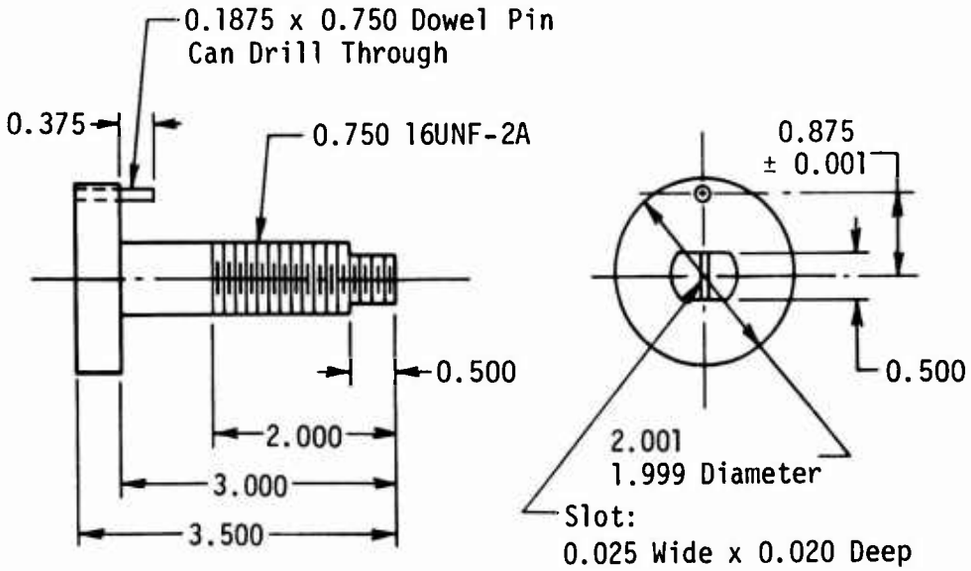

CASE INSTALLATION BOLT

Note: All dimensions are in inches.

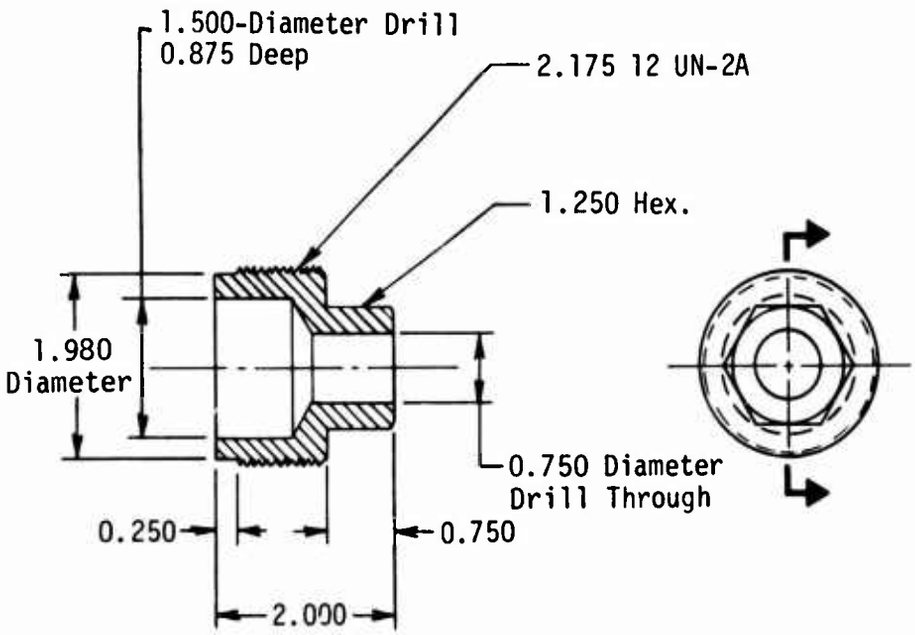

LOCK

APPENDIX B
TRANSDUCER PARTS AND ASSEMBLY PROCEDURE

REQUIRED PARTS

(1) Primary Element and Sleeve
(2) Strain Gage Locating Fixtures
(3) One M9 E-GP350-500 Strain-Gage Package (Kulite)
(4) Two PEP 350-090 Strain-Gage Package (Kulite)
(5) Glass Backing Paper
(6) No. 36 Enamel-Insulated Wire (Belden SGL)
(7) Ten No. 2 Terminal Tabs
(8) Epoxy: M-Bond 610 (Micromeasurements)
(9) Cleaning Solvents (Toluene, MEK, Alcohol) Spectral Grade
(10) Epoxy: Epocast 530 with 9816 Hardener (Furane Plastics)
(11) Embeco 630 Nonshrink Grout (Master Builders)
(12) Alpha No. 1122 Cable (24 ft)
(13) Barrier Water-Proofing GageKote No. 1: MCoatD (Micromeasurements)
(14) Four 4-40 x 1 in Flathead Screws; Eight 6-32 x 3/8 in Screws

MISCELLANEOUS MATERIALS

(1) Cotton Swabs
(2) Flux
(3) Solder: Alloy SN63 Erin Multicore
(4) Masking Tape
(5) Cellophane Tape (1/2-in. Diameter)
(6) Spotter Brushes (No. 00)
(7) Teflon Pads
(8) Soft Rubber Pads
(9) C-95 Blasting Sand
(10) Hose Clamps (1-in. Diameter)

ASSEMBLY PROCEDURE

(1) Insert eight 6-32 x 3/8 in screws into the cups on the two beams such that clearance between the top of each screw and the outer beam surface is 0.030 in.

(2) To 100 parts by weight of Epocast 530 add 15 parts by weight of 9816 hardener and mix thoroughly; to 1 part of this mix by weight add 4 parts by weight of Embeco 630 Grout and mix thoroughly. (Pot life is about 1 hr.)

(3) Carefully place the above mix in the cup on one side of the primary element and allow 4 hr to set.

(4) Repeat step 2.

(5) Repeat step 3 for the other side of the primary element and cure for 24 hr at room temperature.

(6) Thoroughly degrease all parts with solvent (MEK, Toluene, or freon TF).

(7) Apply masking tape around center of primary element (reference mass) and sand blast both element beams only, using C-95 sand.

(8) Using the locating fixture (fig. B1), accurately mark one normal-stress strain-gage pair location on the active beam radially 45° between the two shear axes and 0.650 in. from the free end of the beam. Locate the second mark 180° radially from the first and also 0.650 in. from the free end of the beam.

(9) Locate the shear-stress strain-gage locations accurately as follows: The center of the locating pin is to be considered zero degrees radially from the center of both beam surfaces. The shear-stress strain-gage locations are located exactly 1 in. from the free end of the beams and radially at exactly 0°, 90°, 180°, and 270°. Use both locating fixtures (fig. B1 and B2).

(10) Clean the 10 specimen areas thoroughly with toluene and then with alcohol and cotton swabs.

(11) Place the normal-axis gages (M9 E-GP350-500) as follows:
Using clear cellophane tape, place tape over one gage pair and center gage at one normal-stress specimen point. Secure tape; release one end and remove gage pair from

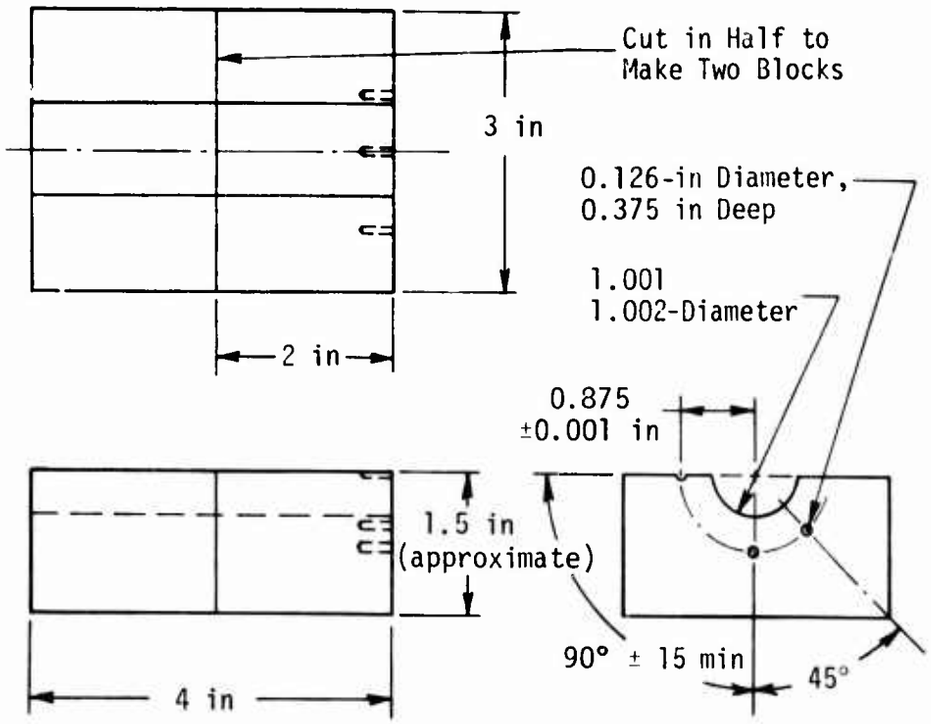

Figure B1. Locating Fixture for Normal-Strain Gage

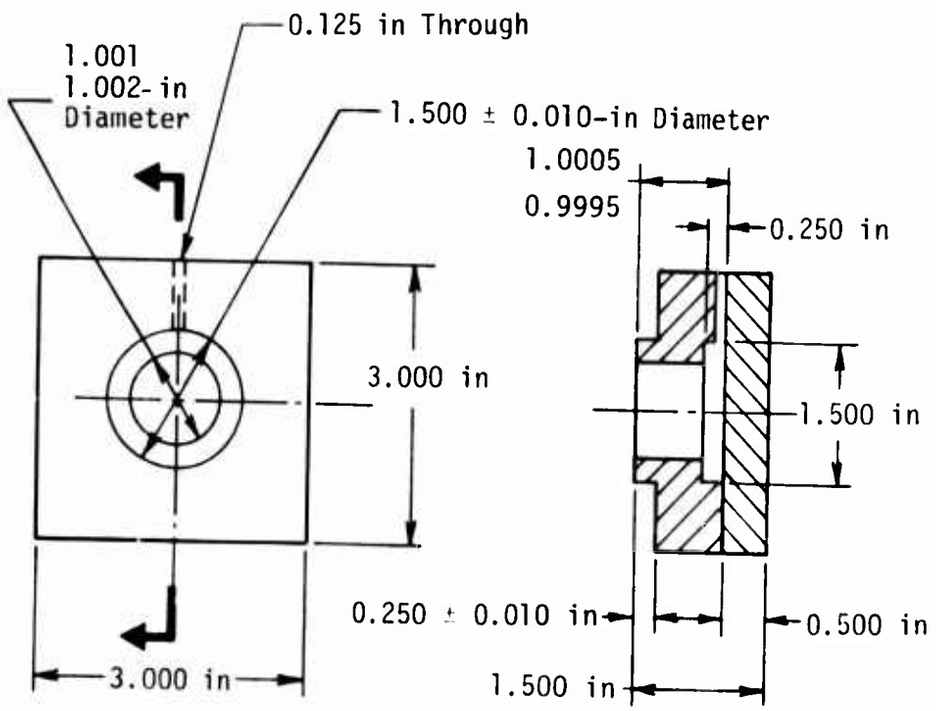

Figure B2. Locating Fixture for Shear-Strain Gage

primary element. Repeat for the second normal-stress specimen point.

(12) Place M-Bond 610 Epoxy on primary element at specimen points and air dry for 20 min.

(13) Using a hose clamp with Teflon and soft rubber pads, clamp gages firmly in place.

(14) Oven cure at 250°F for 4 hr.

(15) Remove pads, clamp, and tape.

(16) Place the shear-stress gages in each of the eight locations as follows: Cut glass paper into three 0.125- by 0.075-in. rectangles. Bend leads up on each strain gage with tweezers. Individually place glass paper segments over specimen areas and apply M-Bond 610 Epoxy to glass papers on two gage locations on the upper working surface. Place gages individually over each paper centering the gages exactly on the specimen points and carefully aligning gage axis with beam axis. Hold leads up until cement dries (10 to 15 min).

(17) After all gages are placed, oven cure at 250°F for 4 hr.

(18) Install 10 gage tabs on the exterior extension of the sleeve using the same epoxy and curing procedure as above.

(19) Examine all strain-gage installations for proper location and bonding.

(20) Wire vertical shear axis (fig. B3). Use No. 36 SGL Belden wire on all wiring in the main body of elements; tape the wire down to the body; then use Gagekote No. 1 over wire and gages; use routing holes in the primary element for interconnections between active beam elements and dummy beam elements.

(21) Wire horizontal shear axis (same as vertical axis wiring).

(22) Wire normal axis (fig. B4). Use No. 36 SGL Belden wire on all wiring in the main body of elements. Tape the wire down to the body; then use Gagekote No. 1 over wire and gages; use routing holes in the primary element for routing leads to the dummy side of the transducer.

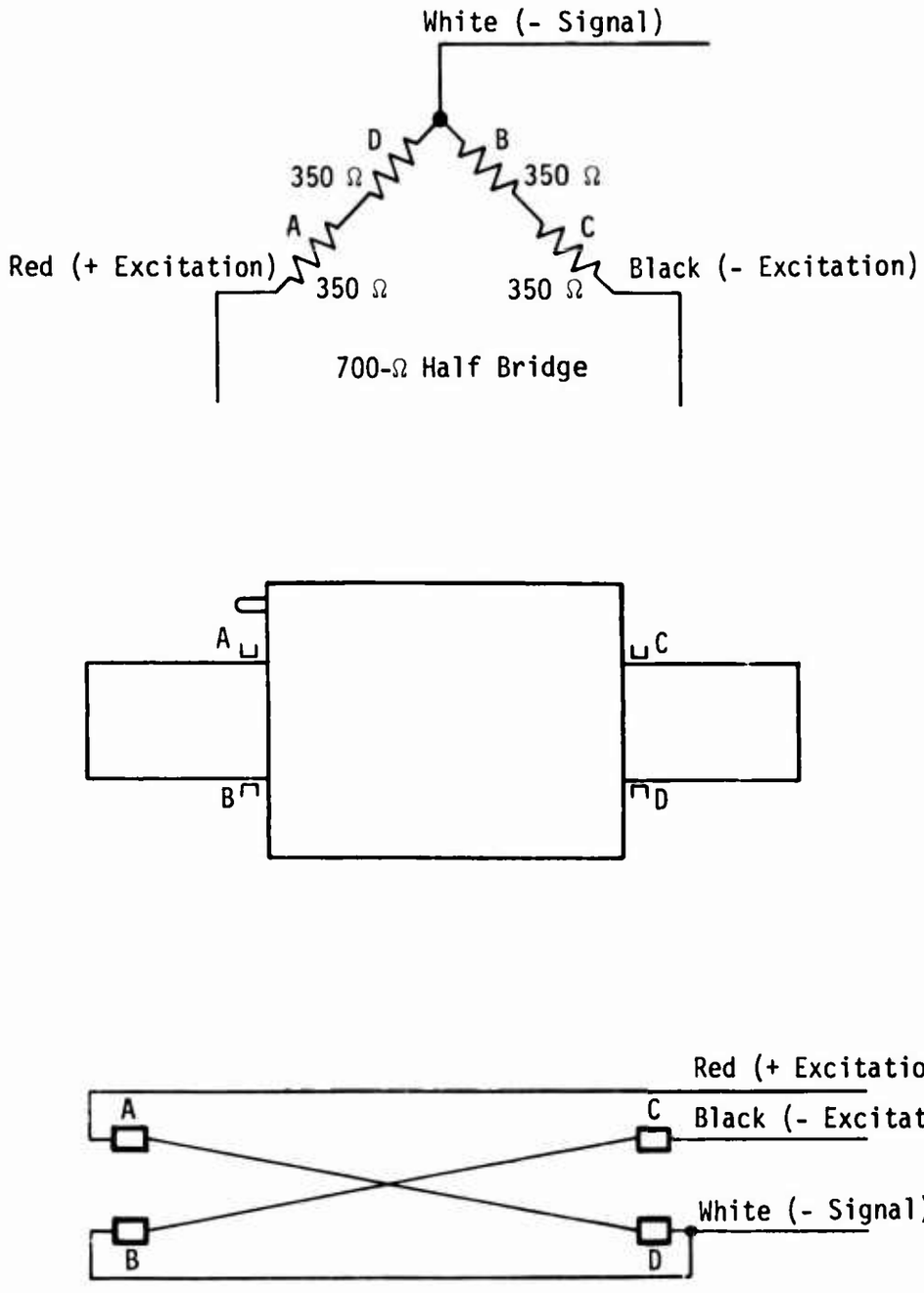

Figure B3. Wiring Diagram for Vertical and Horizontal Shear Axes

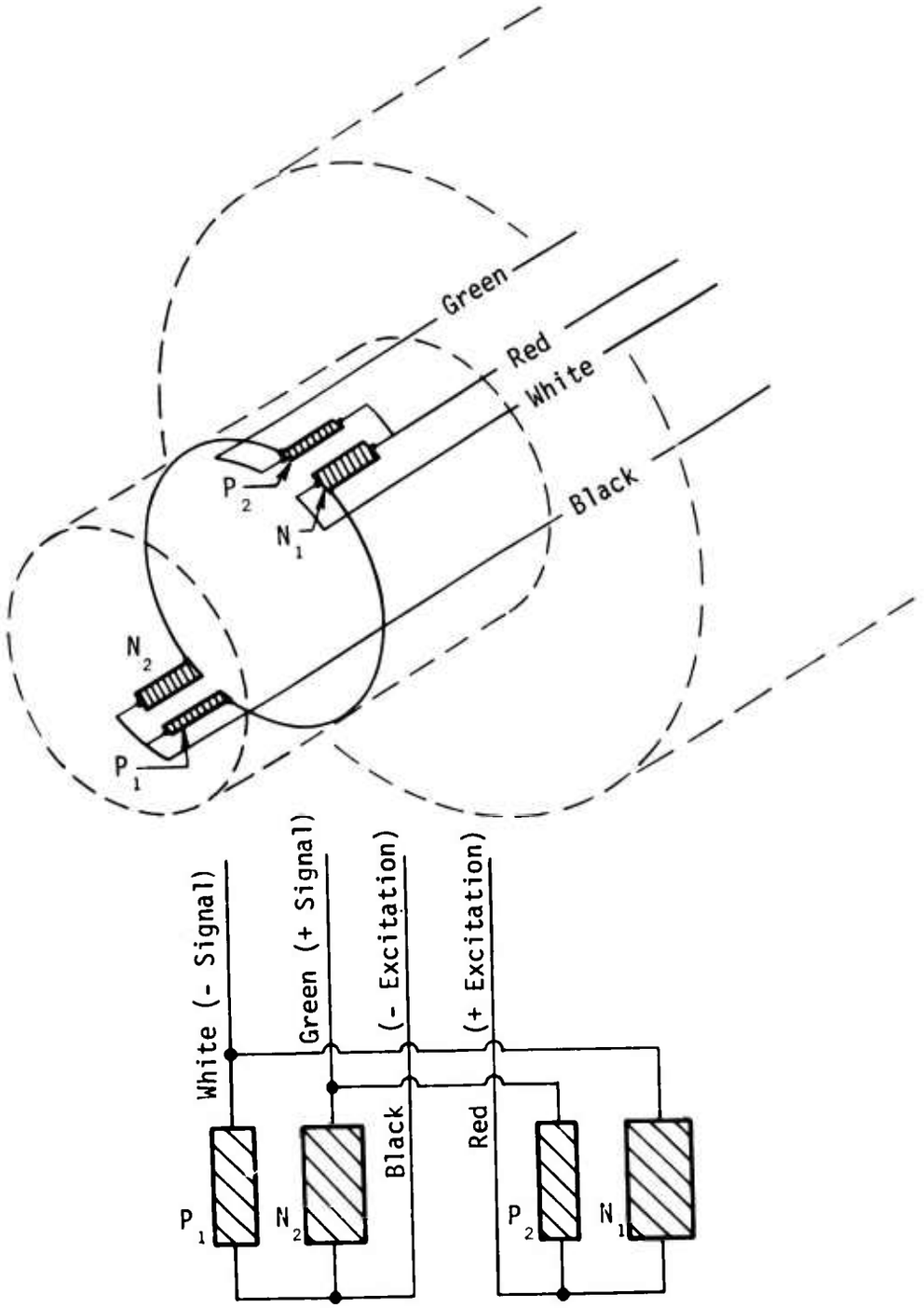

Note: The narrow gage elements are P-type gages; the wide gage elements are N-type gages.

Figure B4. Wiring Diagram for Normal Axis

(23) Route and tape all lead wires between gages on the dummy beam to the end of the dummy beam; apply Gagekote No. 1 over wire leaving about 4 in. of wire extending past the end of the dummy beam.

(24) Pass wires through the wire exit holes in the sleeve and attach sleeve with 4-40 x 1 in flathead screws.

(25) Trim wires and solder to the 10 terminal tabs.

(26) Using three 8-ft lengths of Alpha No. 1122 cable, prepare leads and trim shields, stretching insulation well over shield to prevent shield contact with any part of the transducer.

(27) Insert cables through rear cable exit hole in shield and bring leads through the two side holes near the tabs.

(28) Solder cable leads to the appropriate tabs (figs. B3 and B4); apply RTV to solder tabs and fill cable exit holes and allow adequate time for curing.

(29) Check all circuits on external cable leads for ohmic leakage (readings should be greater than $10^{10}\Omega$). Transducer is now ready for calibration.

APPENDIX C
TRANSDUCER CASE INSTALLATION PROCEDURE

(1) On the outside surface of the form, mark the direction of the sensitive shear axis with a line; also mark the location of the hole for the transducer.

(2) Drill a 13/16-in. diameter hole in the form at the location marked.

(3) Remove the nut, washer, and rubber shipping block from the case assembly; discard the rubber shipping block and retain the nut and washer for installing the case to the form.

CAUTION

Be careful in handling the case so that lip is not dented.

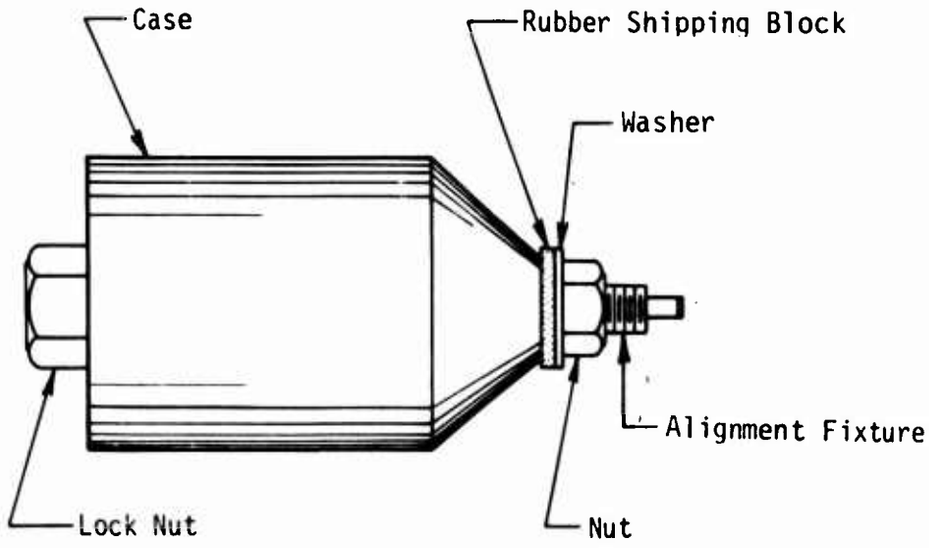

(4) Insert the bolt through the hole in the form so that the case will be cast into the concrete with the tapered portion toward the outside of the form; attach the nut loosely to the bolt.

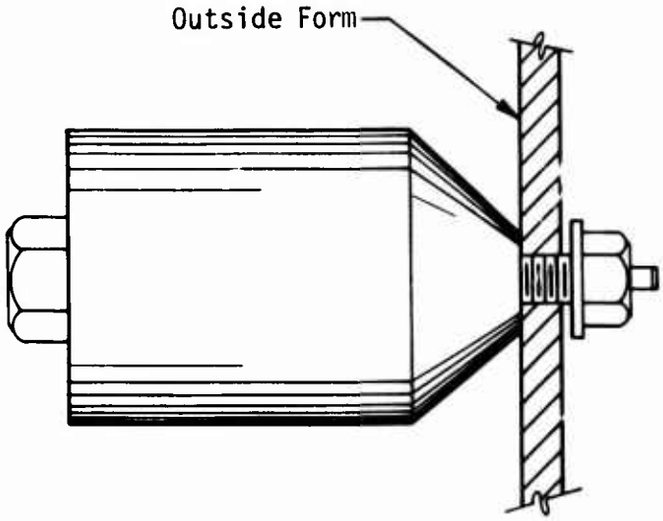

(5) Align the slot in the positioning fixture with the line drawn in step 1 to mark the sensitive shear axis; point the arrowhead on the positioning fixture in the direction chosen for positive shear.

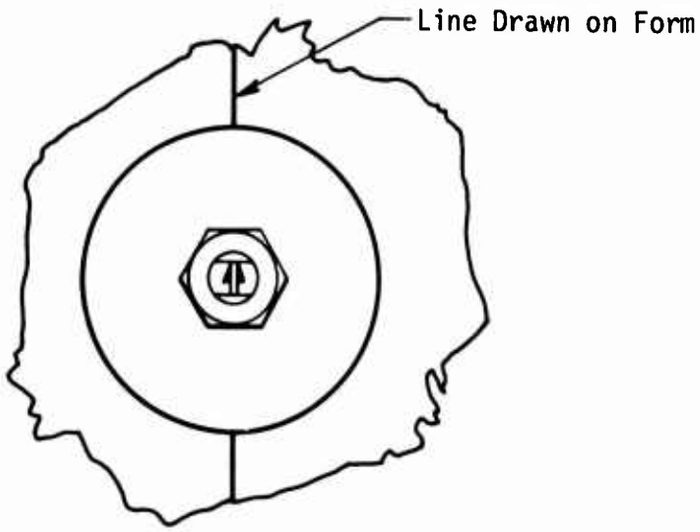

(6) Hold the positioning fixture in place with a 1/2-in. open-end wrench and tighten the nut until the case is held snuggly against the form.

CAUTION

Do not overtighten.

(7) Insert three 1/2-in. diameter 20 UNF bolts of a convenient length (6-in. long bolts are furnished) into the three tapped holes in the case and hand tighten.

CAUTION

Be careful not to disturb the alignment of the case.

(8) Tie or weld the three bolts installed in step 7 to reinforcing steel.

CAUTION

Do not weld on the case and do not attempt to bend the bolts once they have been installed in the case. Even slight deformation of the case will make it unfit for its intended use.

(9) Cut a 3-in. diameter cardboard tube long enough to extend from 1/2 in. behind the three bolts in the case to the inner form, and place the tube over the case; before pouring the concrete, be sure that the cardboard tube fits snuggly against the inner form; caulk between the tube and the inner form if needed to prevent concrete from entering the tube.

(10) Check to see that the slot and arrow on the positioning fixture are still in proper alignment.

(11) While pouring the concrete, be especially conscientious to insure that the concrete completely fills the region between the case and the outside form.

(12) Before removing the forms, remove the nut and positioning fixture from the case; replace the large lock nut in the case after the positioning fixture is removed.

APPENDIX D

STATIC-SHEAR TEST DATA

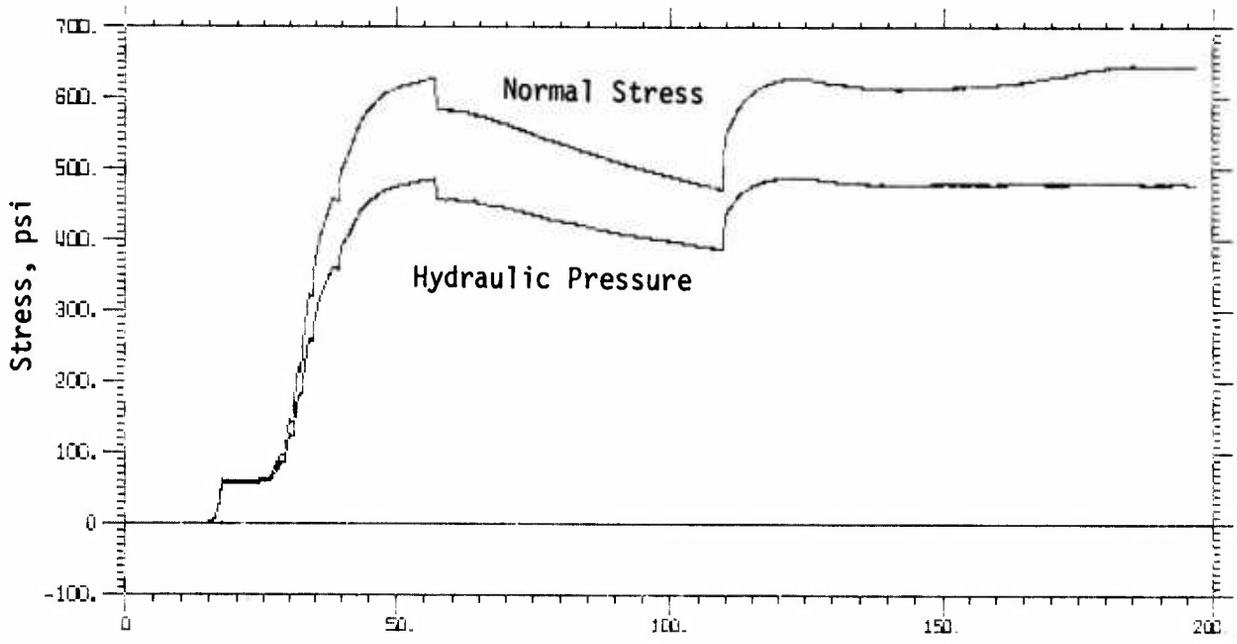

Hydraulic Pressure and Normal Stress

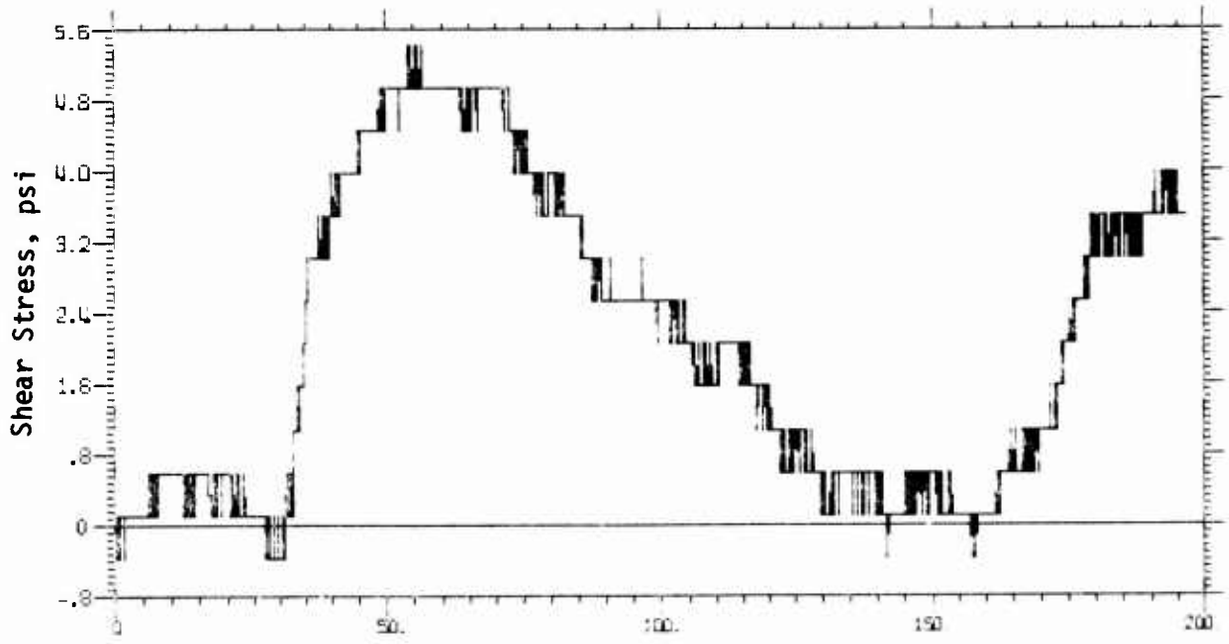

Horizontal Shear Stress

TEST 3 (1 of 2)

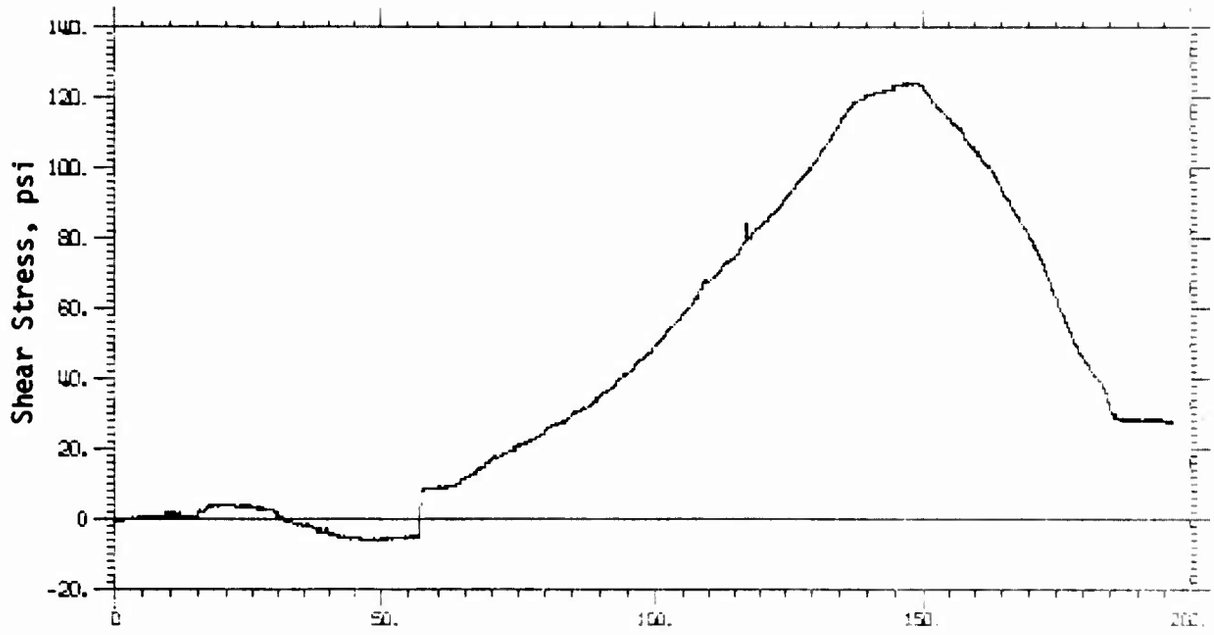

Time, sec

Vertical Shear Stress

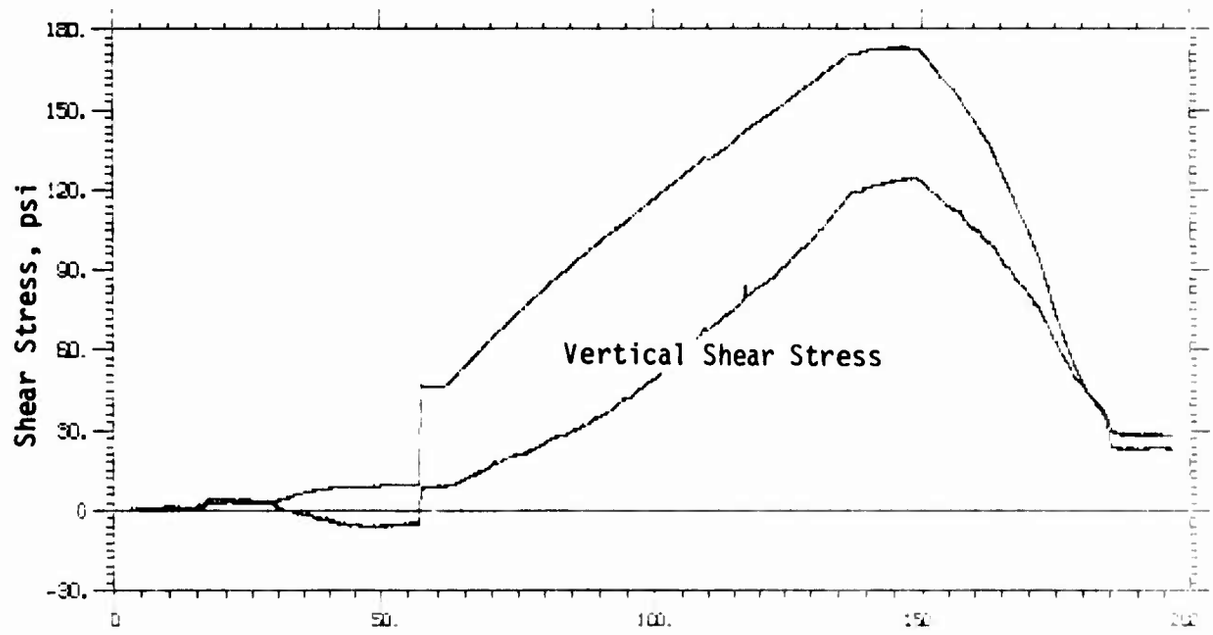

Time, sec

Inferred Vertical Shear Stress

TEST 3 (2 of 2)

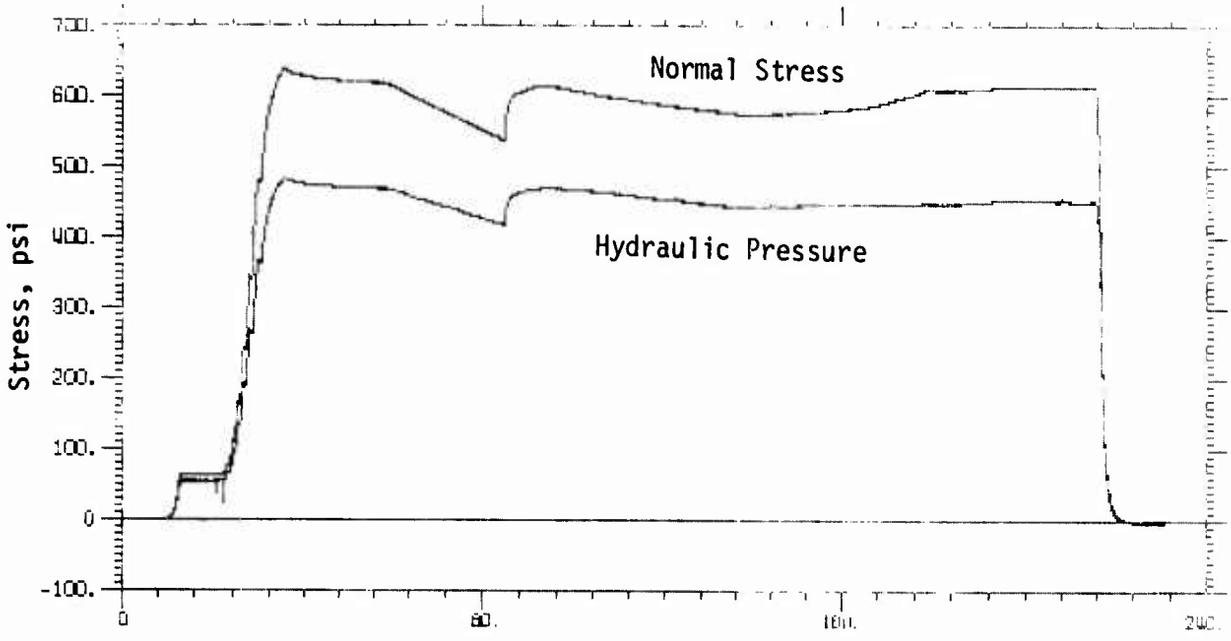

Time, sec

Hydraulic Pressure and Normal Stress

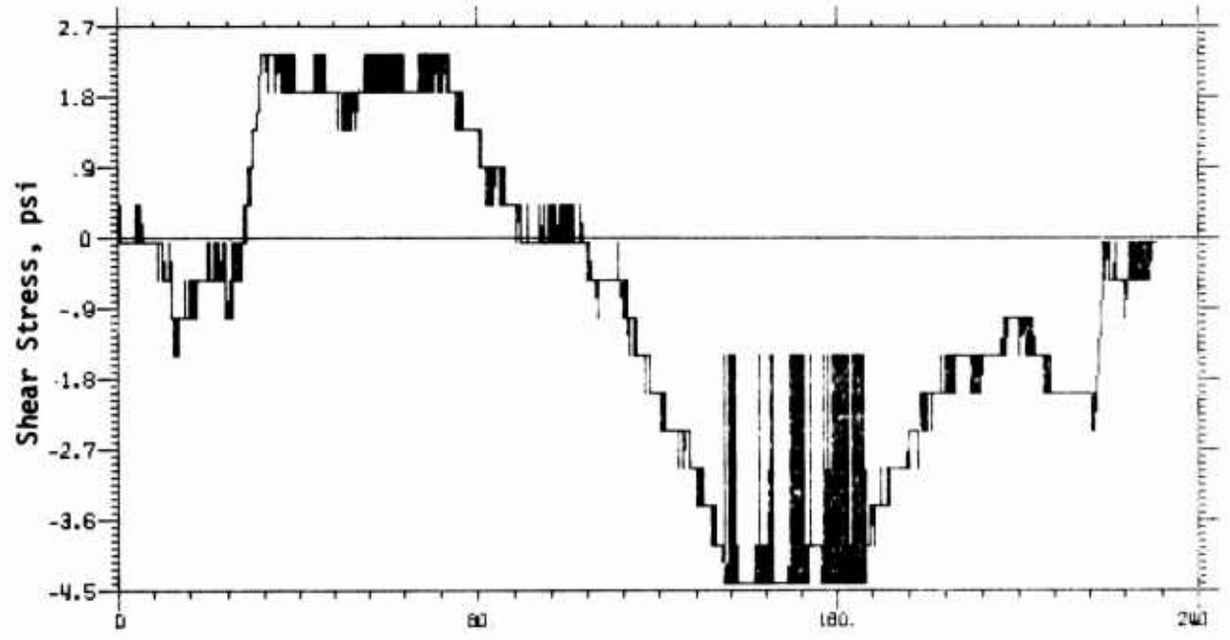

Time, sec

Horizontal Shear Stress

TEST 4 (1 of 2)

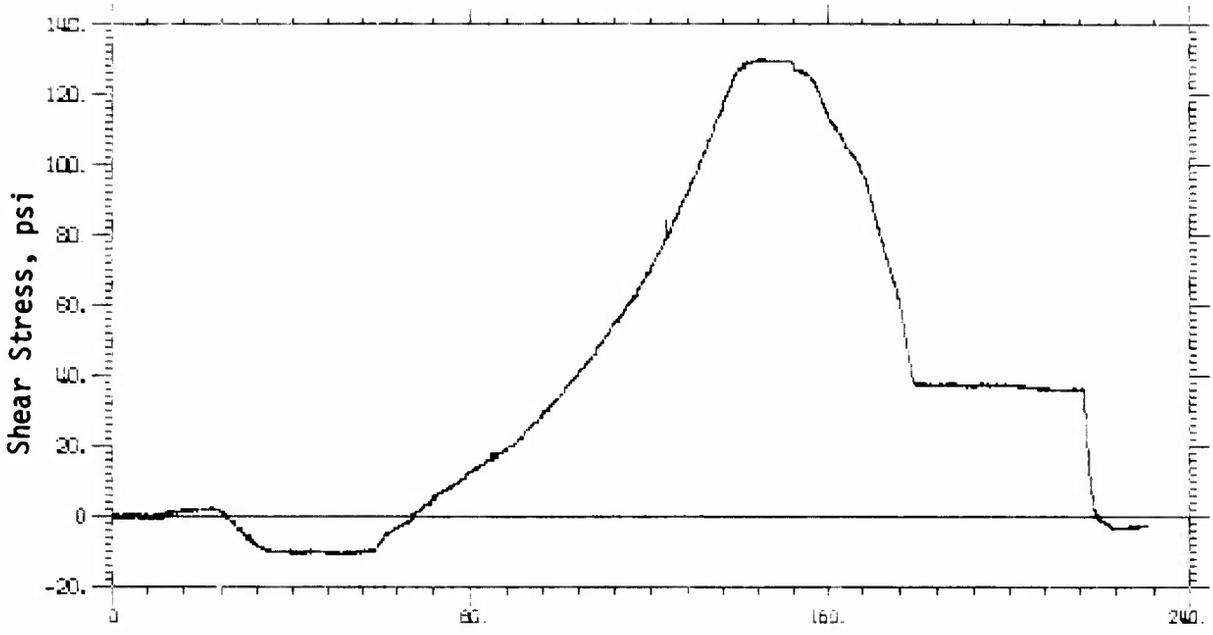

Time, sec

Vertical Shear Stress

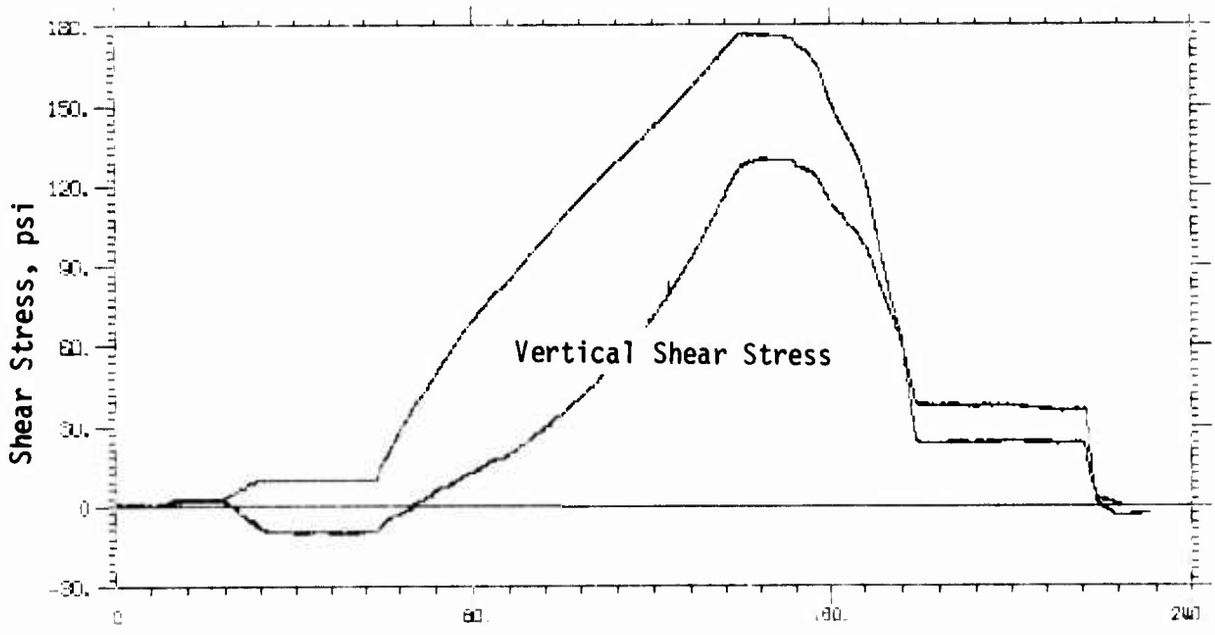

Time, sec

Inferred Vertical Shear Stress

TEST 4 (2 of 2)

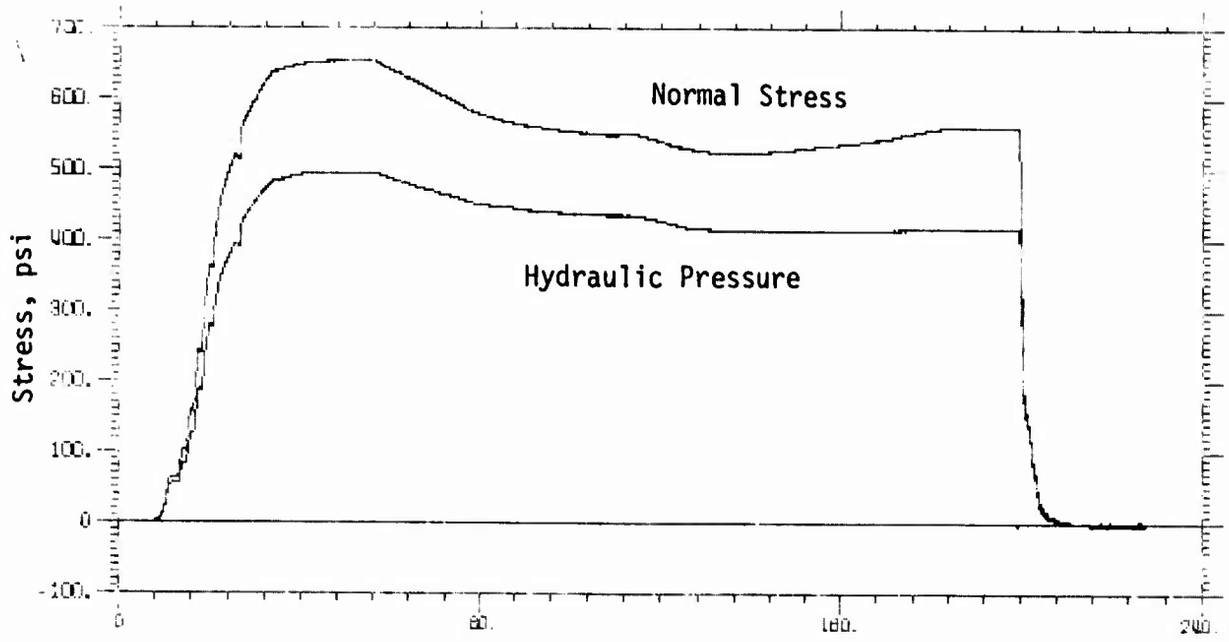

Time, sec

Hydraulic Pressure and Normal Stress

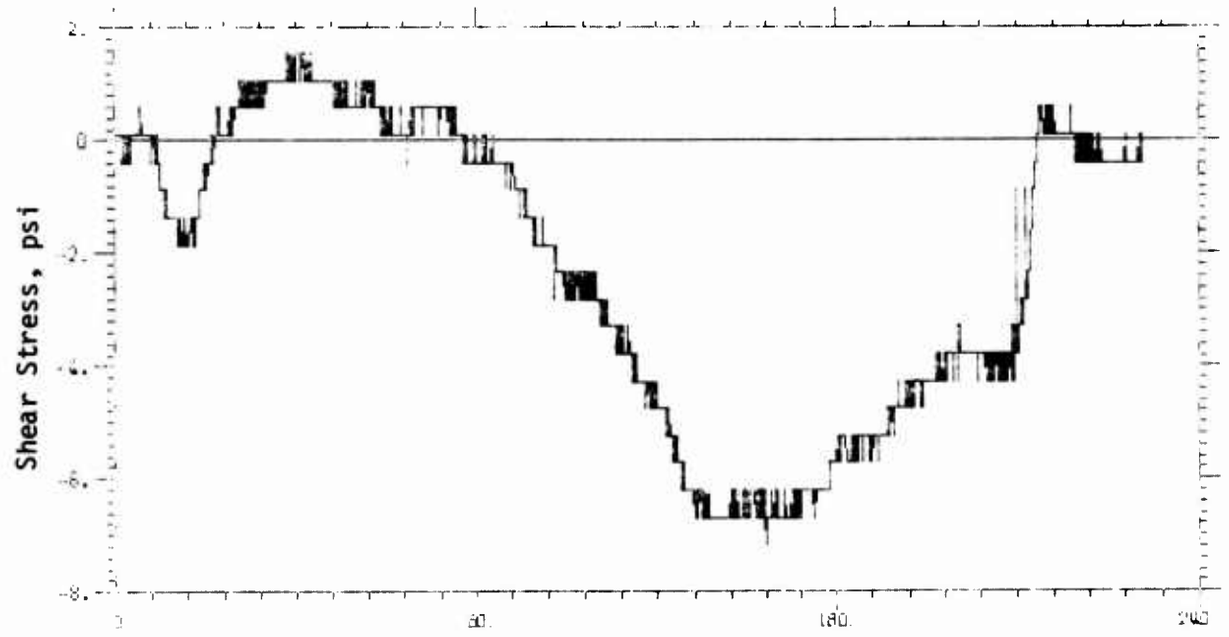

Time, sec

Horizontal Shear Stress

TEST 5 (1 of 2)

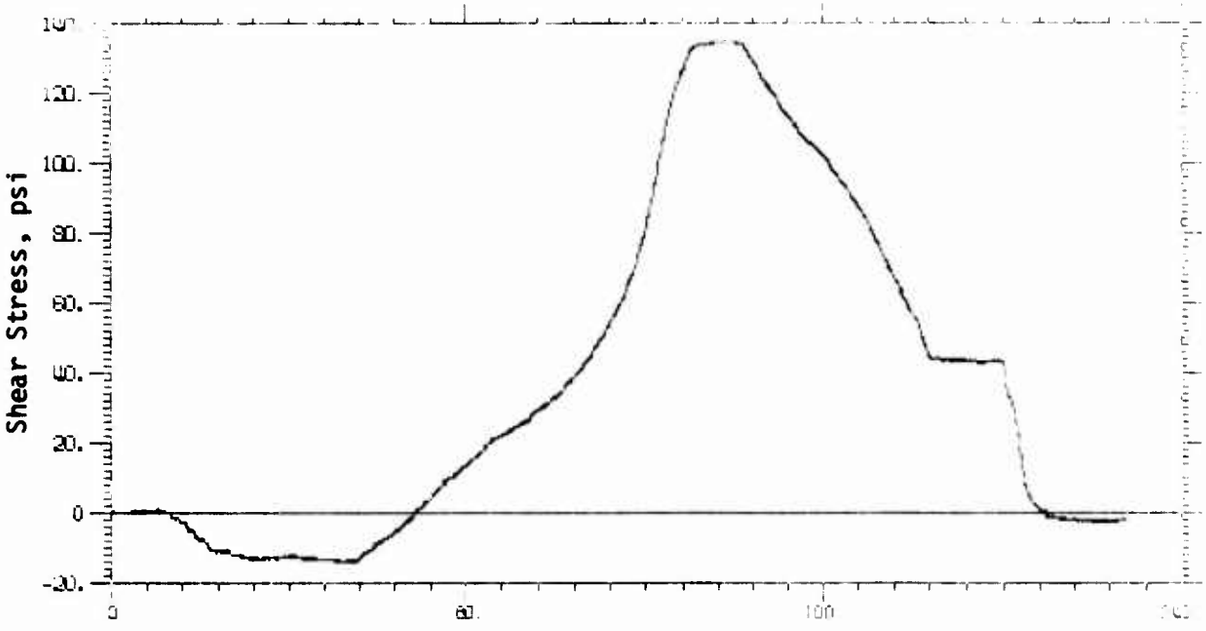

Time, sec

Vertical Shear Stress

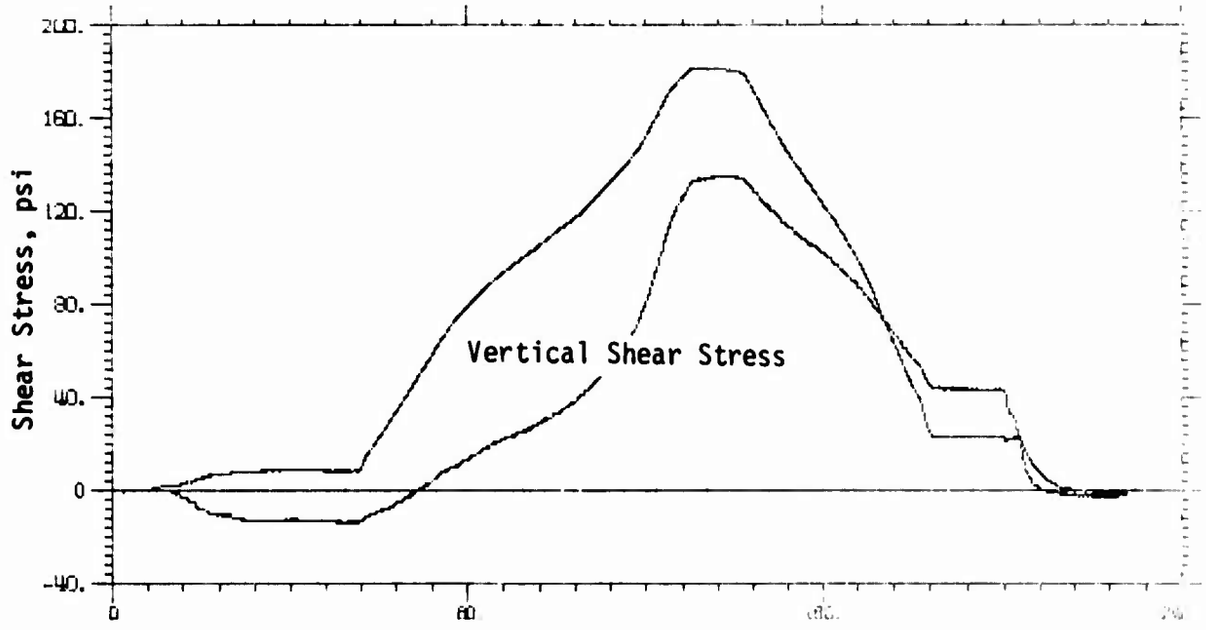

Time, sec

Inferred Vertical Shear Stress

TEST 5 (2 of 2)

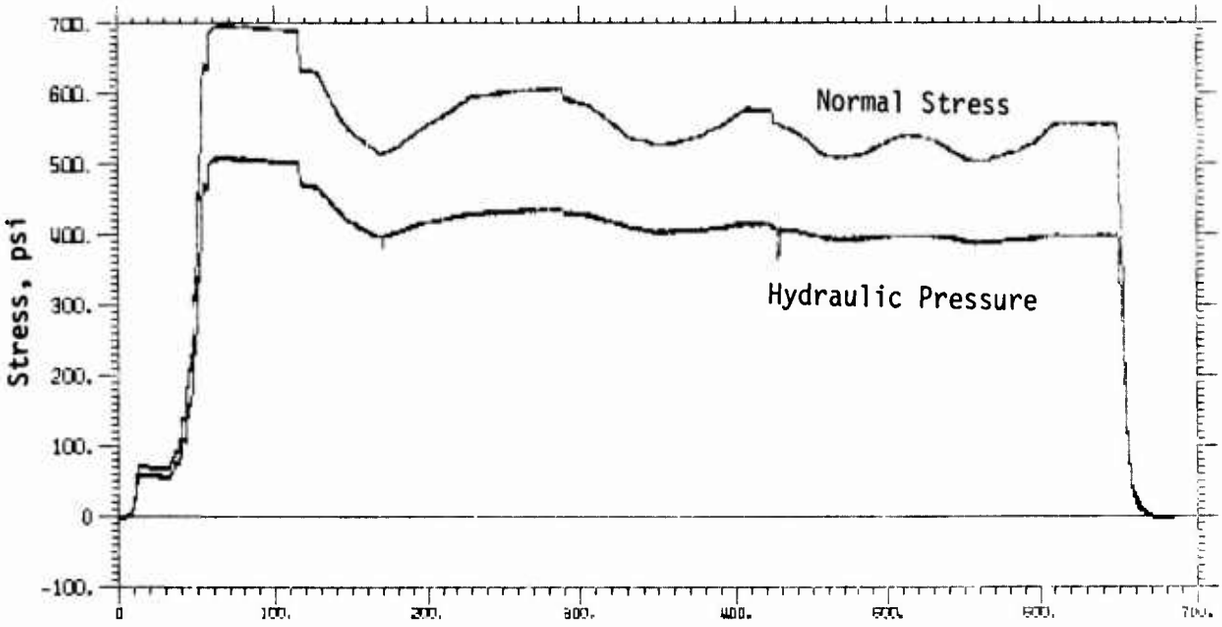

Time, sec

Hydraulic Pressure and Normal Stress

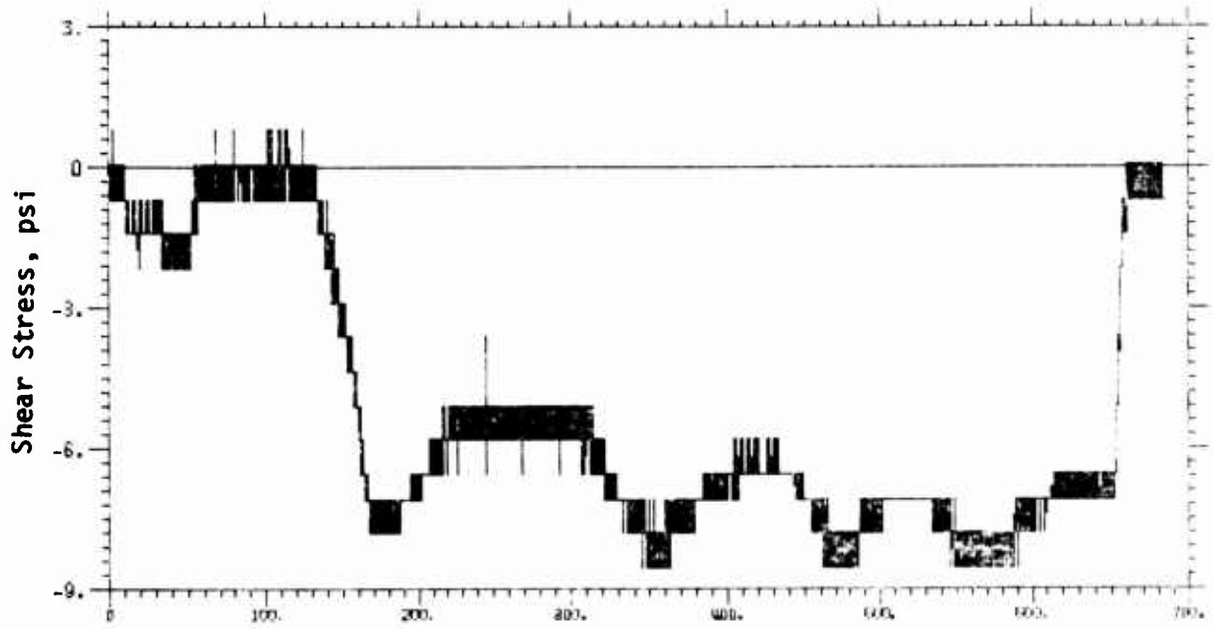

Time, sec

Horizontal Shear Stress

TEST 6 (1 of 2)

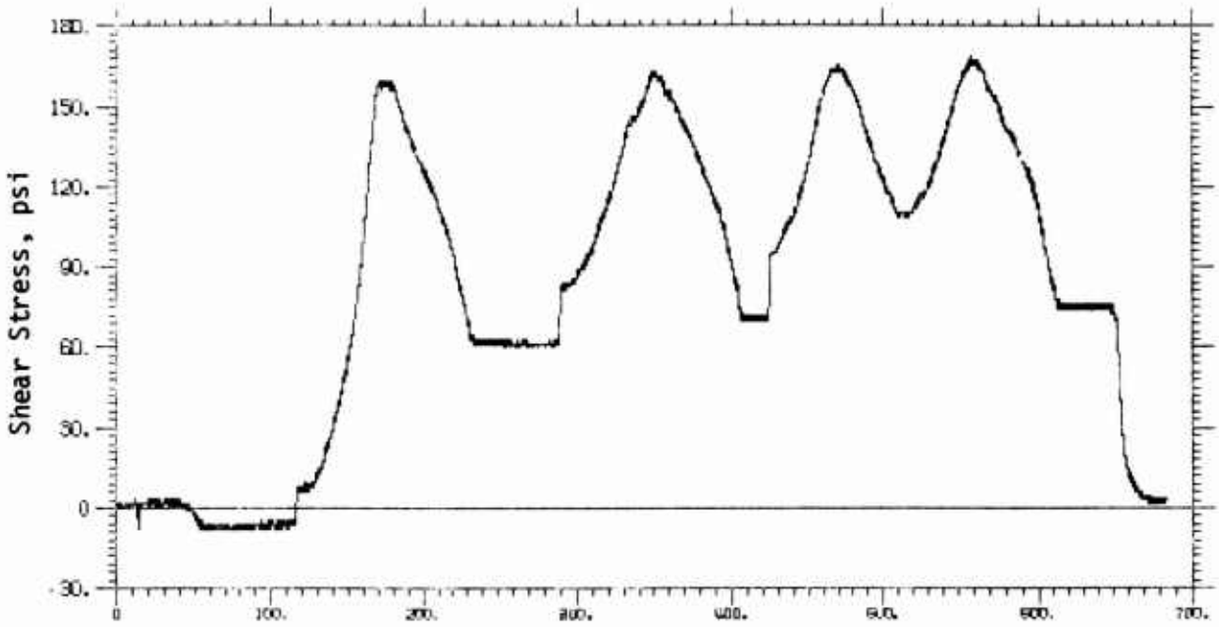

Time, sec

Vertical Shear Stress

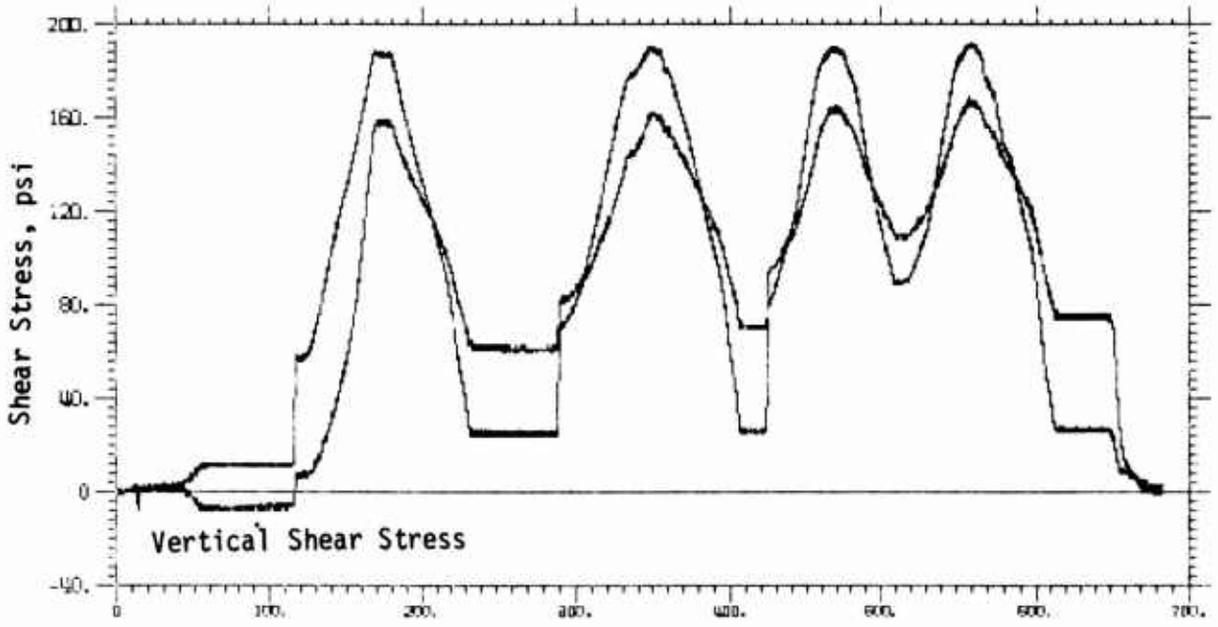

Time, sec

Inferred Vertical Shear Stress

TEST 6 (2 of 2)

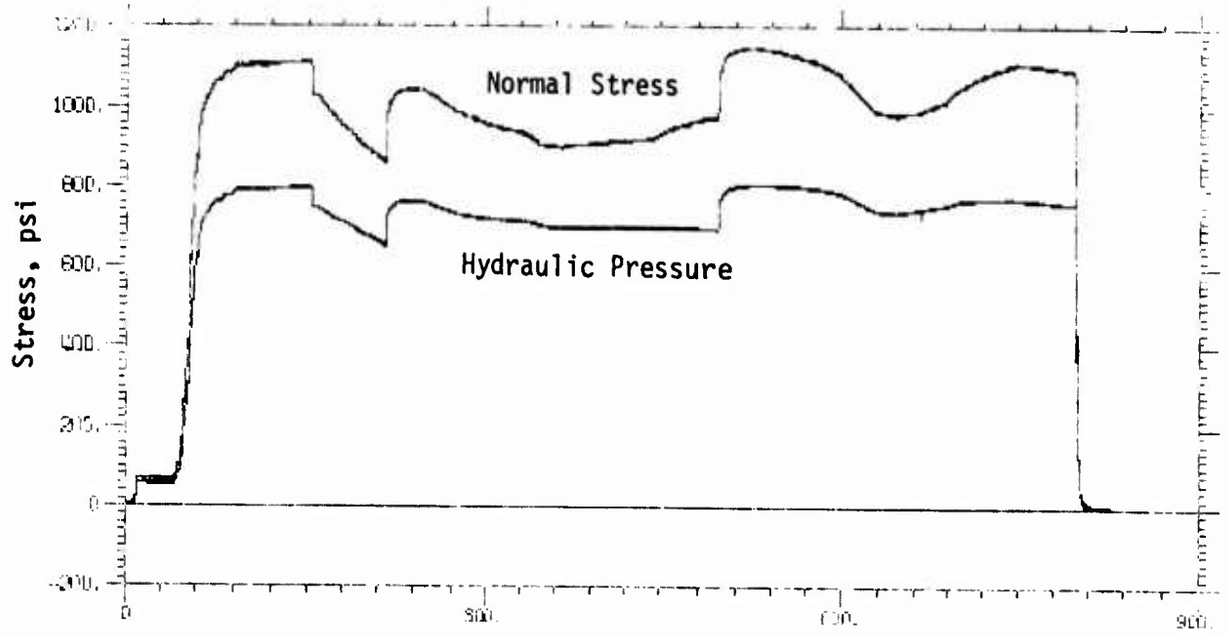

Time, sec

Hydraulic Pressure and Normal Stress

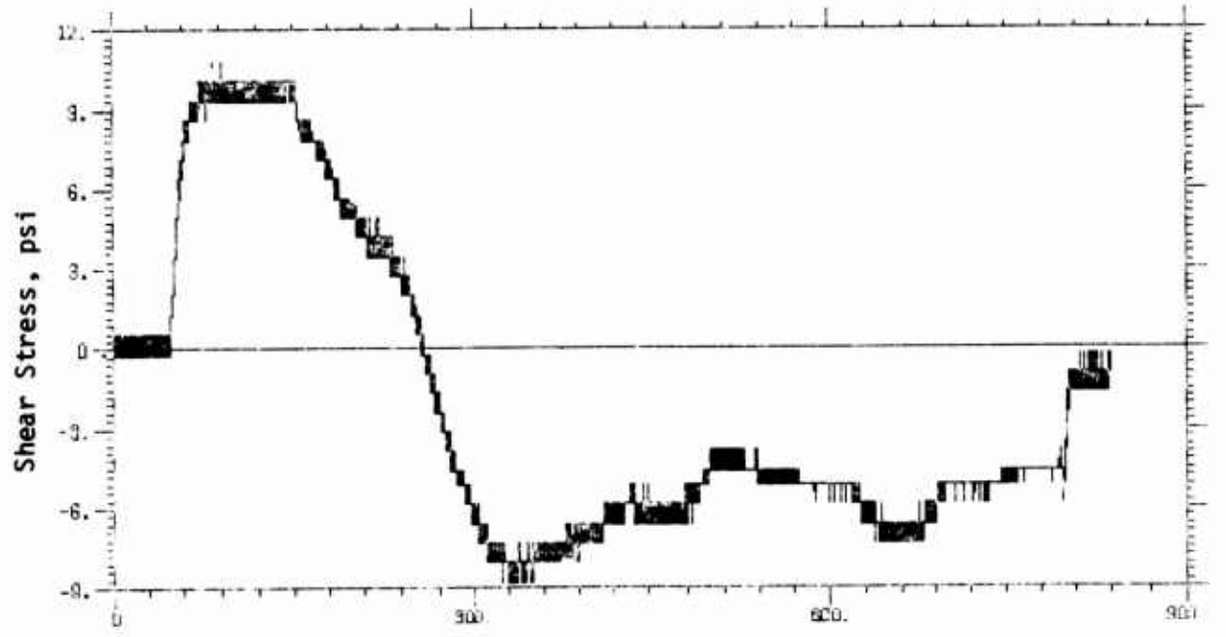

Time, sec

Horizontal Shear Stress

TEST 8 (1 of 2)

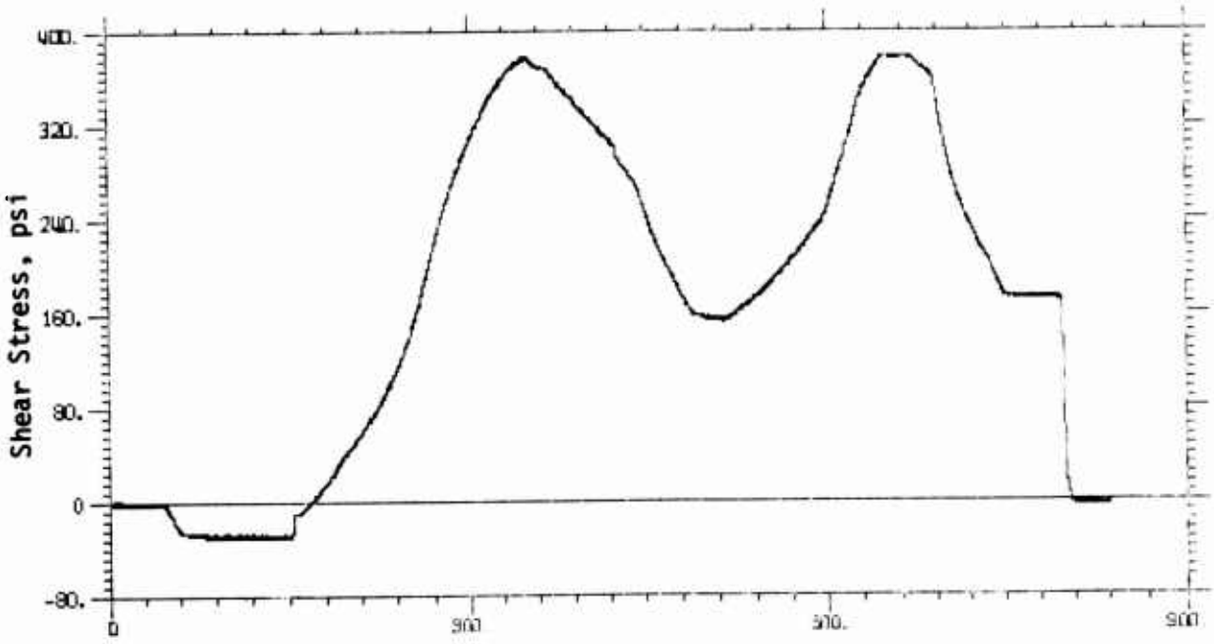

Time, sec

Vertical Shear Stress

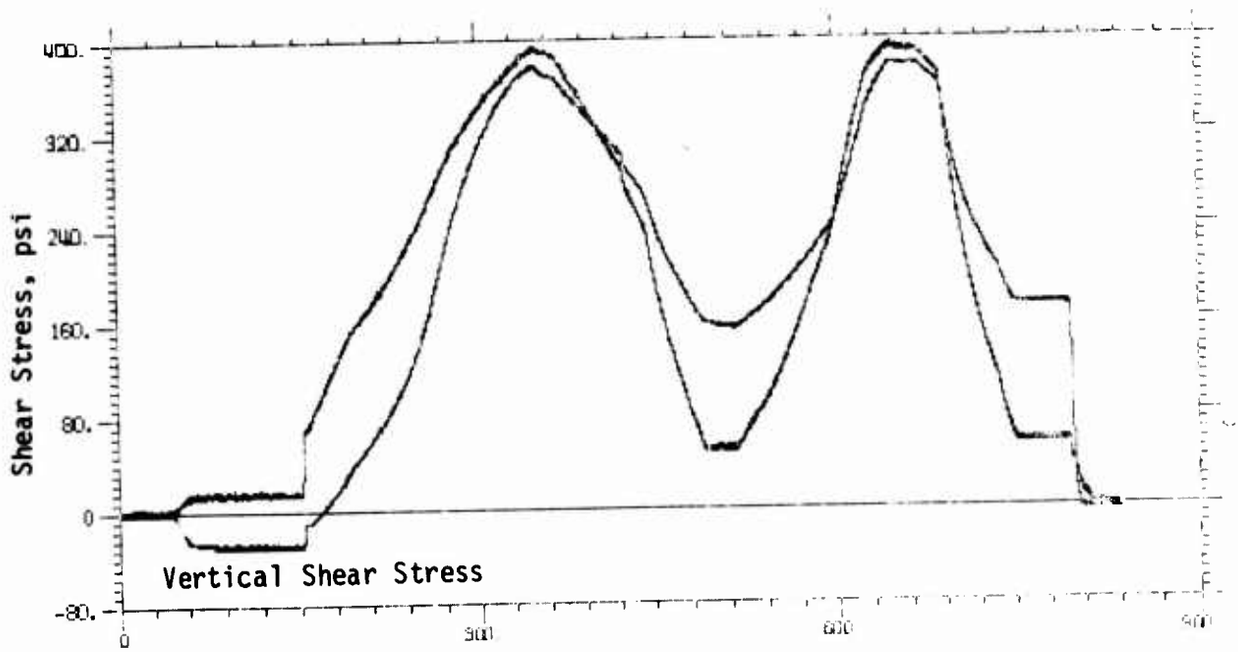

Time, sec

Inferred Vertical Shear Stress

TEST 8 (2 of 2)

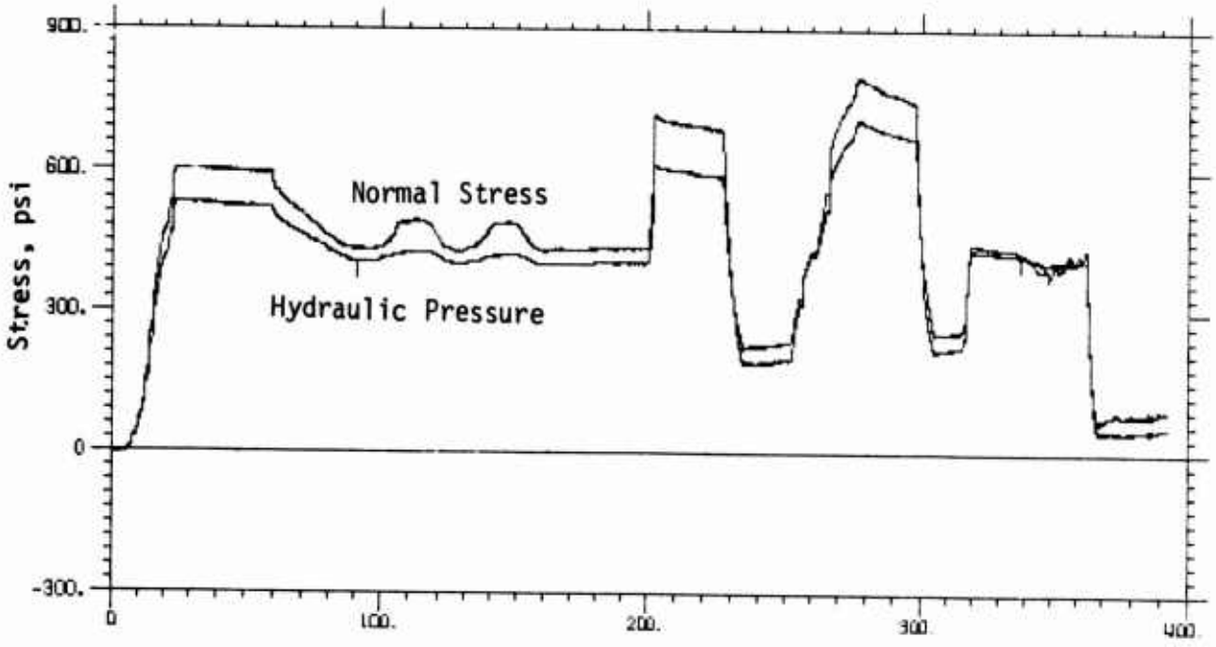

Hydraulic Pressure and Normal Stress

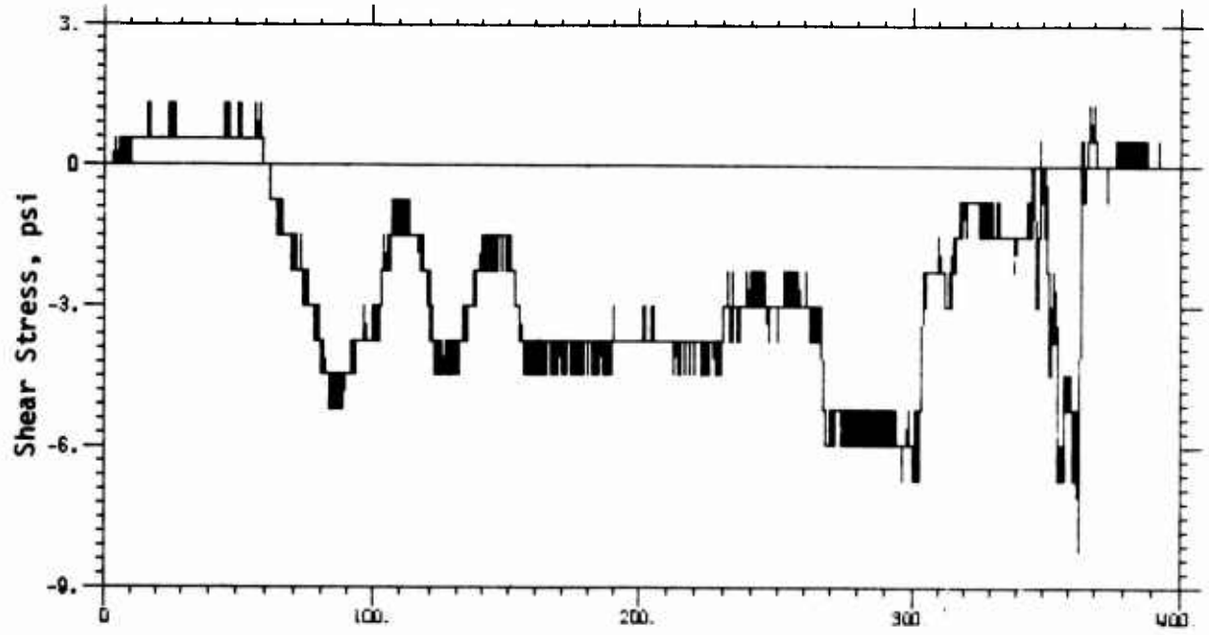

Horizontal Shear Stress

TEST 11 (1 of 2)

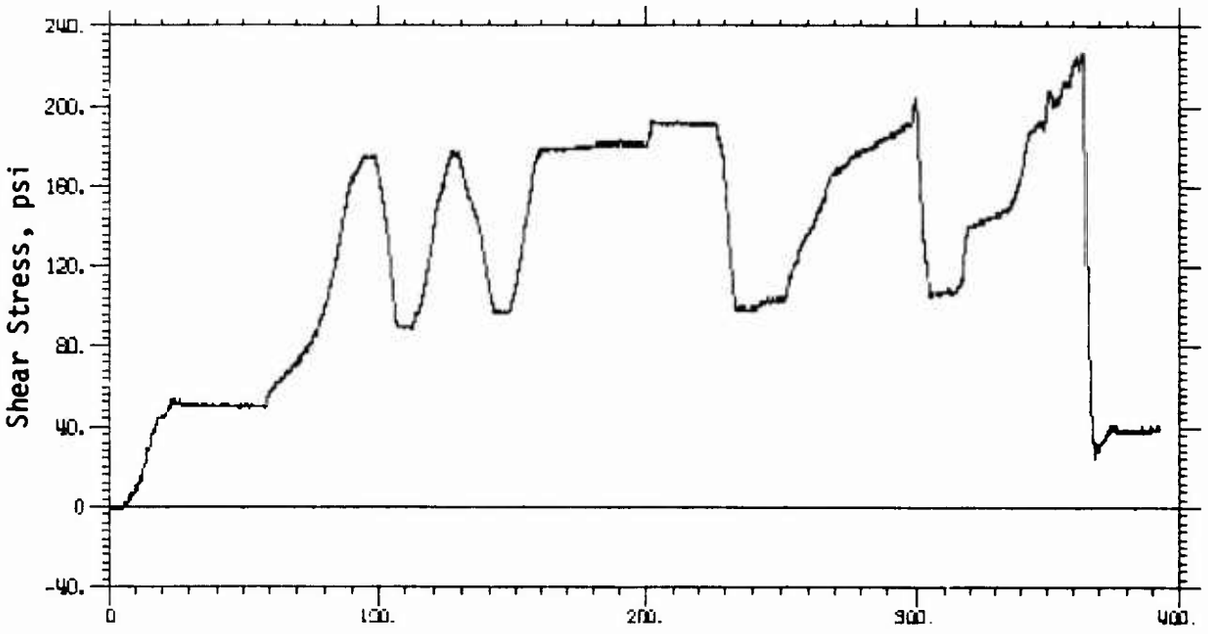

Time, sec

Vertical Shear Stress

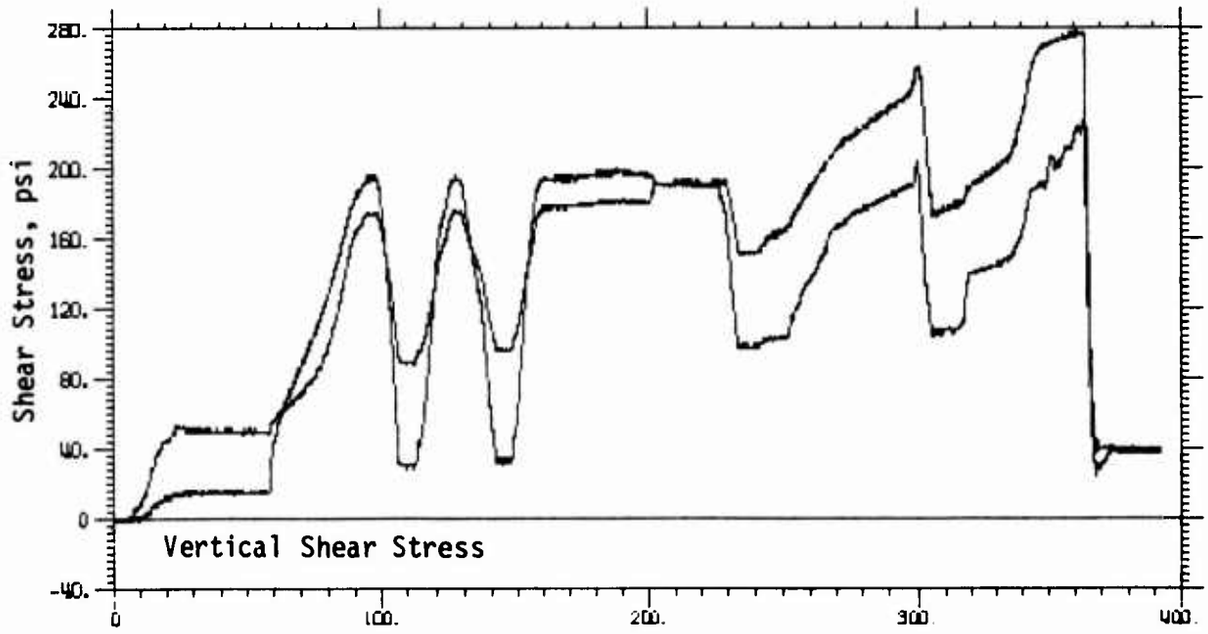

Time, sec

Inferred Vertical Shear Stress

TEST 11 (2 of 2)

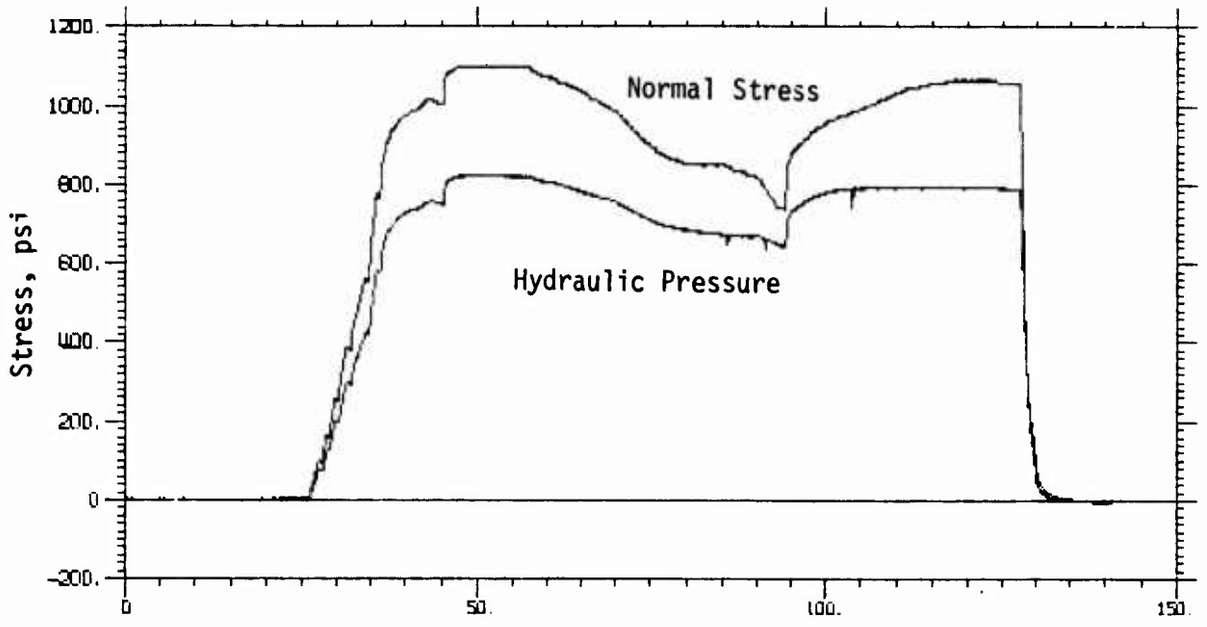

Time, sec

Hydraulic Pressure and Normal Stress

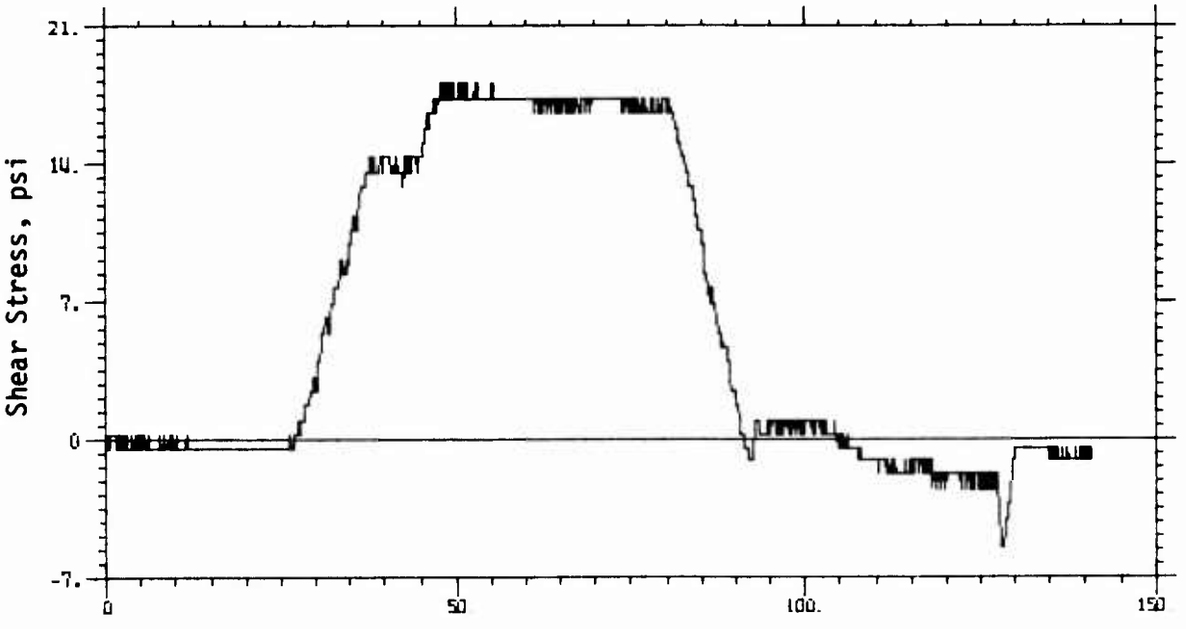

Time, sec

Horizontal Shear Stress

TEST 16 (1 of 2)

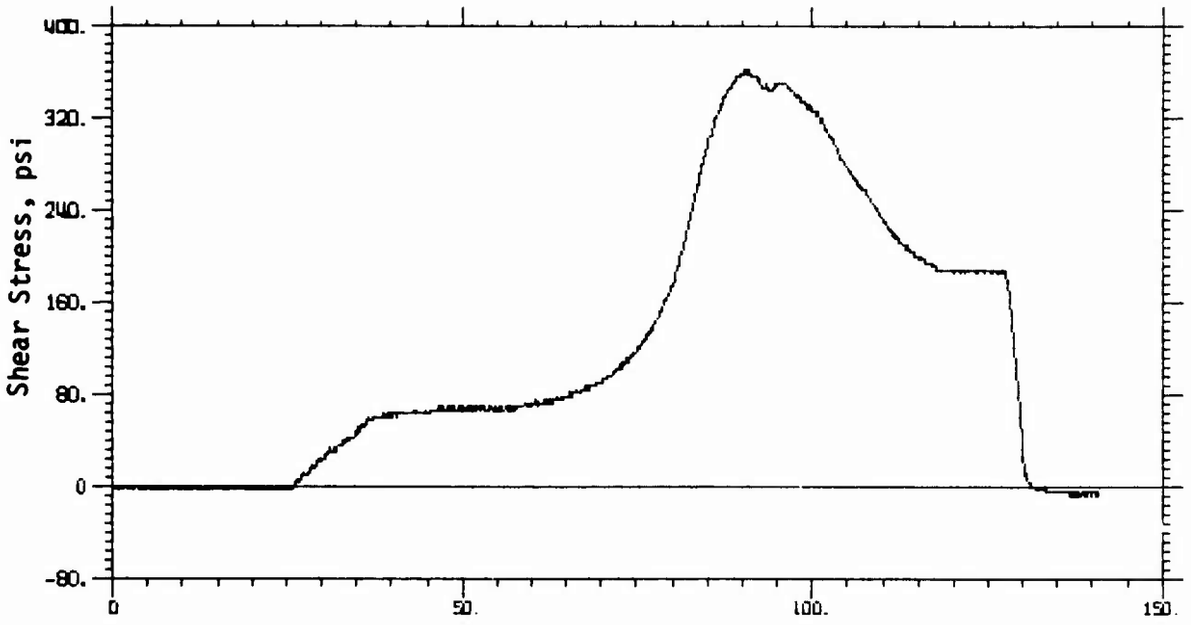

Vertical Shear Stress

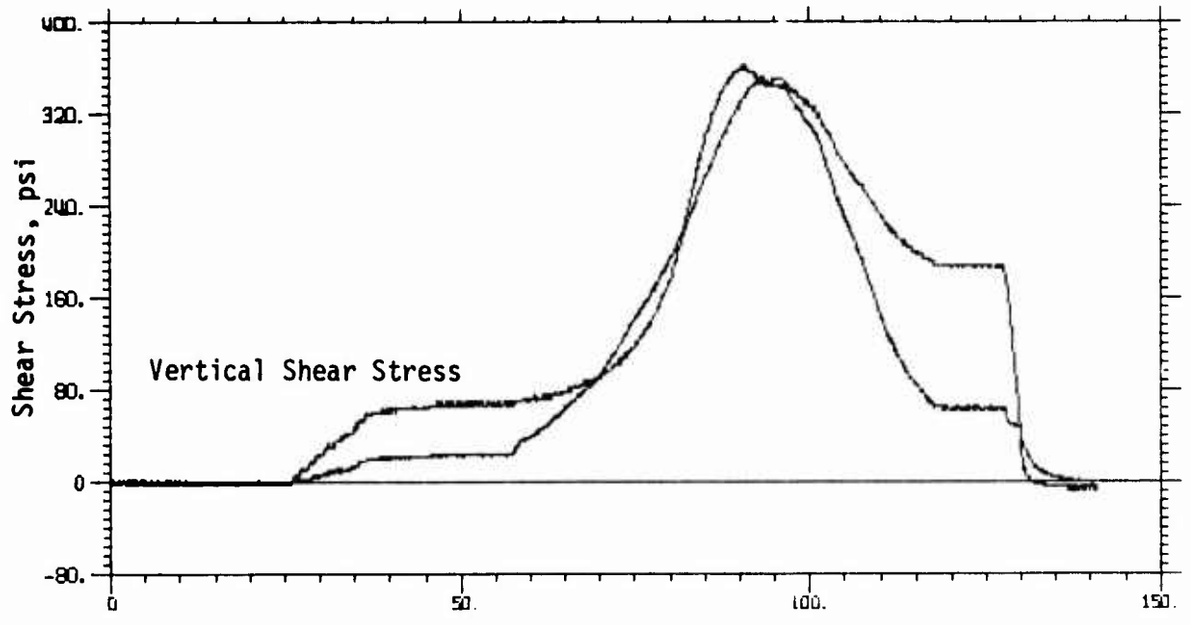

Inferred Vertical Shear Stress

TEST 16 (2 of 2)

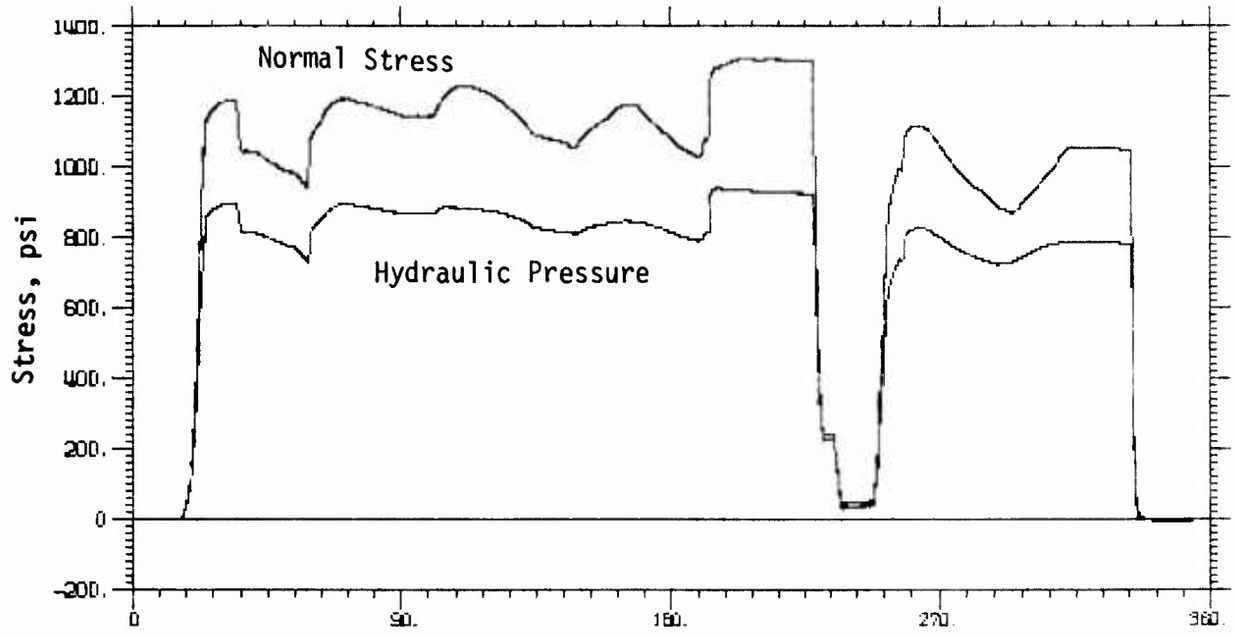

Hydraulic Pressure and Normal Stress

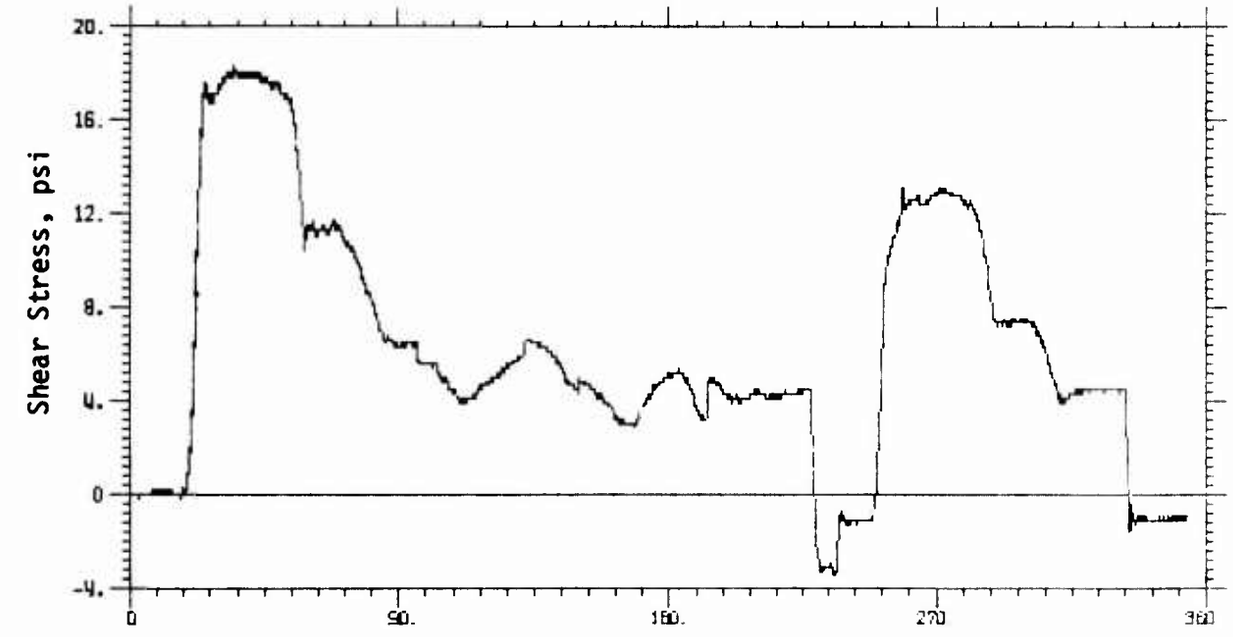

Horizontal Shear Stress

TEST 17 (1 of 2)

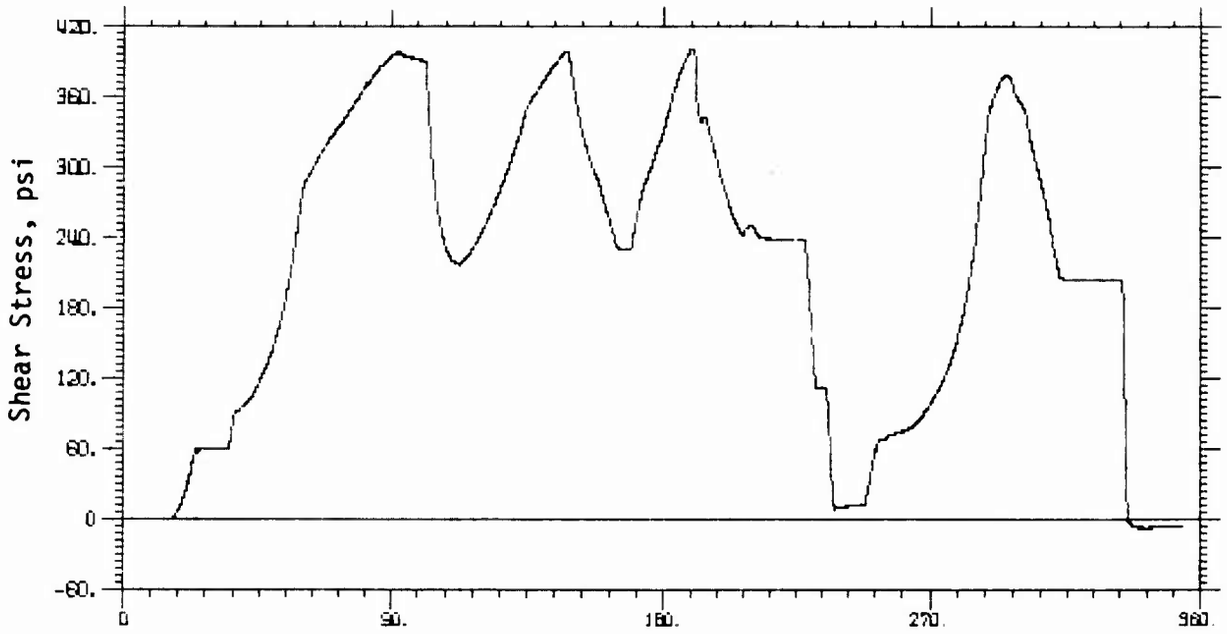

Time, sec

Vertical Shear Stress

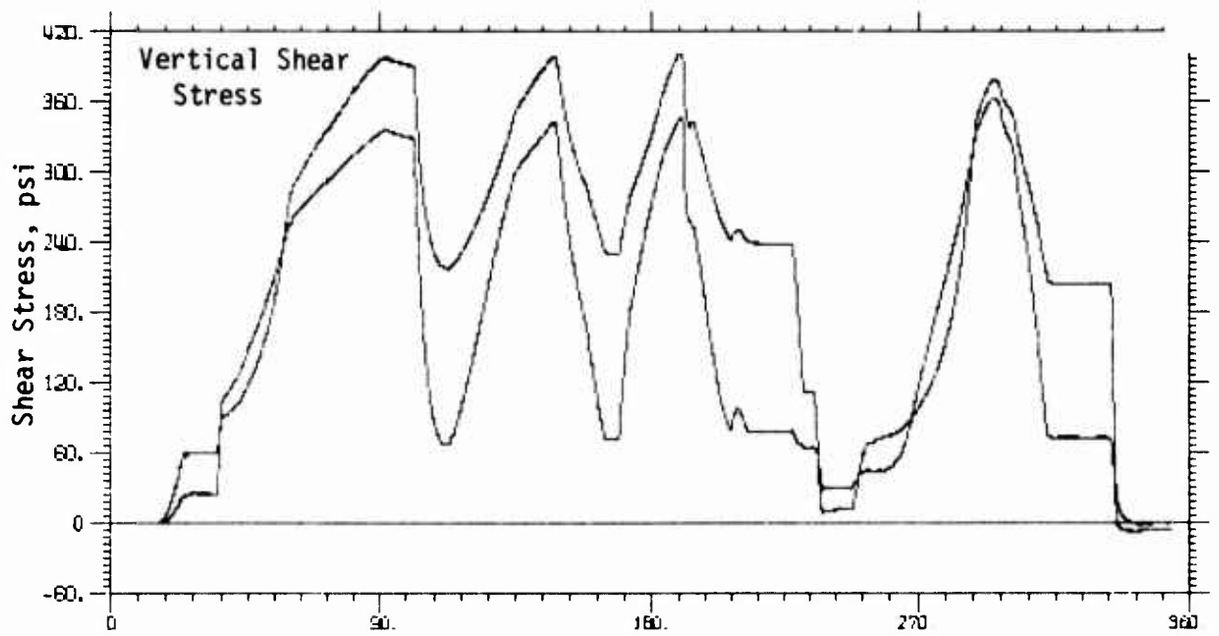

Time, sec

Inferred Vertical Shear Stress

TEST 17 (2 of 2)

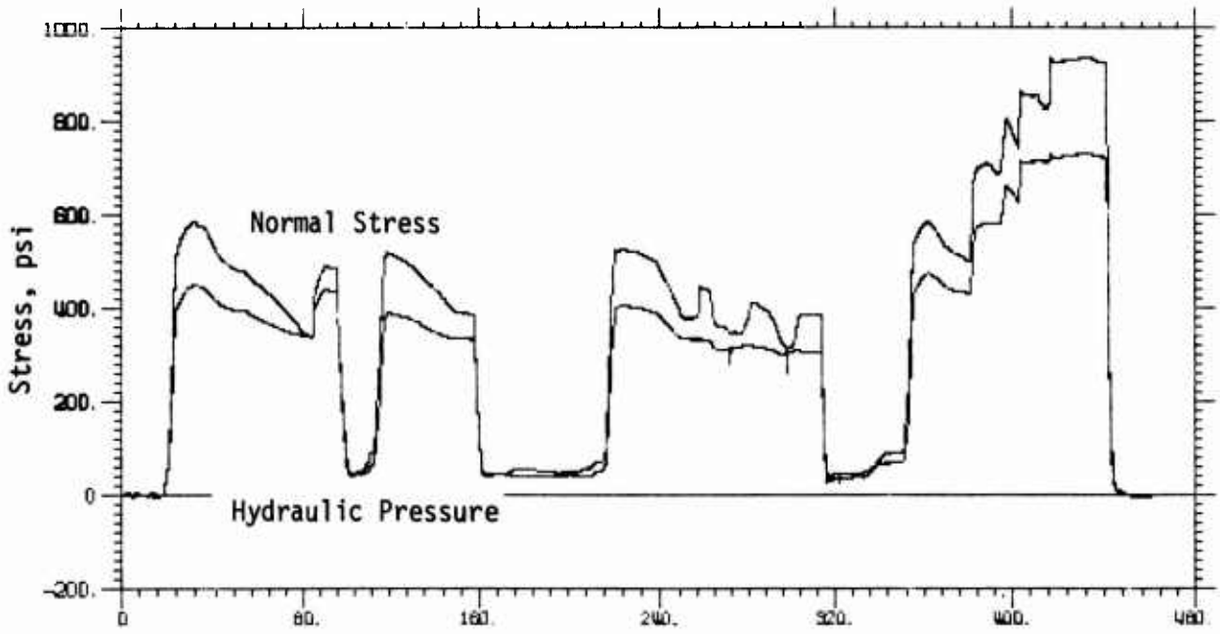

Time, sec

Hydraulic Pressure and Normal Stress

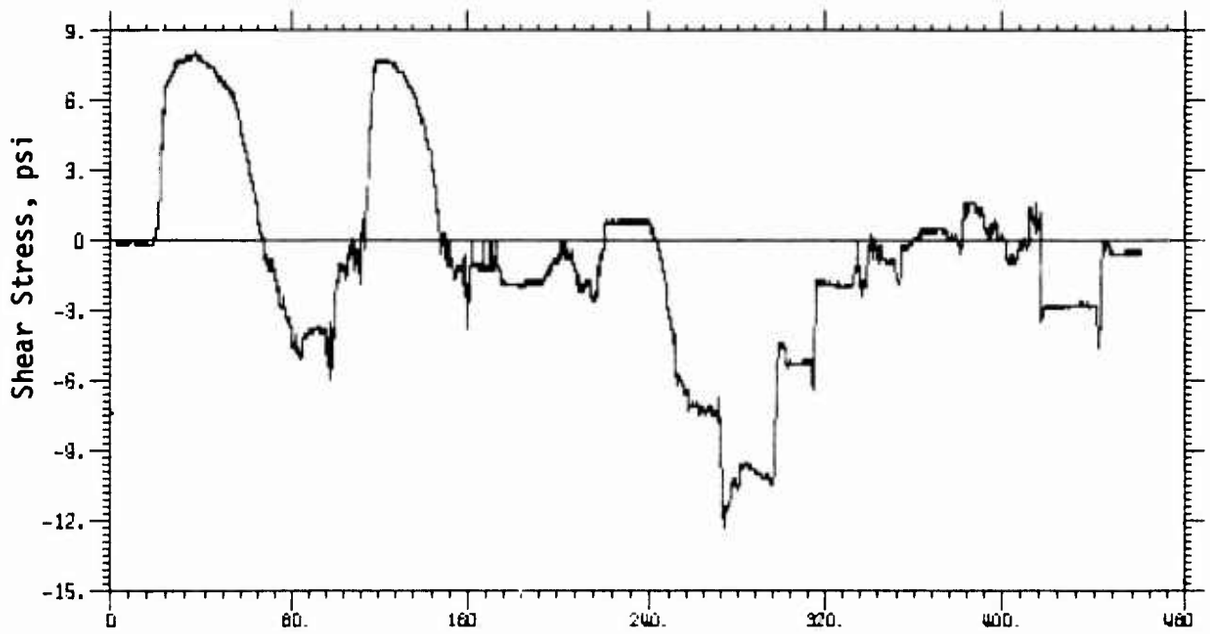

Time, sec

Horizontal Shear Stress

TEST 18 (1 of 2)

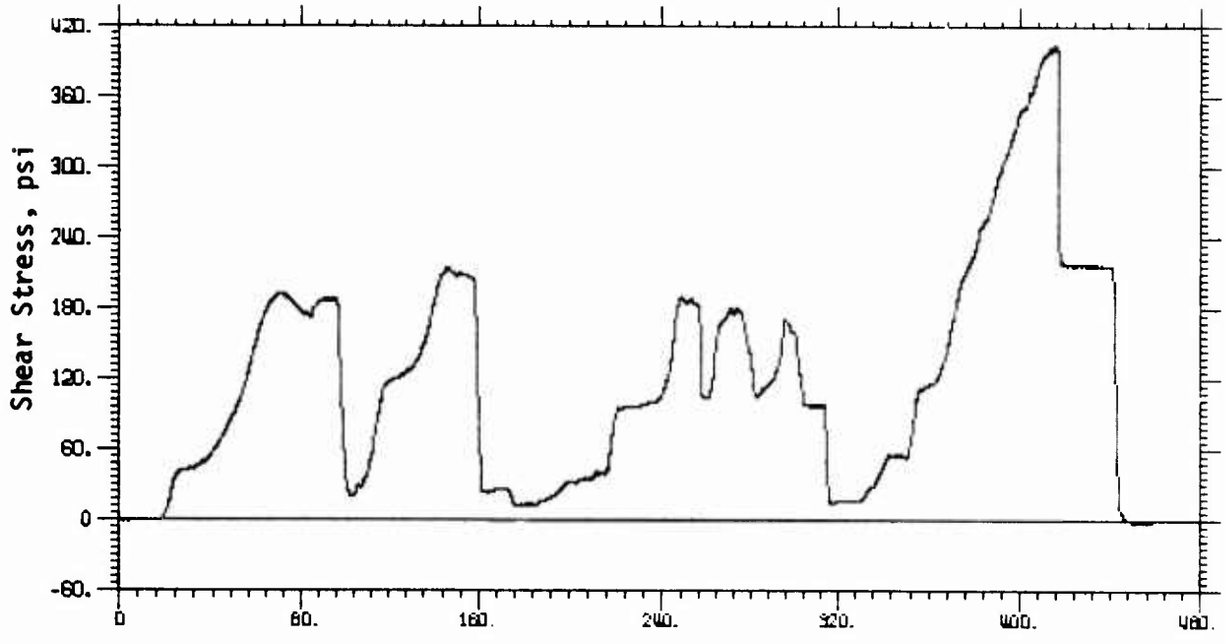

Time, sec

Vertical Shear Stress

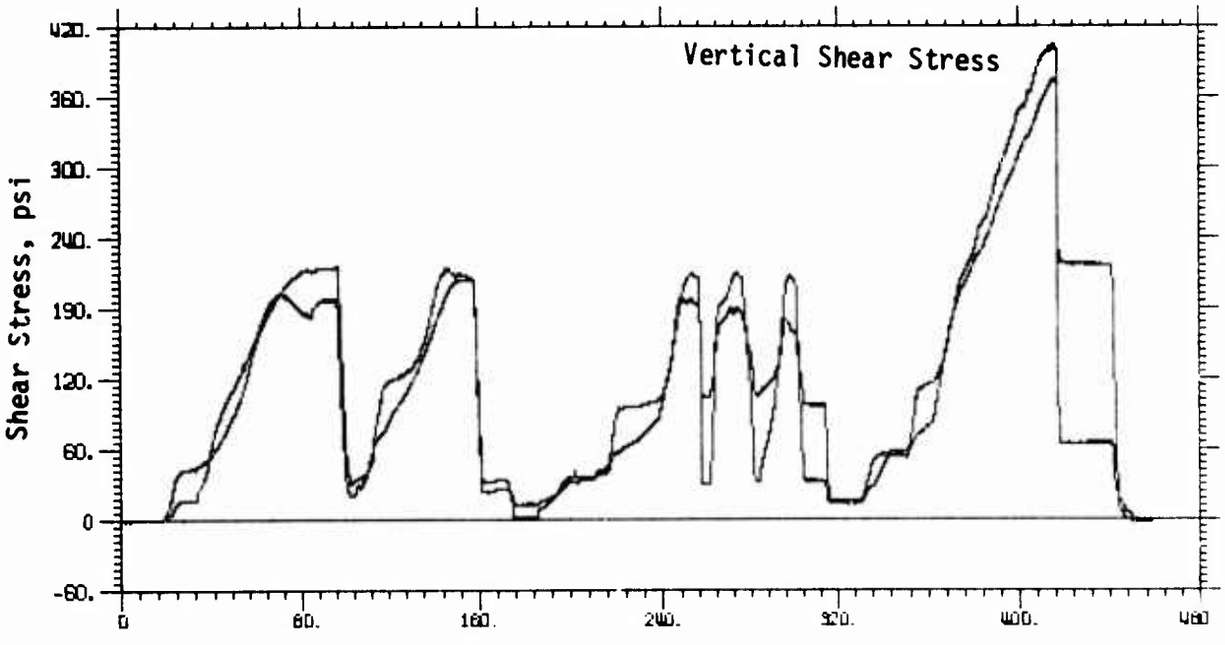

Time, sec

Inferred Vertical Shear Stress

TEST 18 (2 of 2)

APPENDIX E

DYNAMIC-SHEAR TEST DATA

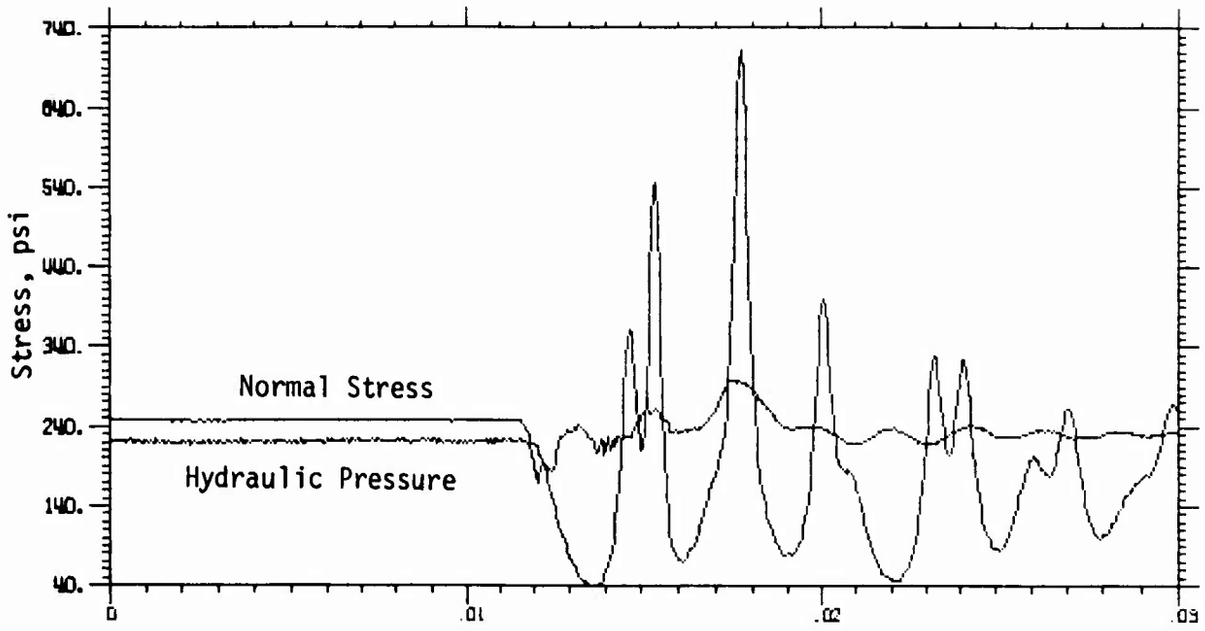

Time, sec

Hydraulic Pressure and Normal Stress

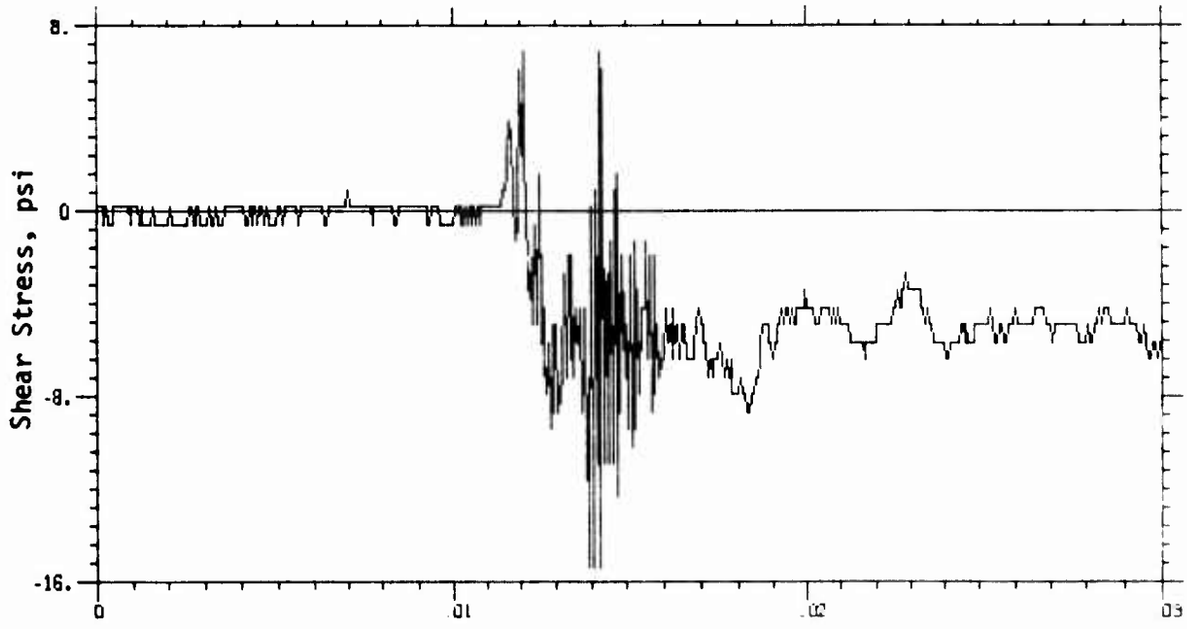

Time, sec

Horizontal Shear Stress

TEST 10 (1 of 3)

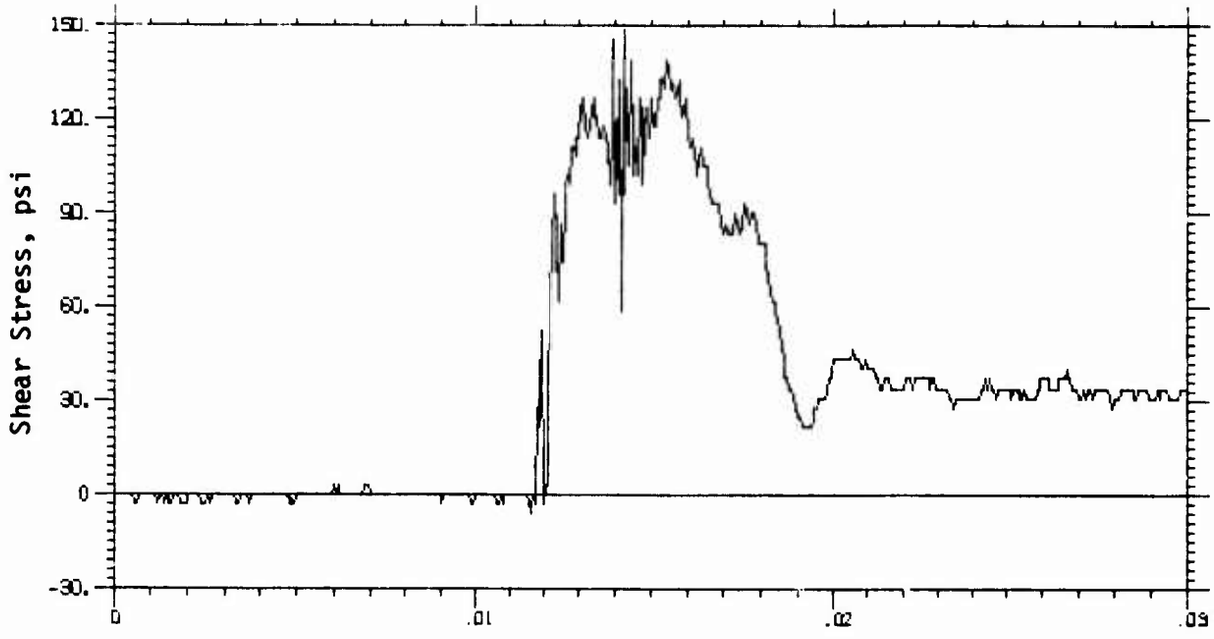

Time, sec

Vertical Shear Stress

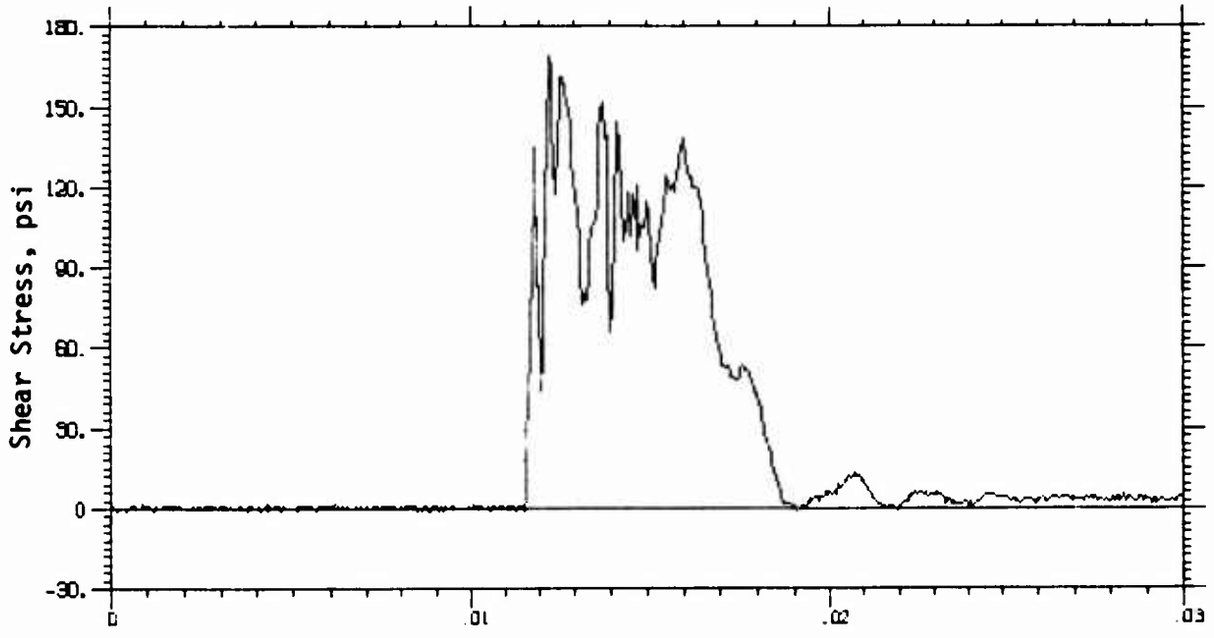

Time, sec

Inferred Vertical Shear Stress

TEST 10 (2 of 3)

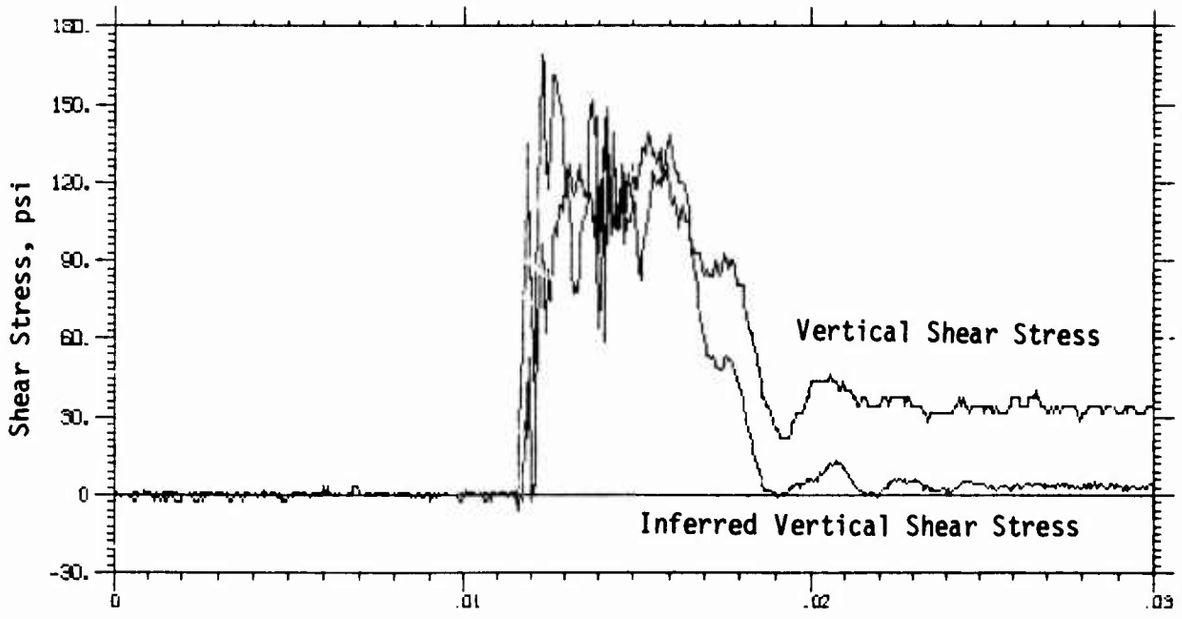

Time, sec

Vertical Shear Stresses (Comparison)

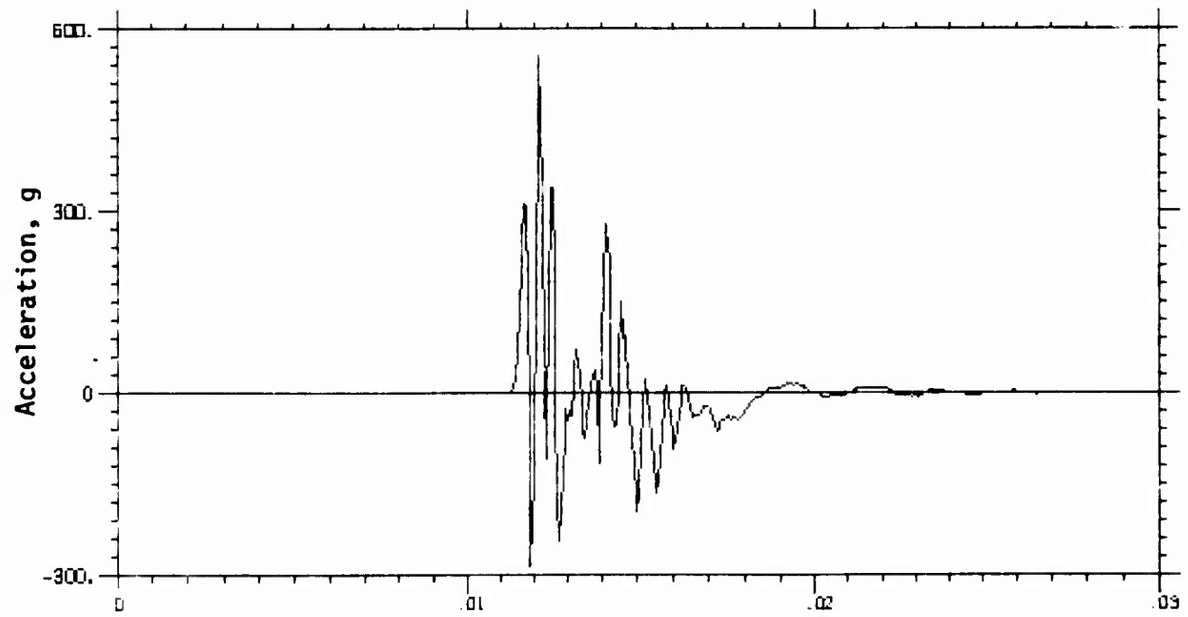

Time, sec

Acceleration

TEST 10 (3 of 3)

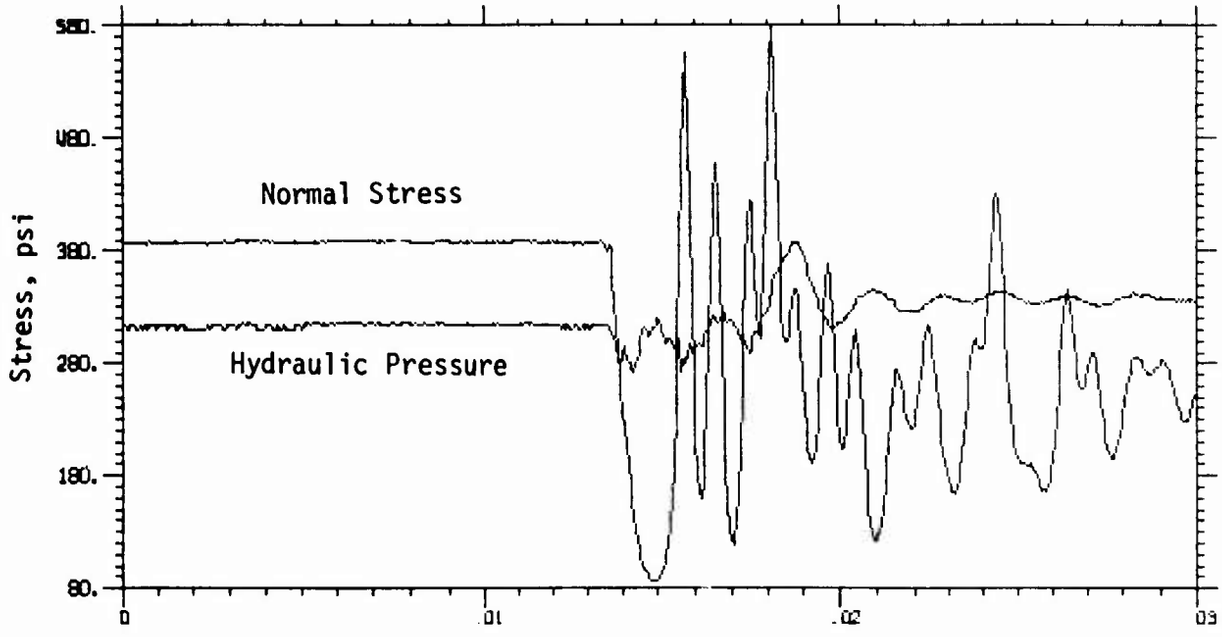

Time, sec

Hydraulic Pressure and Normal Stress

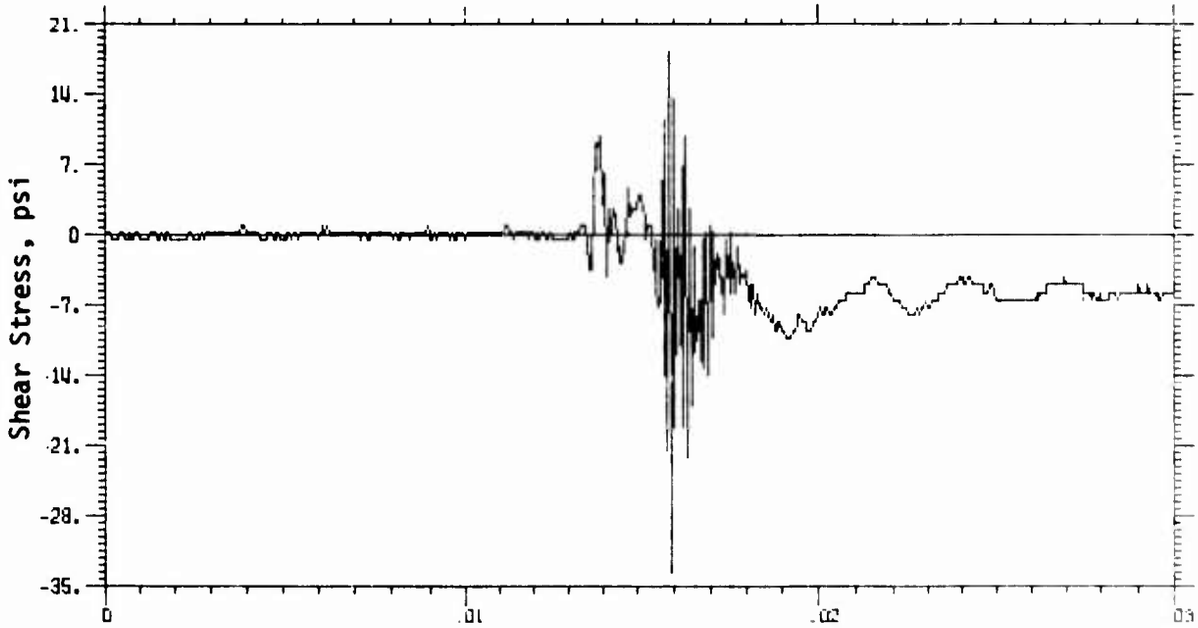

Time, sec

Horizontal Shear Stress

TEST 11 (1 of 3)

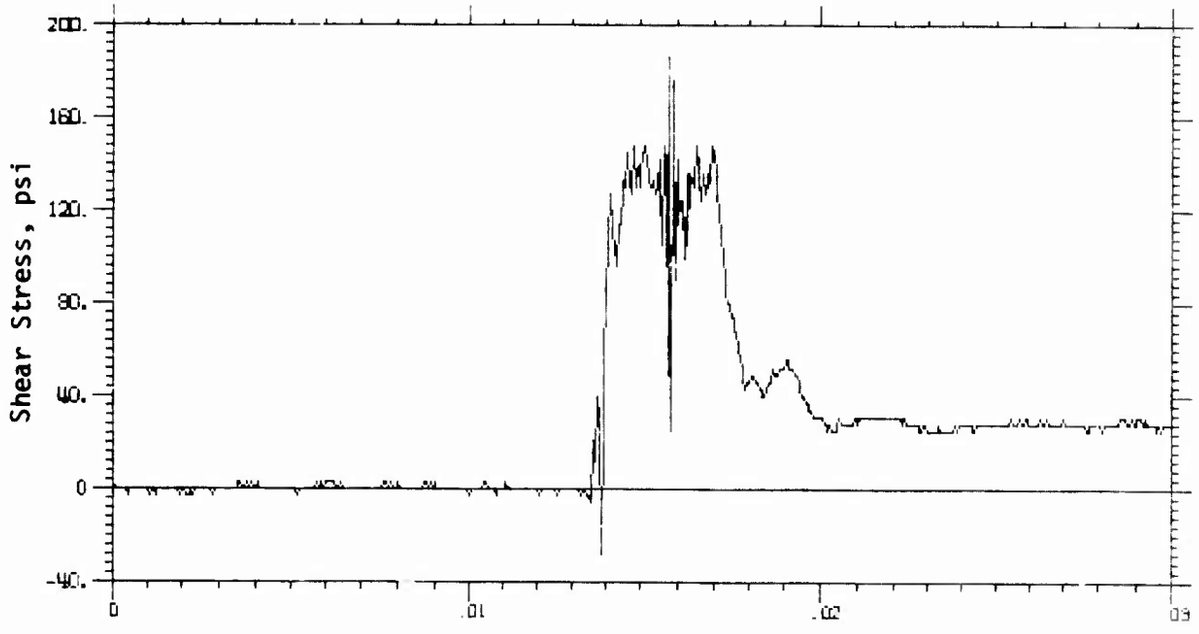

Time, sec

Vertical Shear Stress

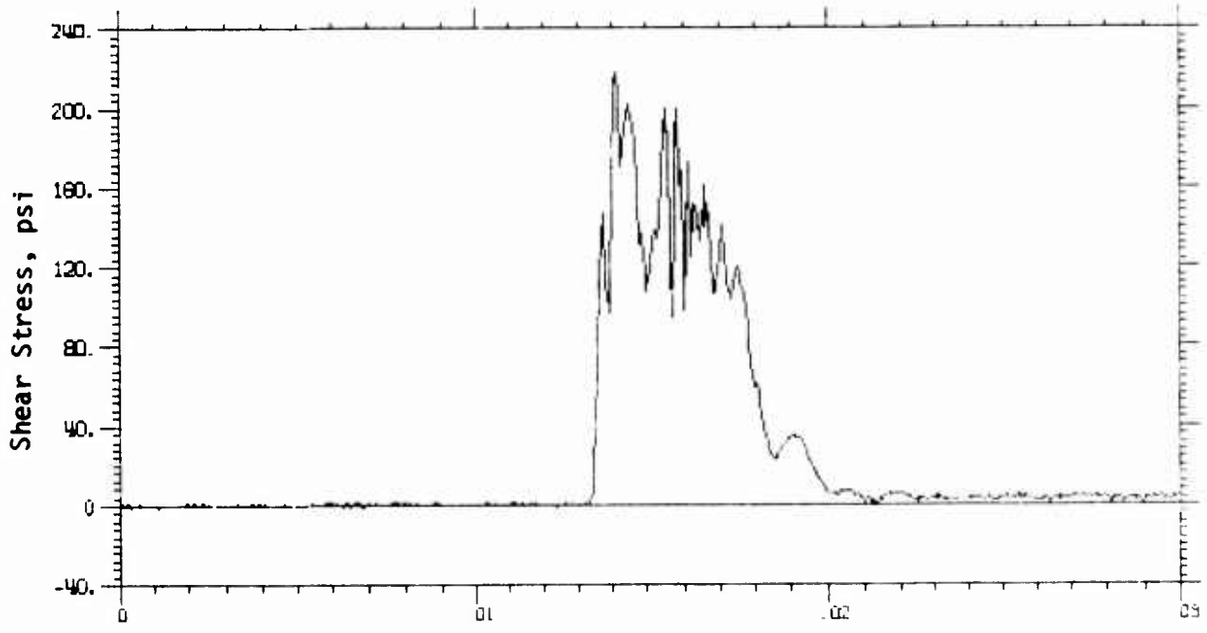

Time, sec

Inferred Vertical Shear Stress

TEST 11 (2 of 3)

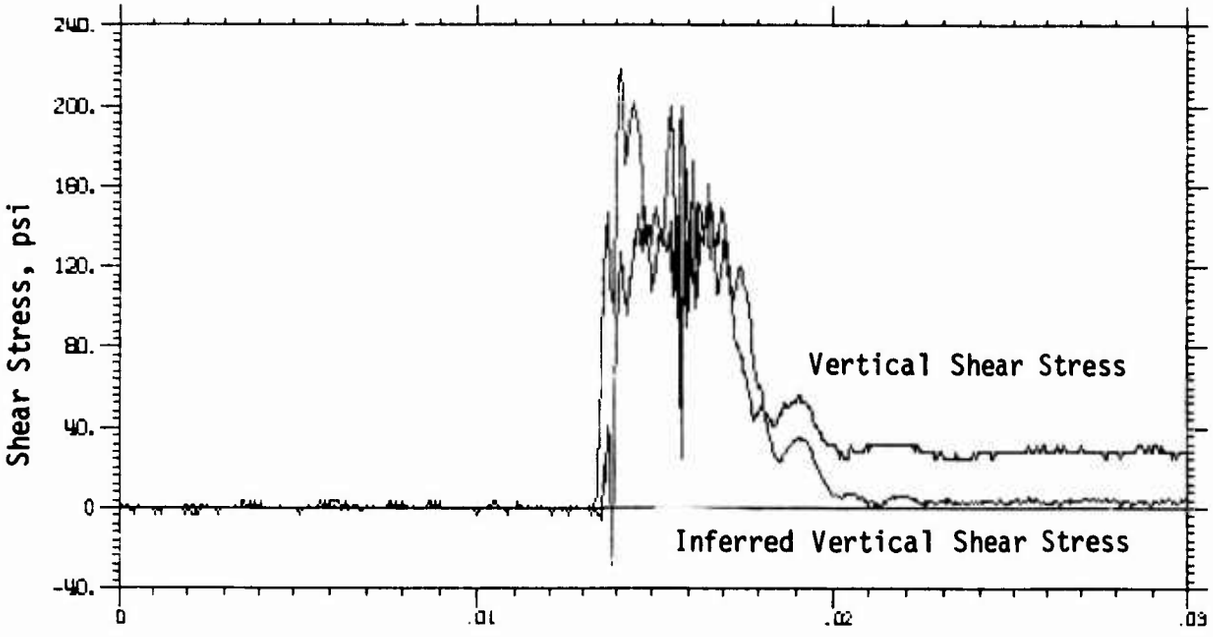

Vertical Shear Stresses (Comparison)

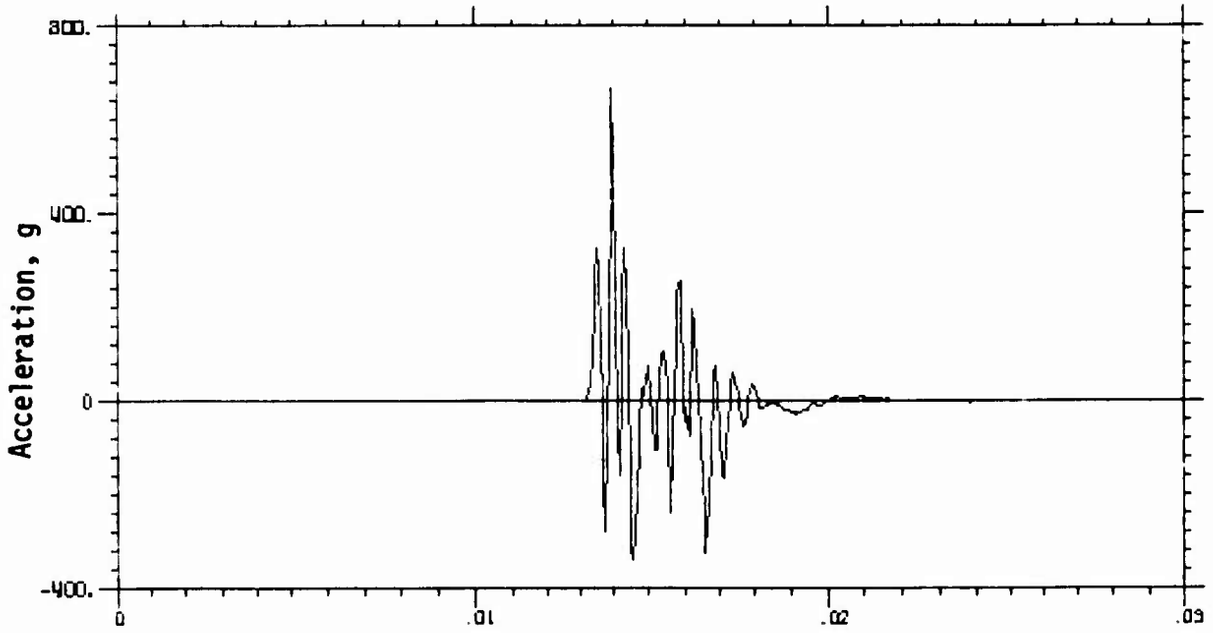

Acceleration

TEST 11 (3 of 3)

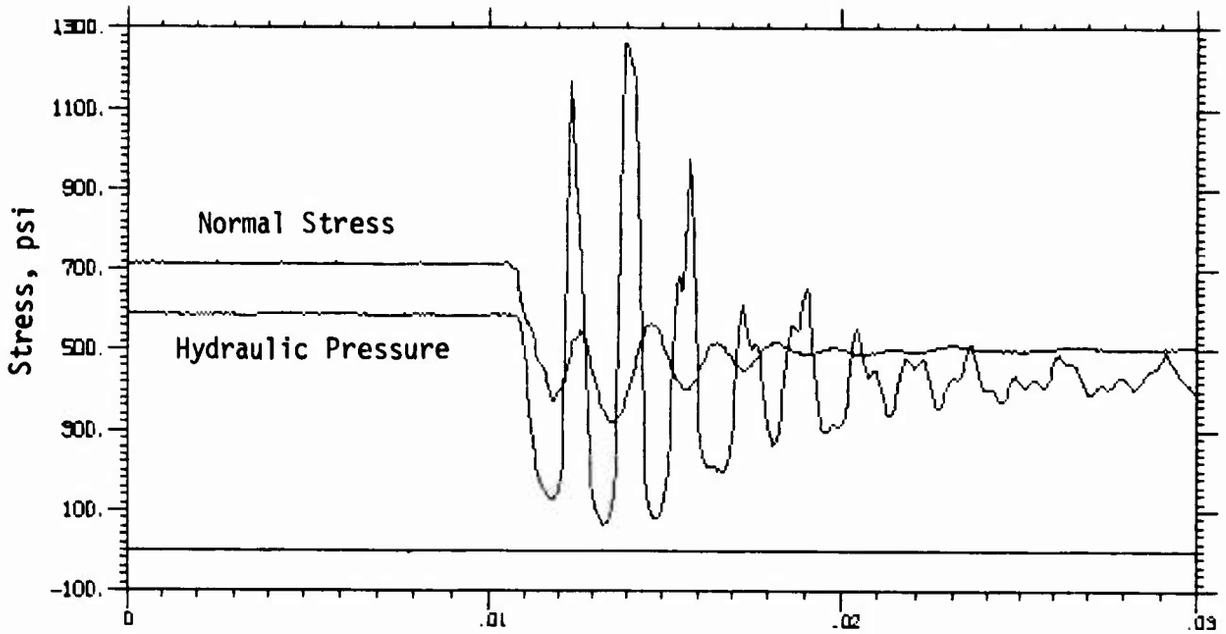

Hydraulic Pressure and Normal Stress

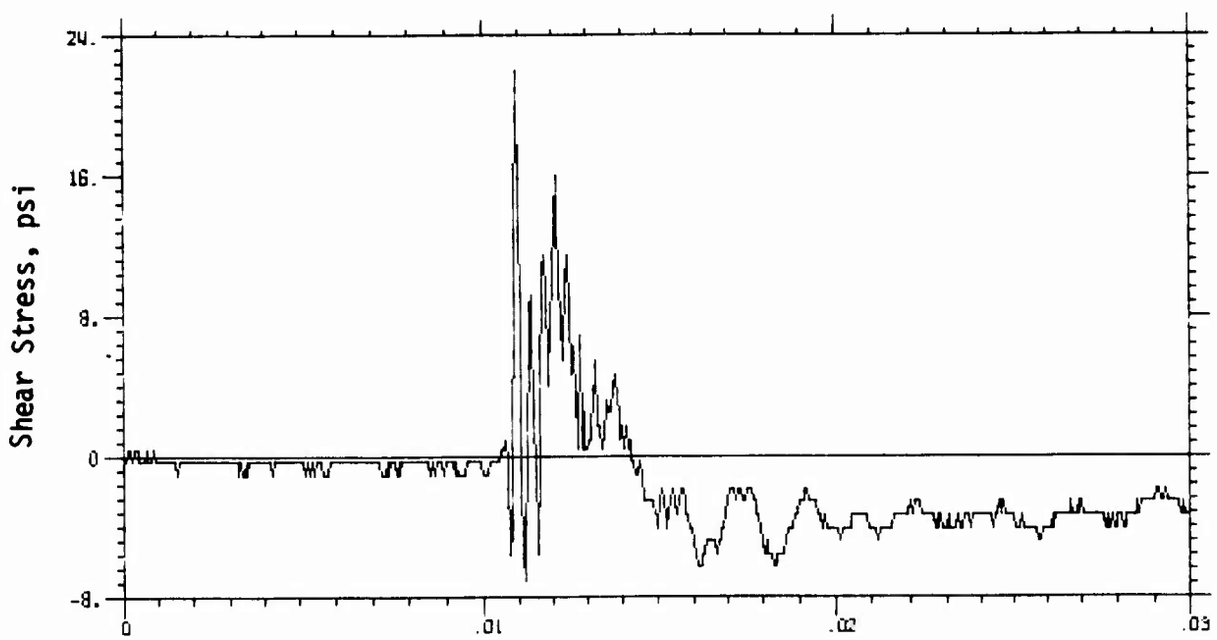

Horizontal Shear Stress

TEST 13 (1 of 3)

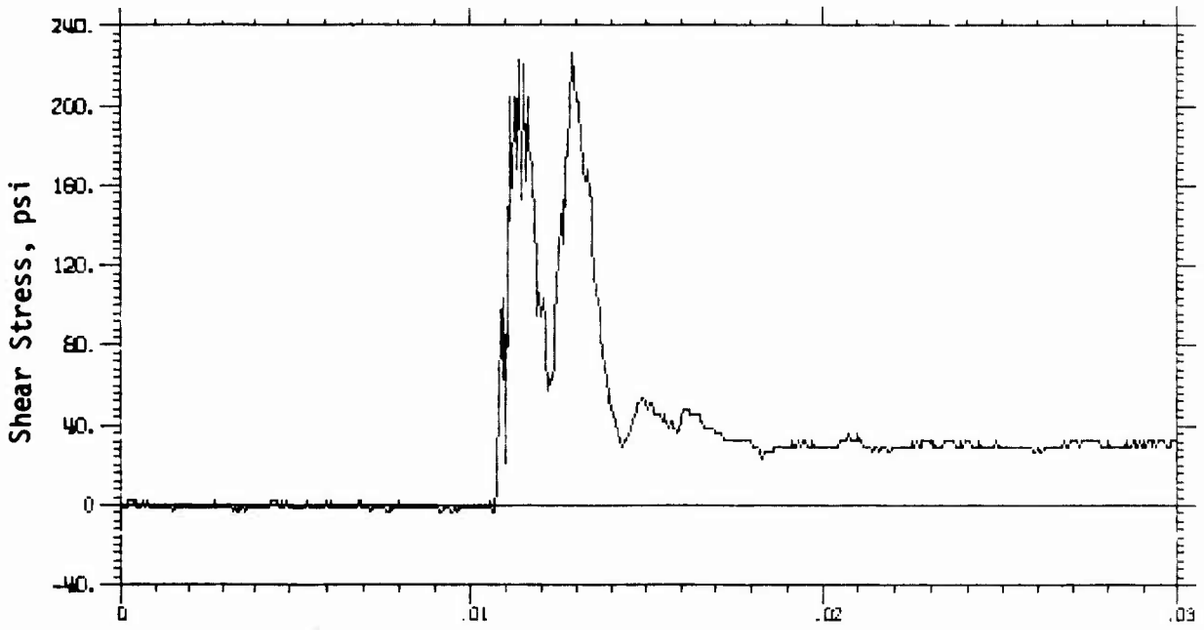

Time, sec

Vertical Shear Stress

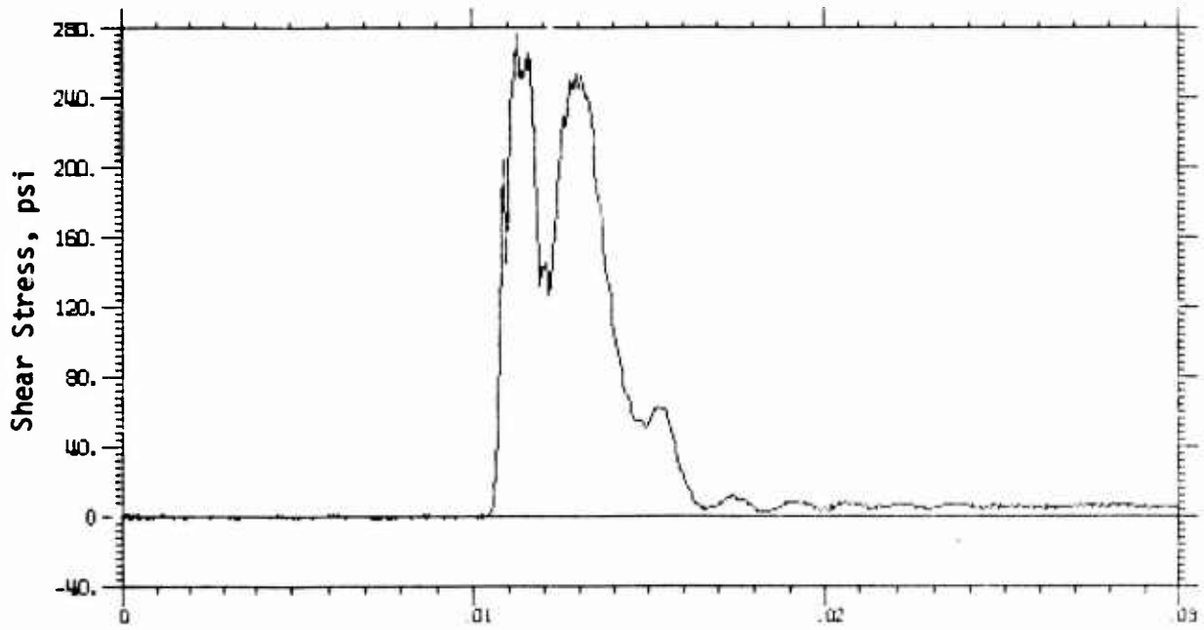

Time, sec

Inferred Vertical Shear Stress

TEST 13 (2 of 3)

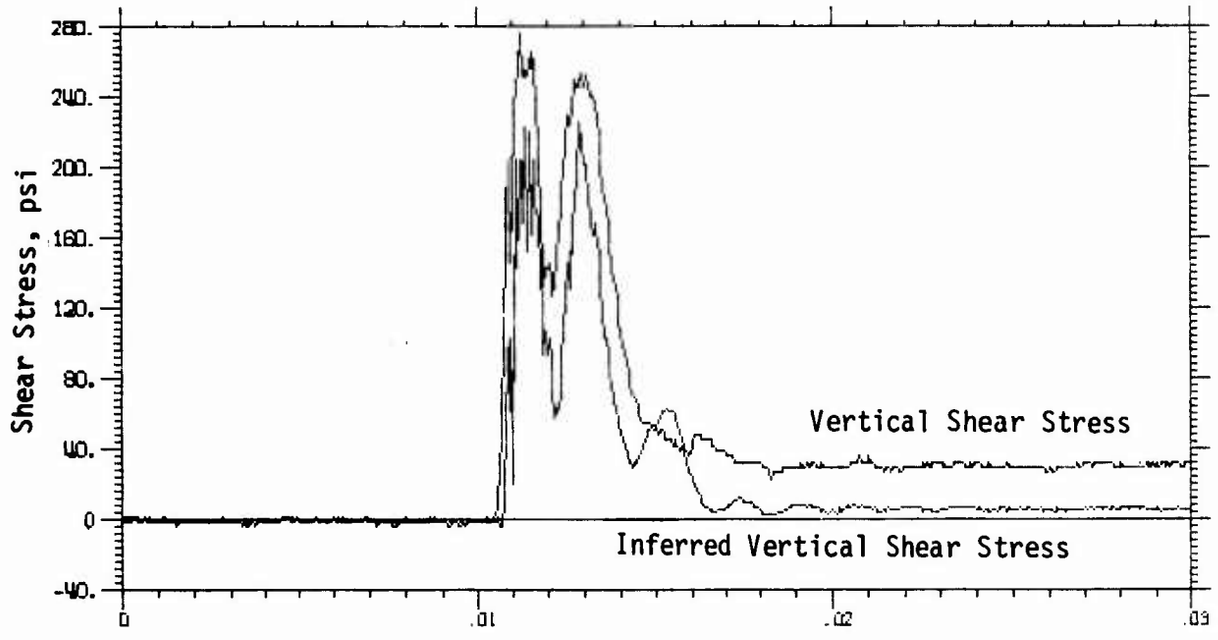

Time, sec

Vertical Shear Stresses (Comparison)

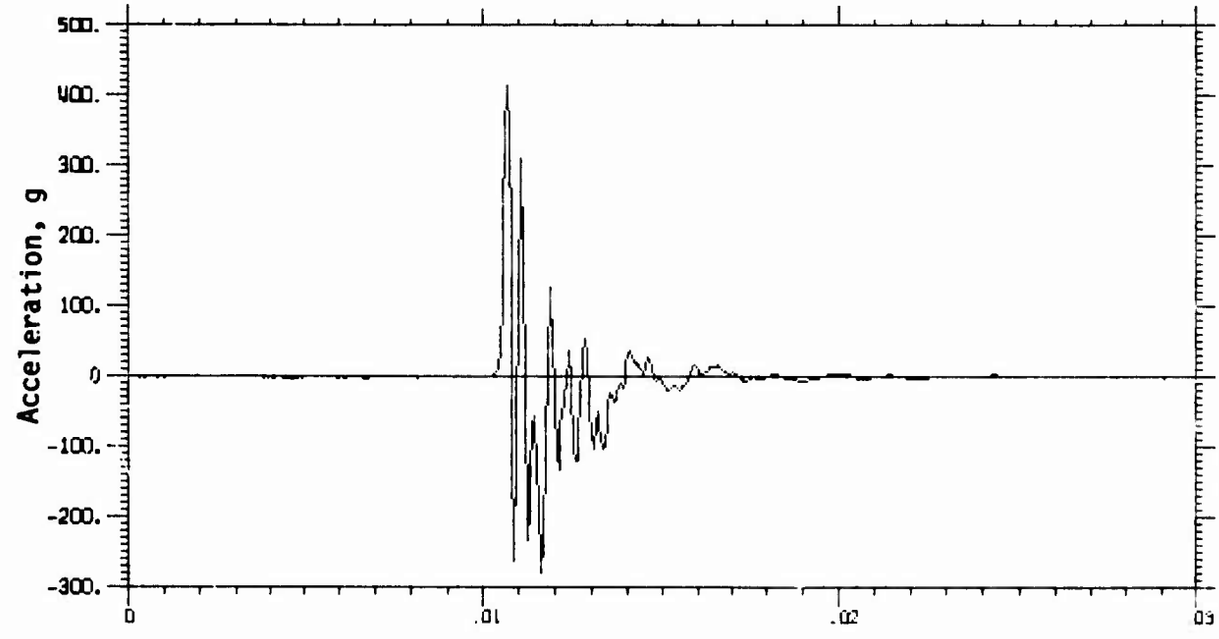

Time, sec

Acceleration

TEST 13 (3 of 3)

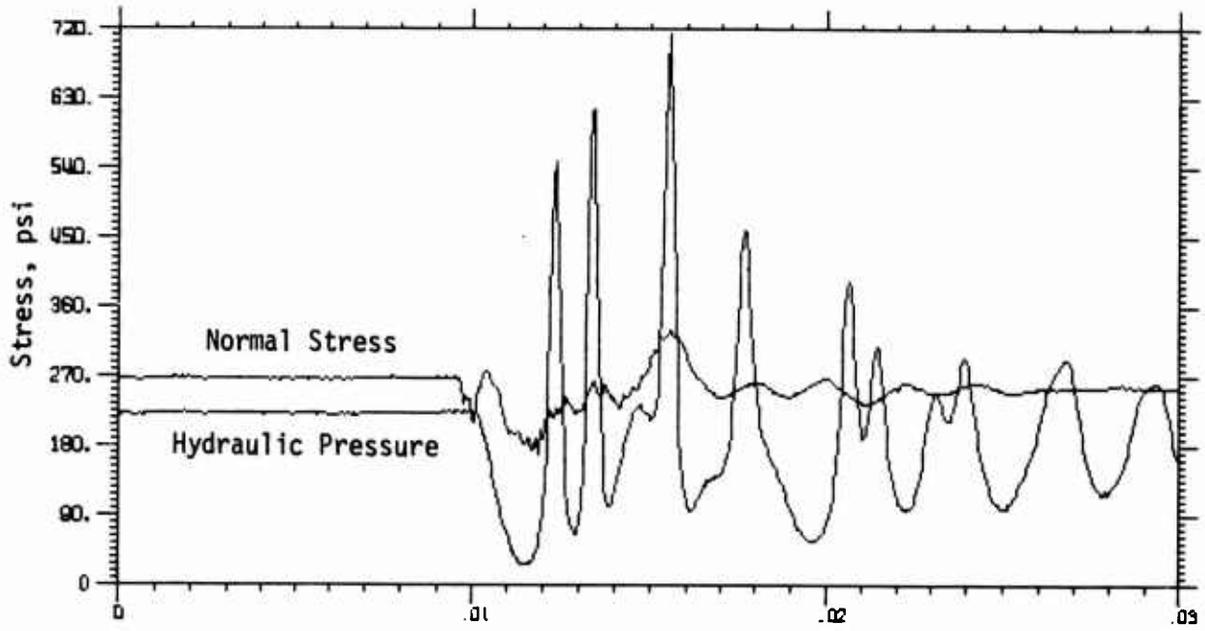

Hydraulic Pressure and Normal Stress

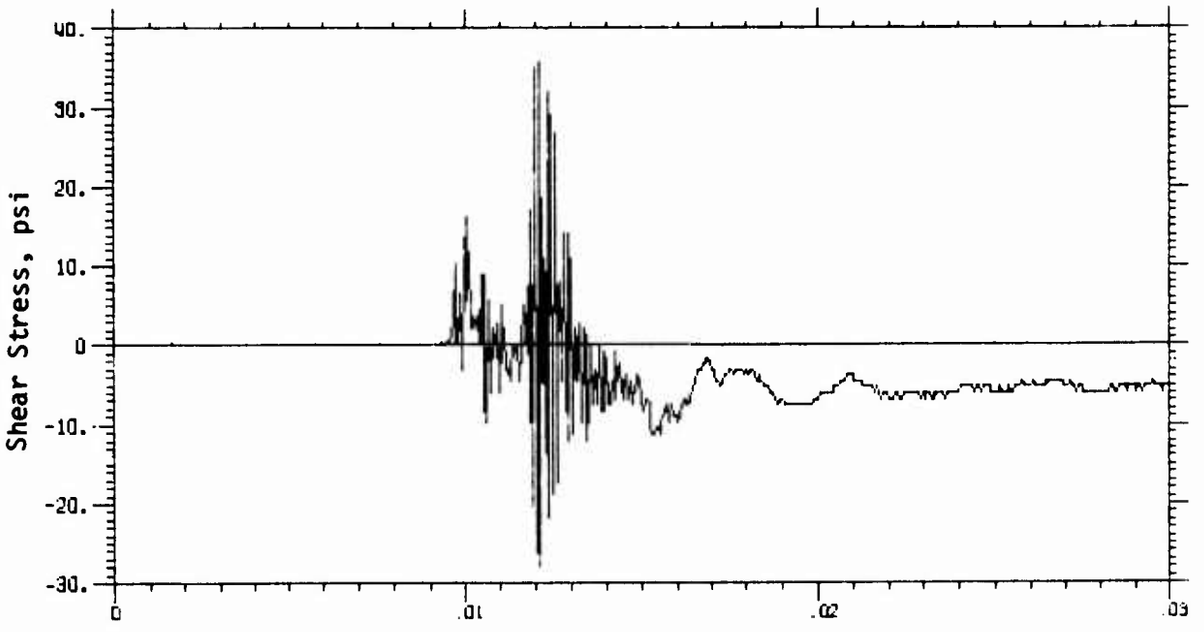

Horizontal Shear Stress

TEST 14 (1 of 3)

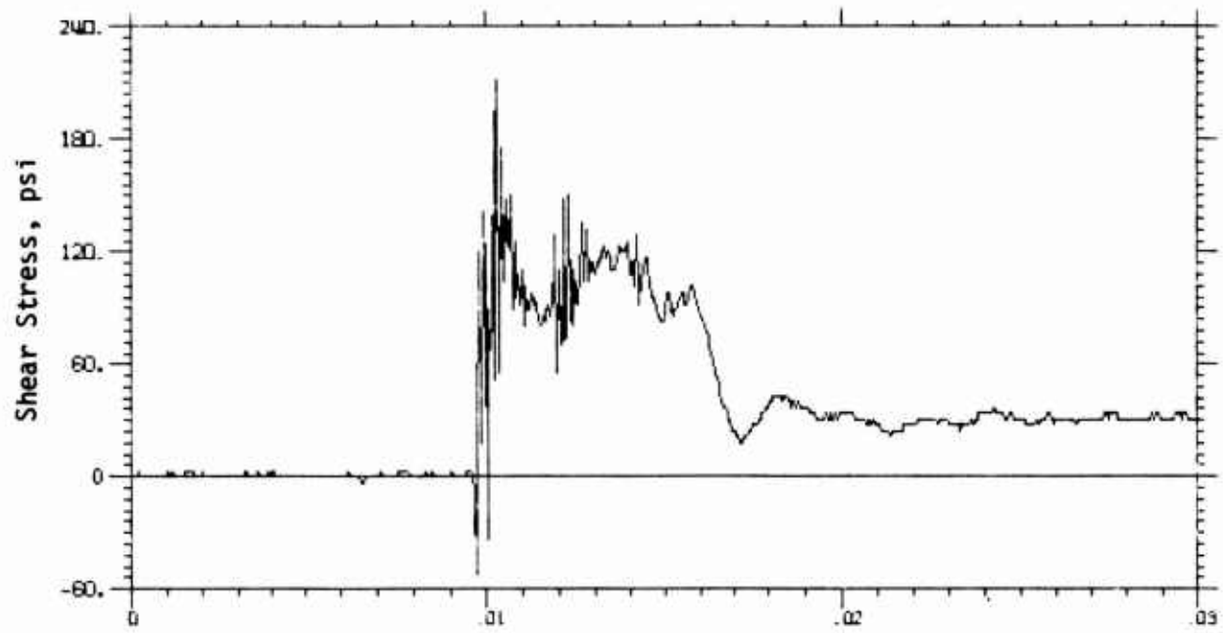

Time, sec

Vertical Shear Stress

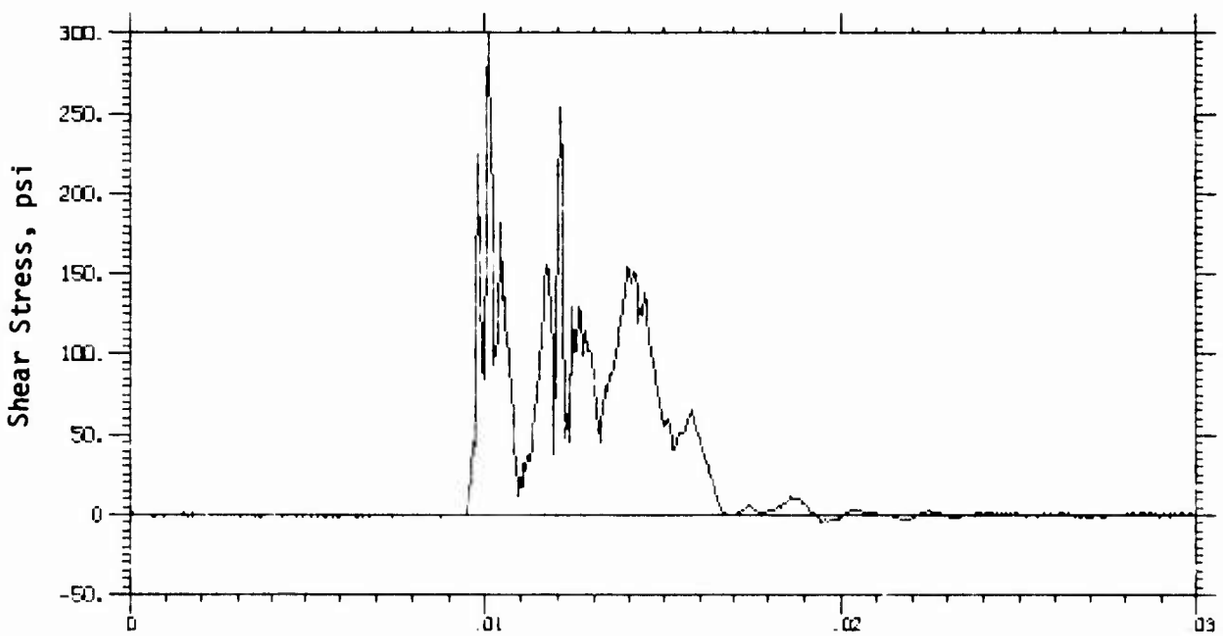

Time, sec

Inferred Vertical Shear Stress

TEST 14 (2 of 3)

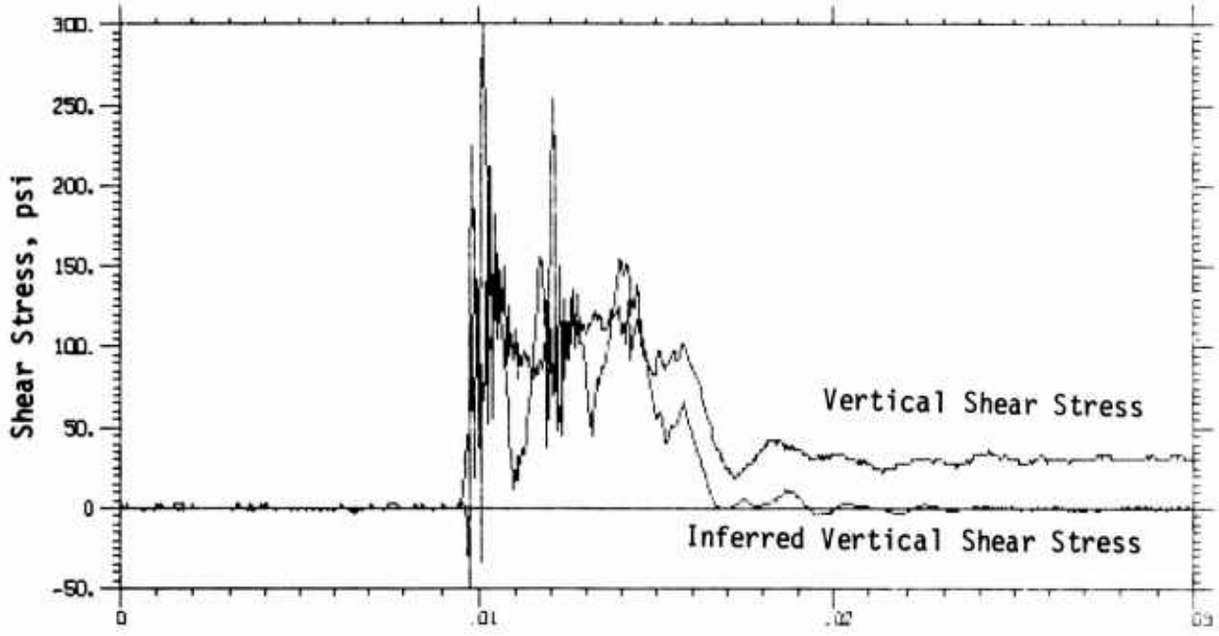

Time, sec

Vertical Shear Stresses (Comparison)

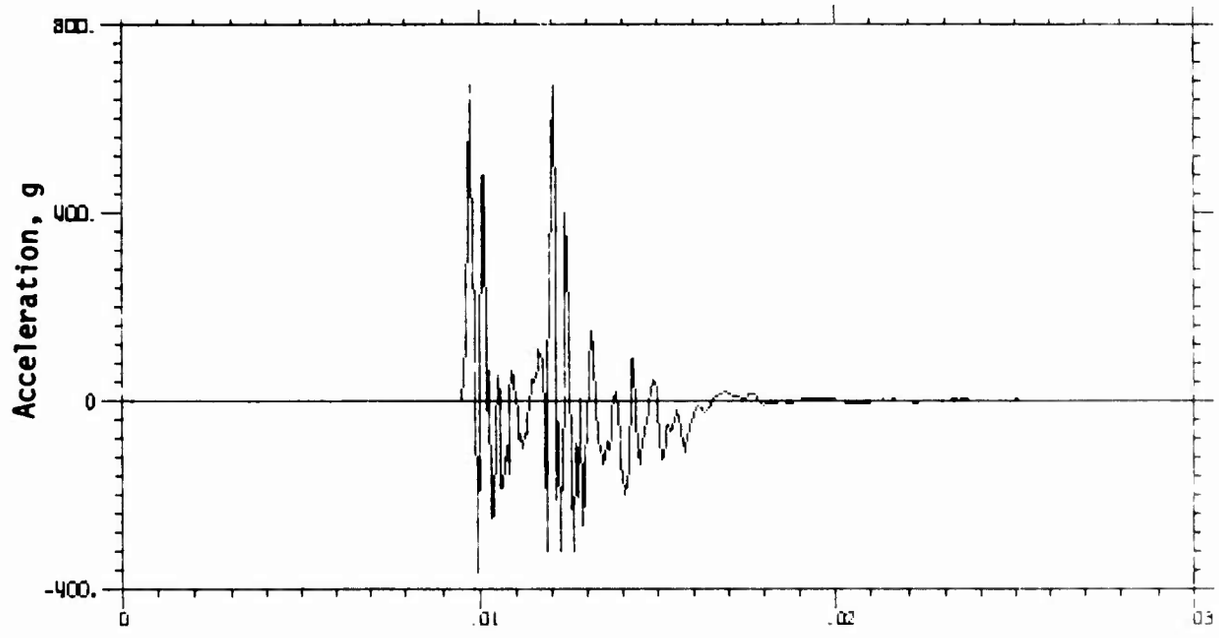

Time, sec

Acceleration

TEST 14 (3 of 3)

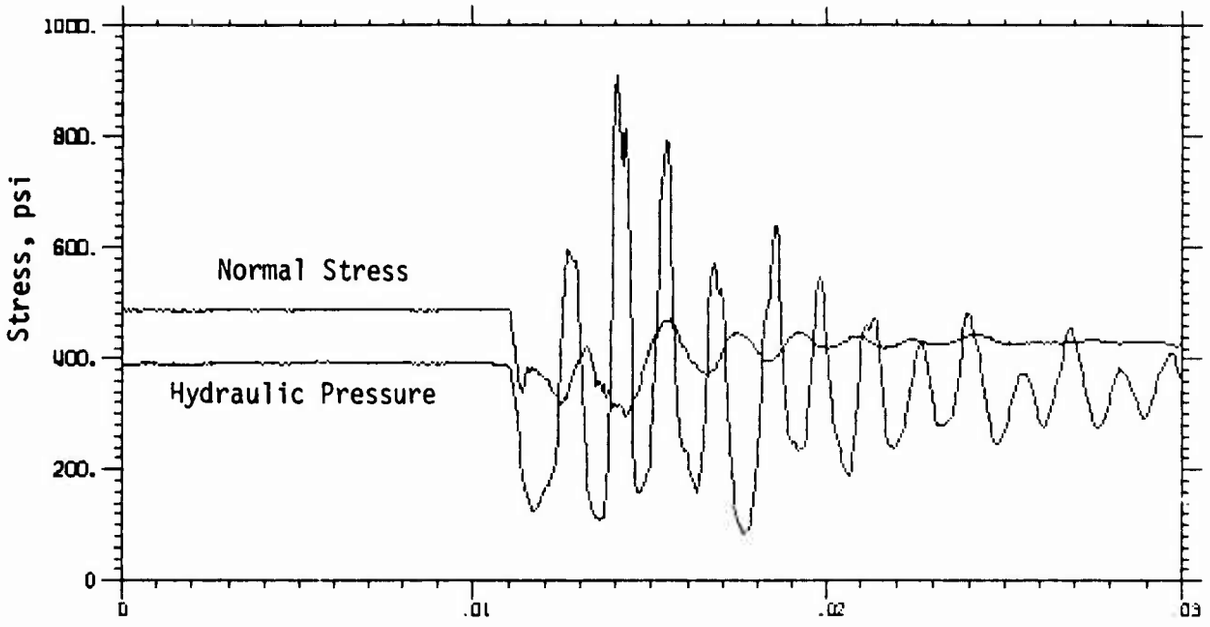

Time, sec

Hydraulic Pressure and Normal Stress

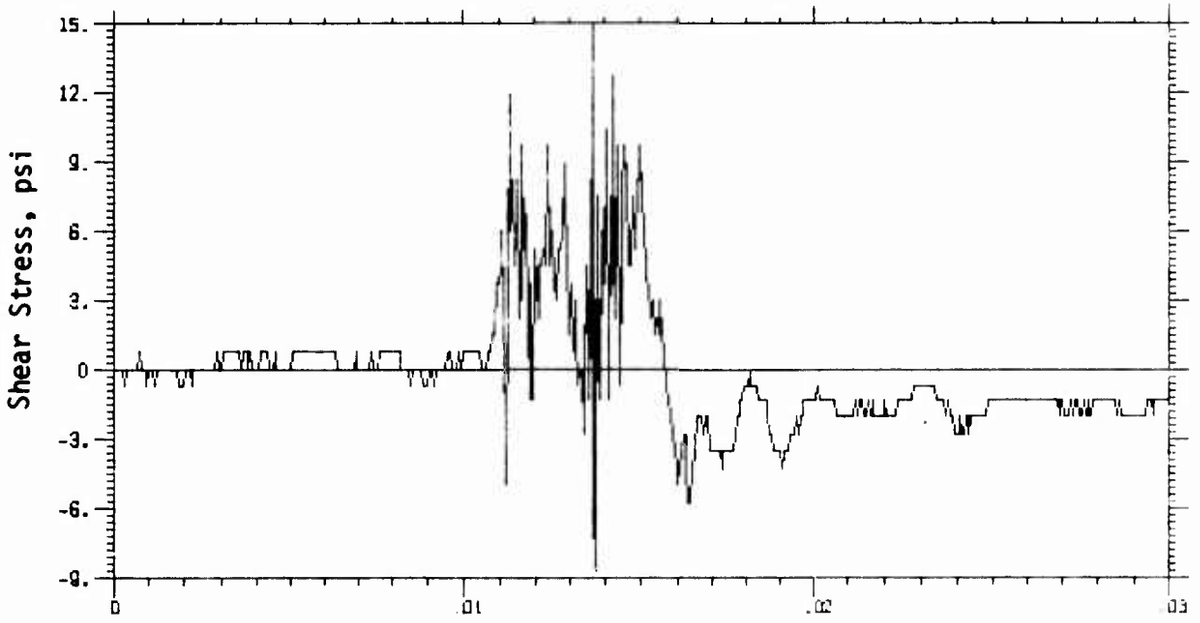

Time, sec

Horizontal Shear Stress

TEST 17 (1 of 3)

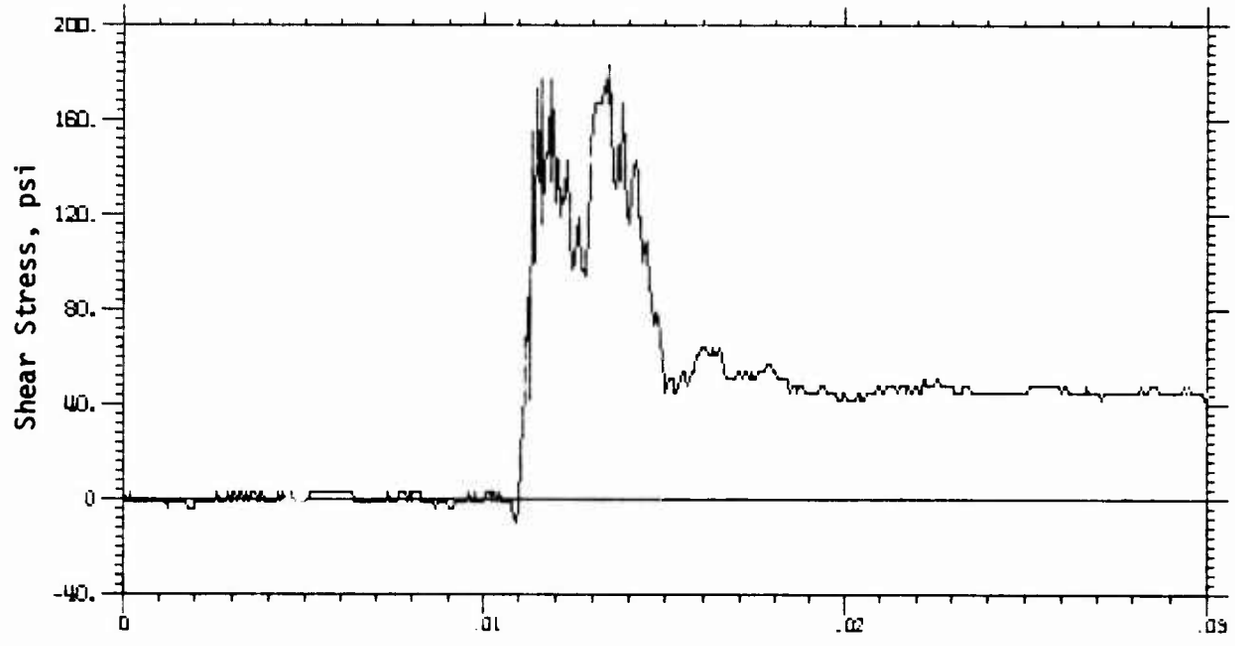

Time, sec

Vertical Shear Stress

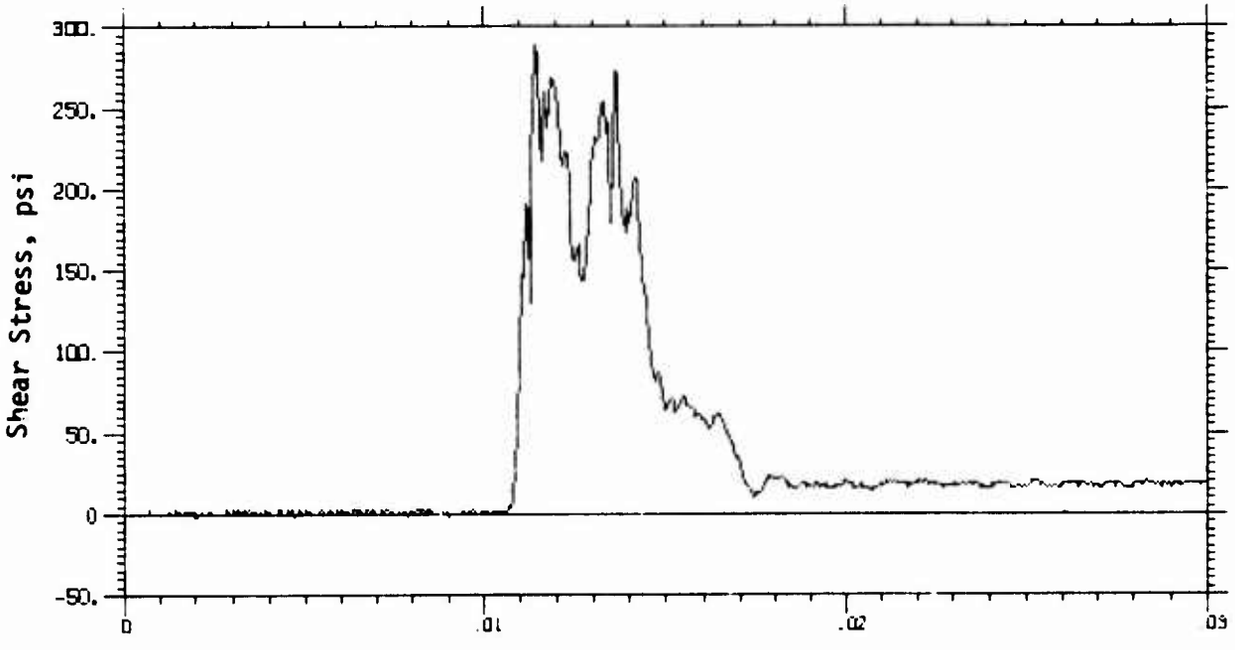

Time, sec

Inferred Vertical Shear Stress

TEST 17 (2 of 3)

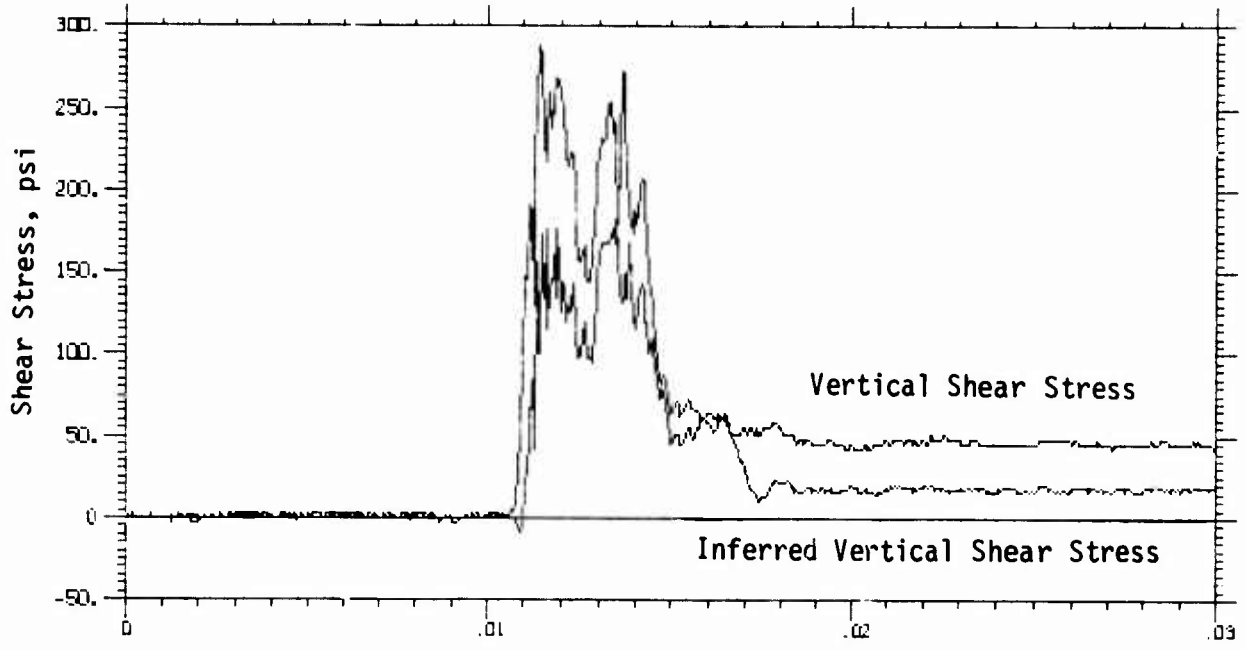

Time, sec

Vertical Shear Stresses (Comparison)

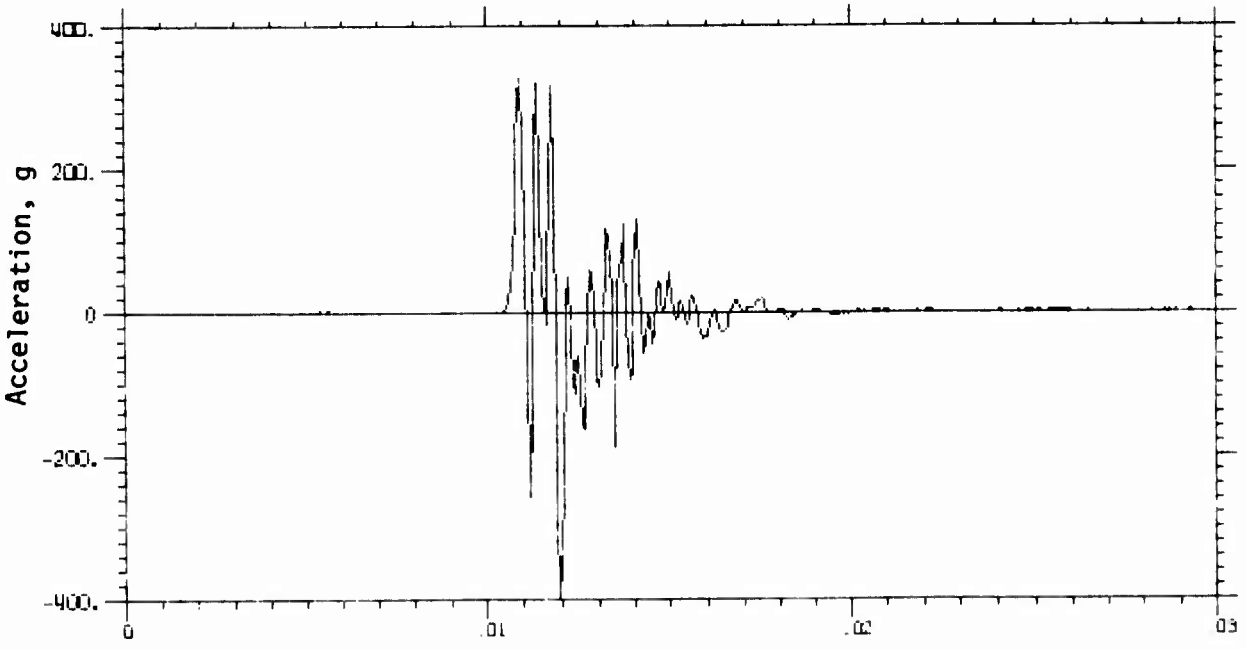

Time, sec

Acceleration

TEST 17 (3 of 3)

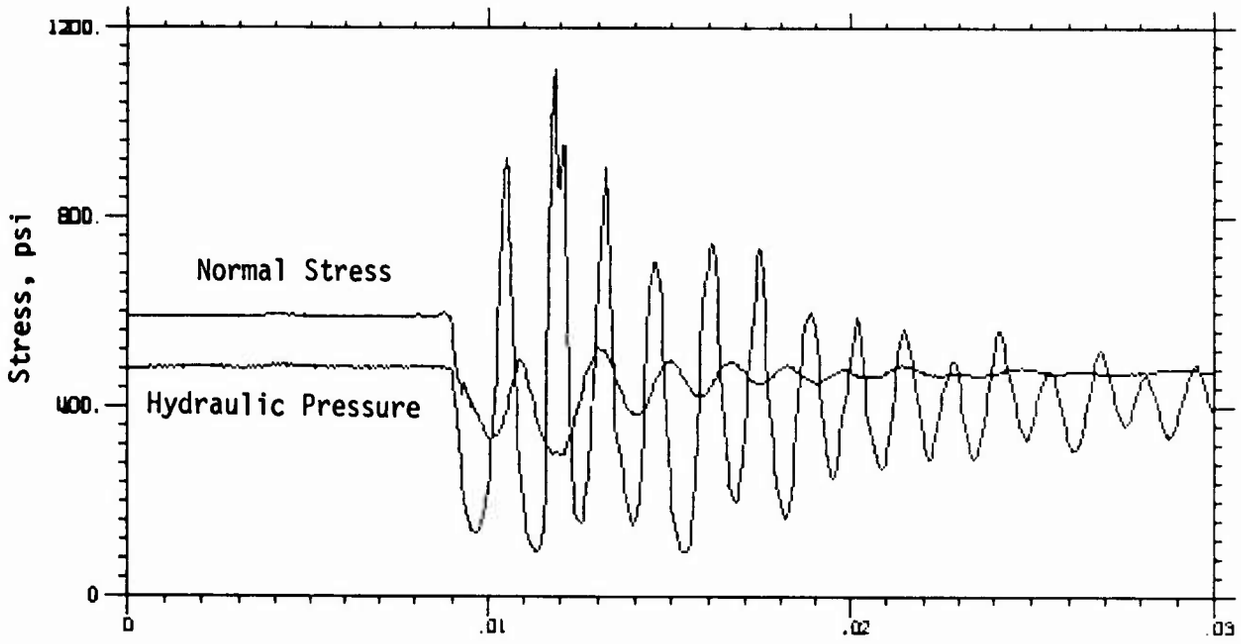

Hydraulic Pressure and Normal Stress

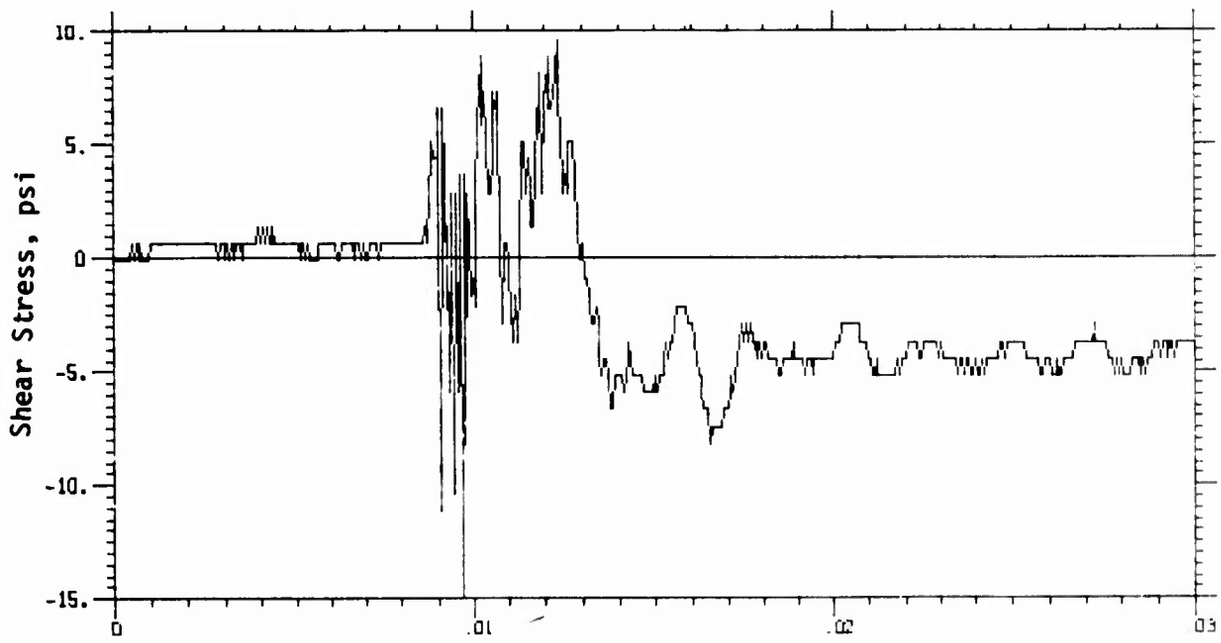

Horizontal Shear Stress

TEST 18 (1 of 3)

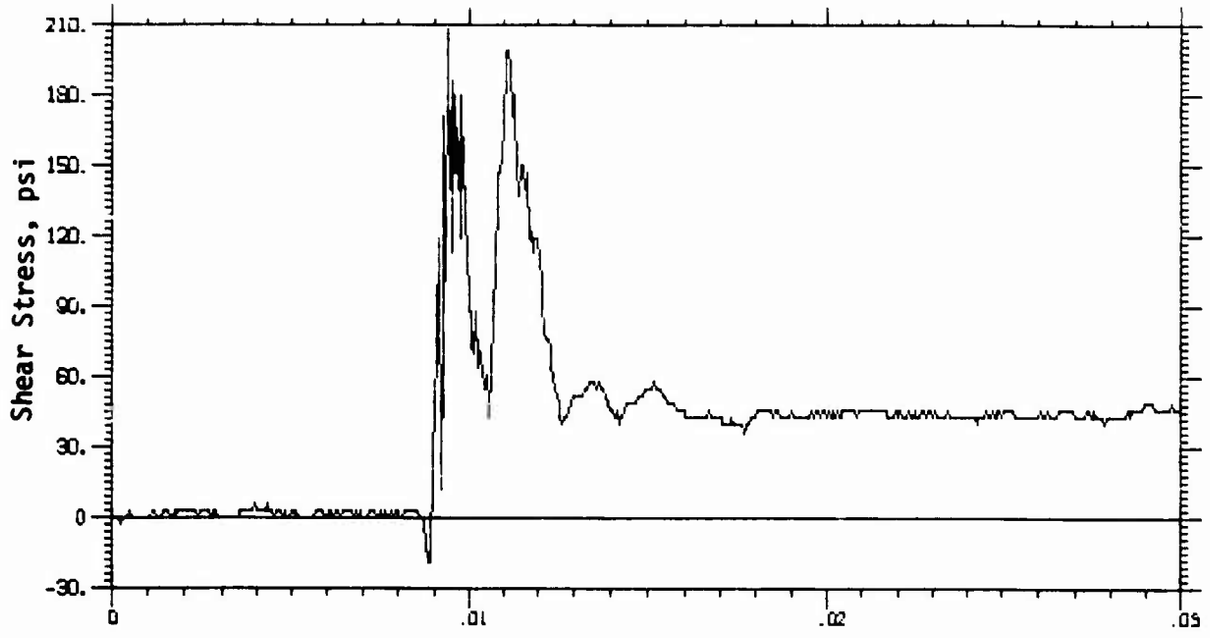

Time, sec

Vertical Shear Stress

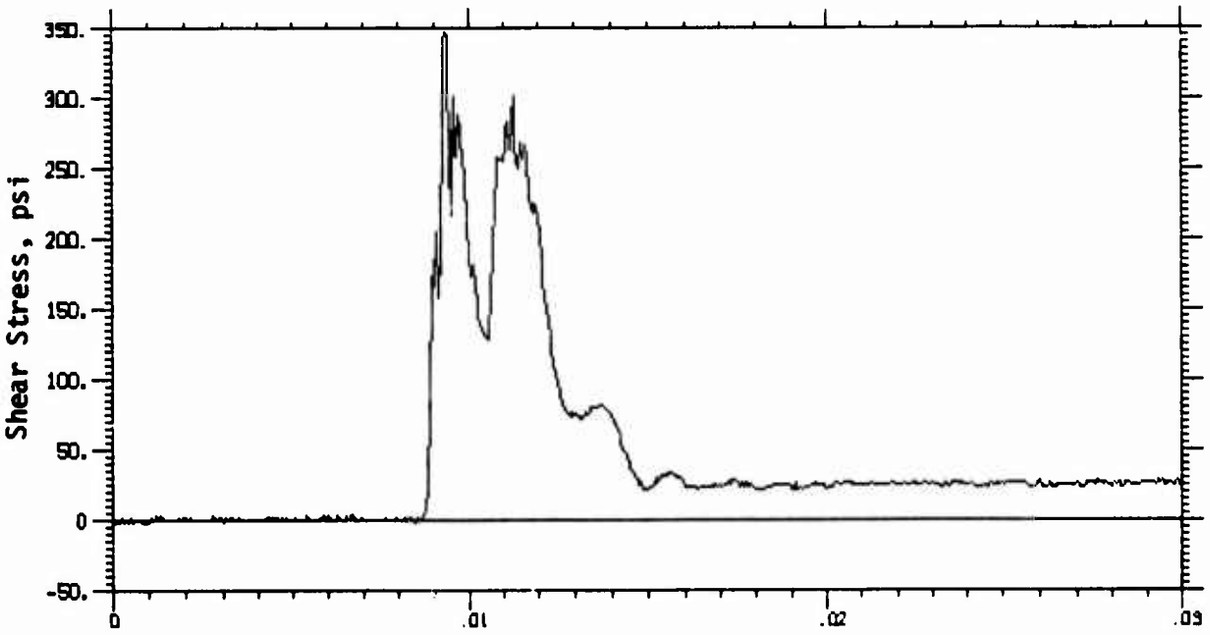

Time, sec

Inferred Vertical Shear Stress

TEST 18 (2 of 3)

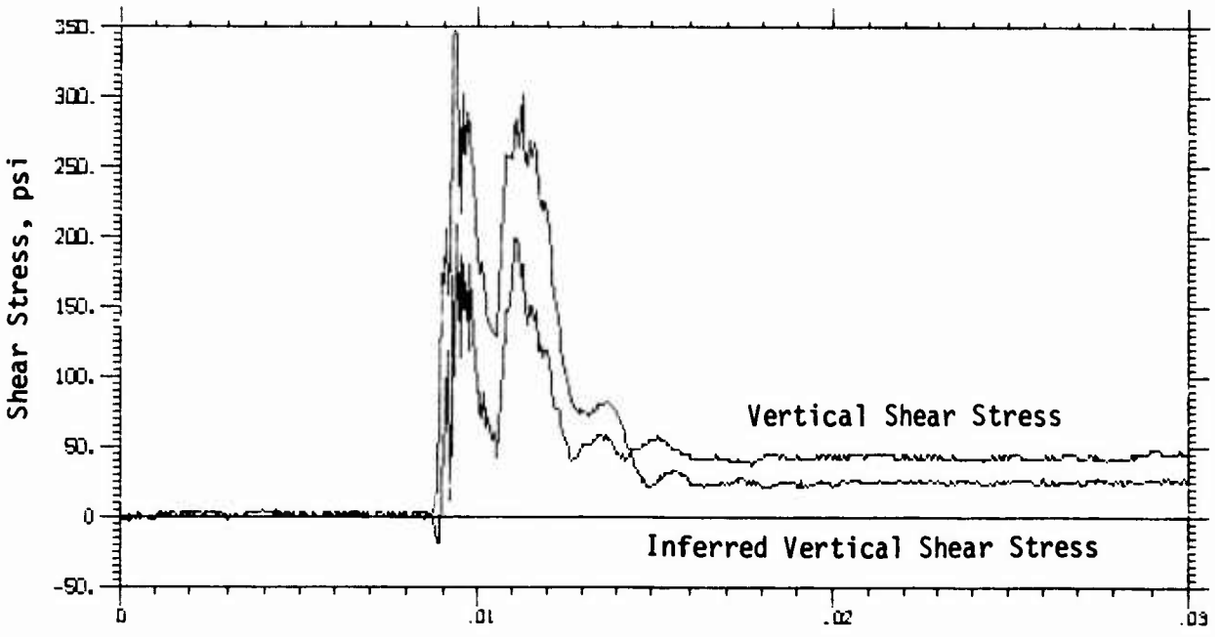

Vertical Shear Stresses (Comparison)

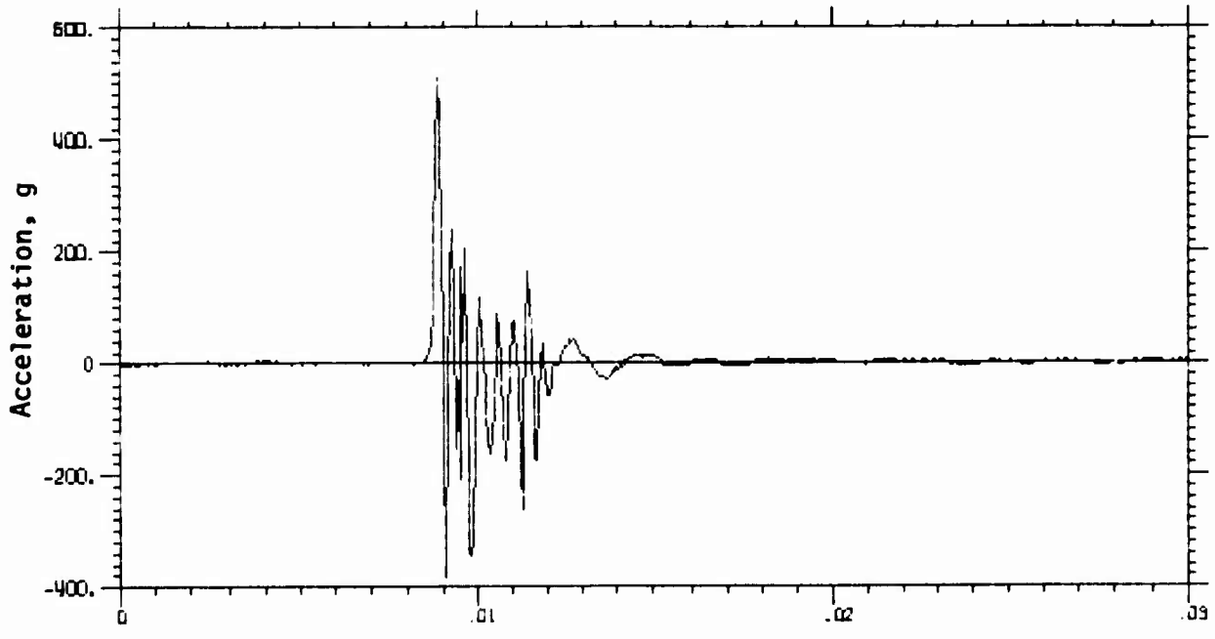

Acceleration

TEST 18 (3 of 3)

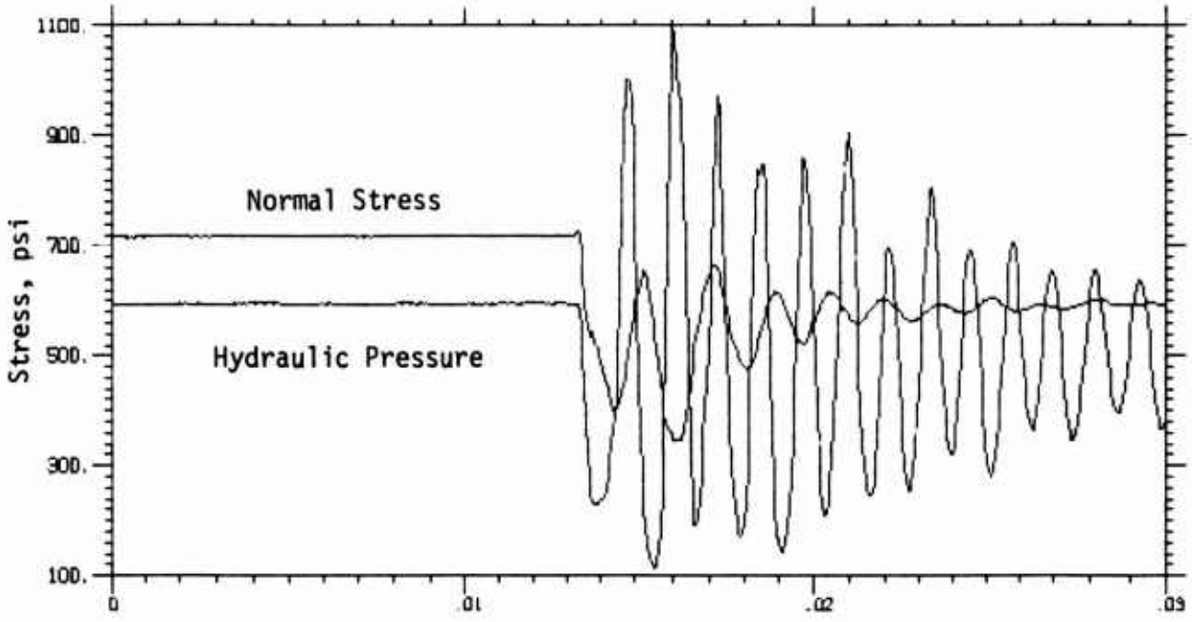

Time, sec

Hydraulic Pressure and Normal Stress

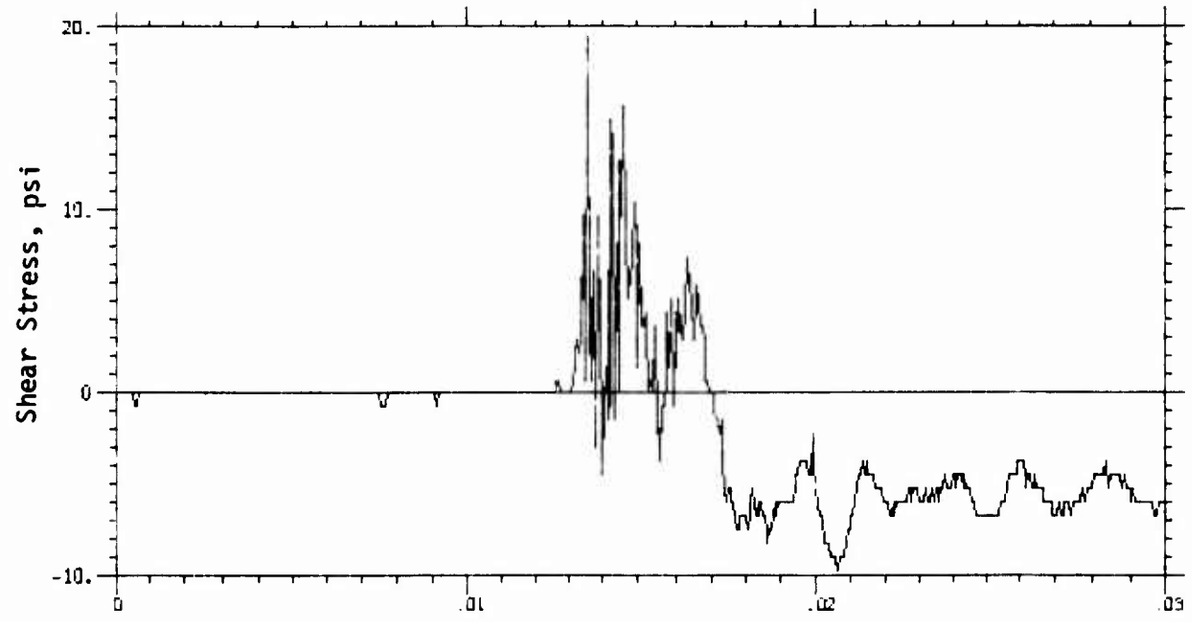

Time, sec

Horizontal Shear Stress

TEST 19 (1 of 3)

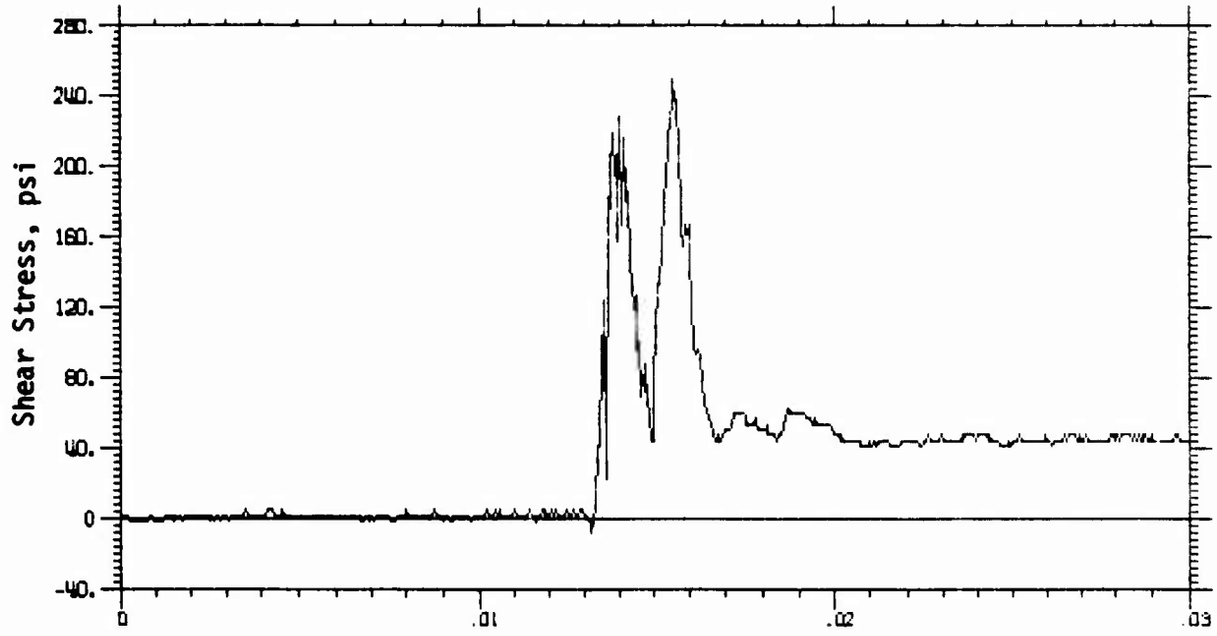

Time, sec

Vertical Shear Stress

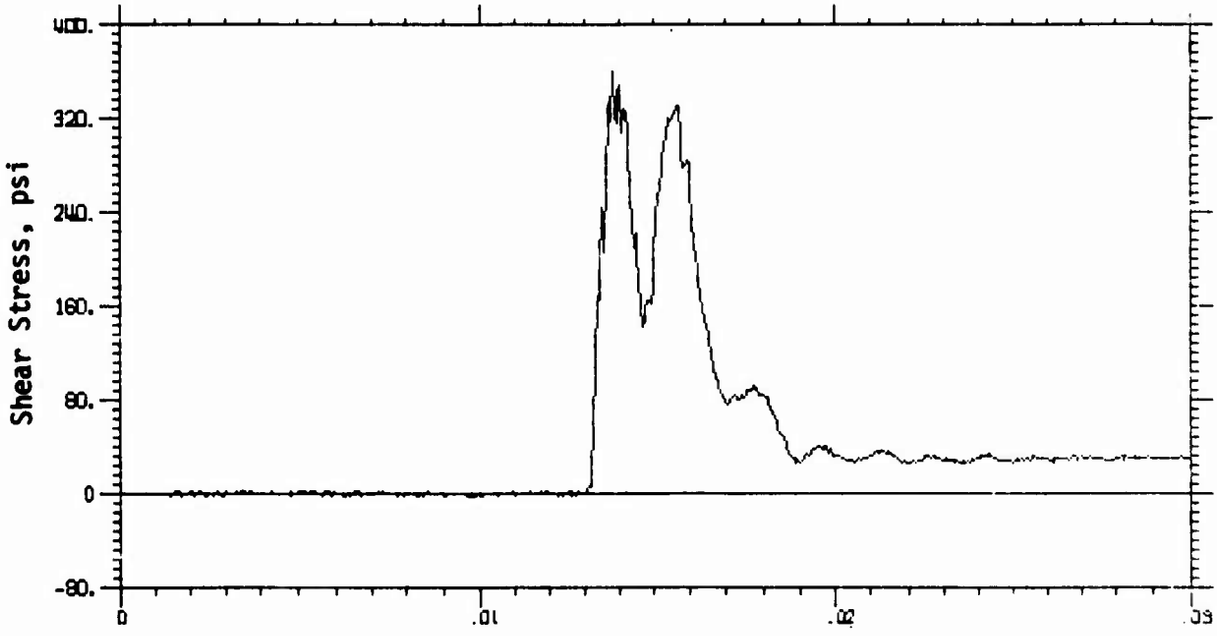

Time, sec

Inferred Vertical Shear Stress

TEST 19 (2 of 3)

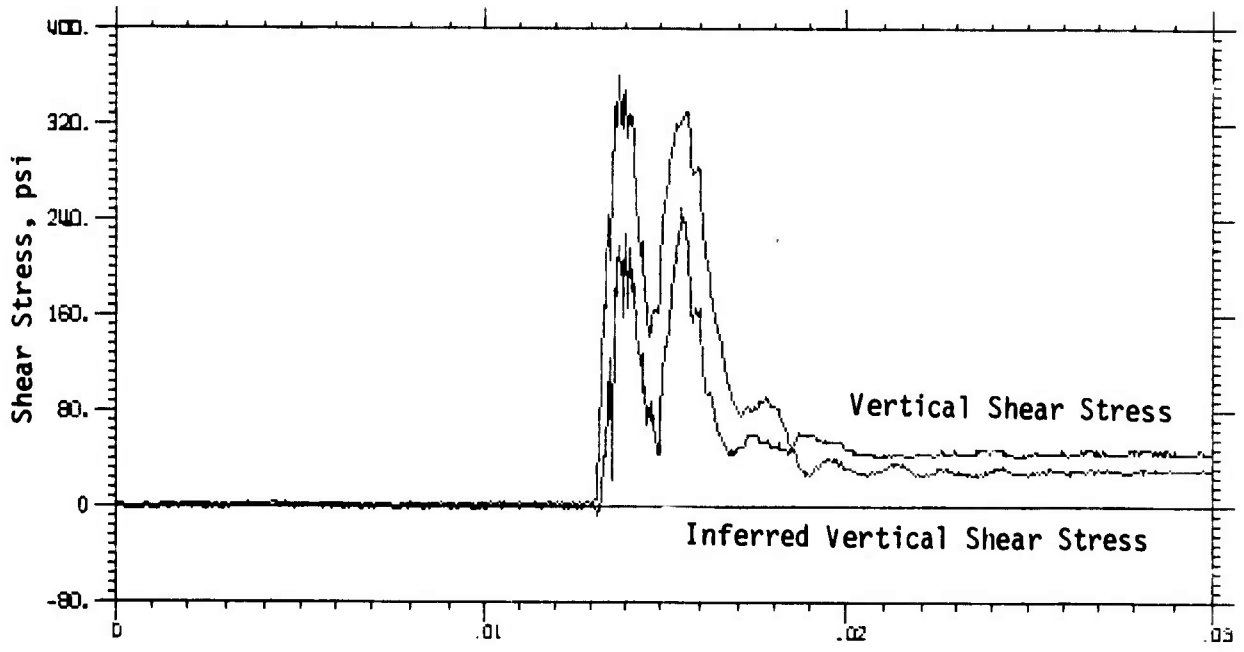

Vertical Shear Stresses (Comparison)

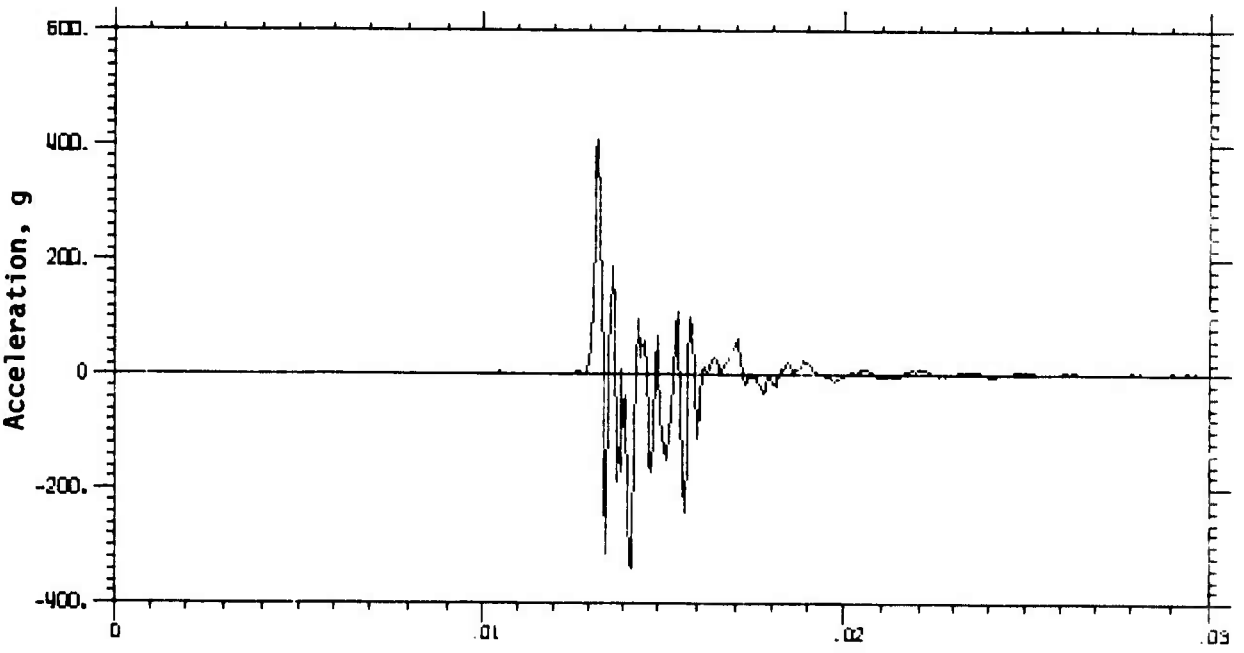

Acceleration

TEST 19 (3 of 3)

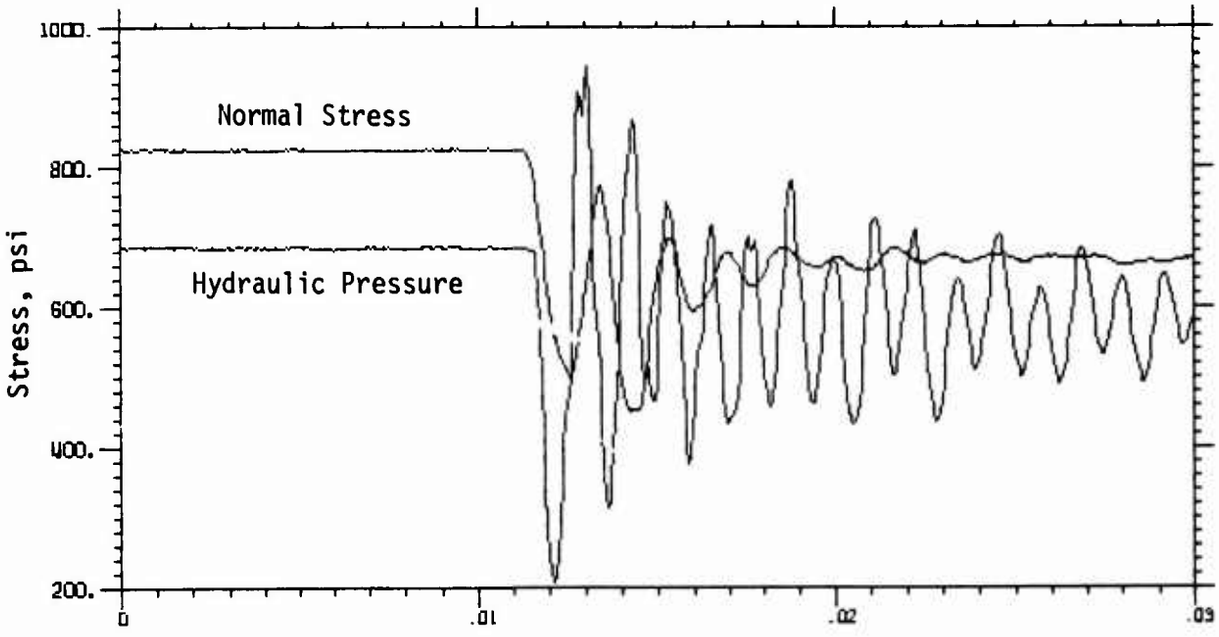

Time, sec

Hydraulic Pressure and Normal Stress

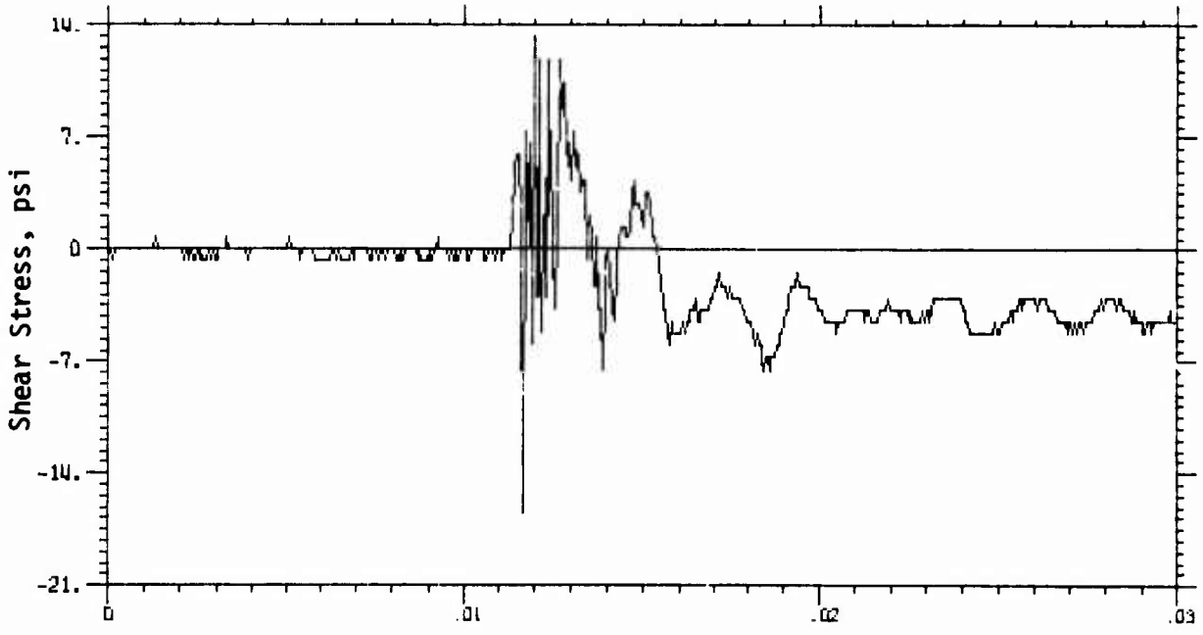

Time, sec

Horizontal Shear Stress

TEST 20 (1 of 3)

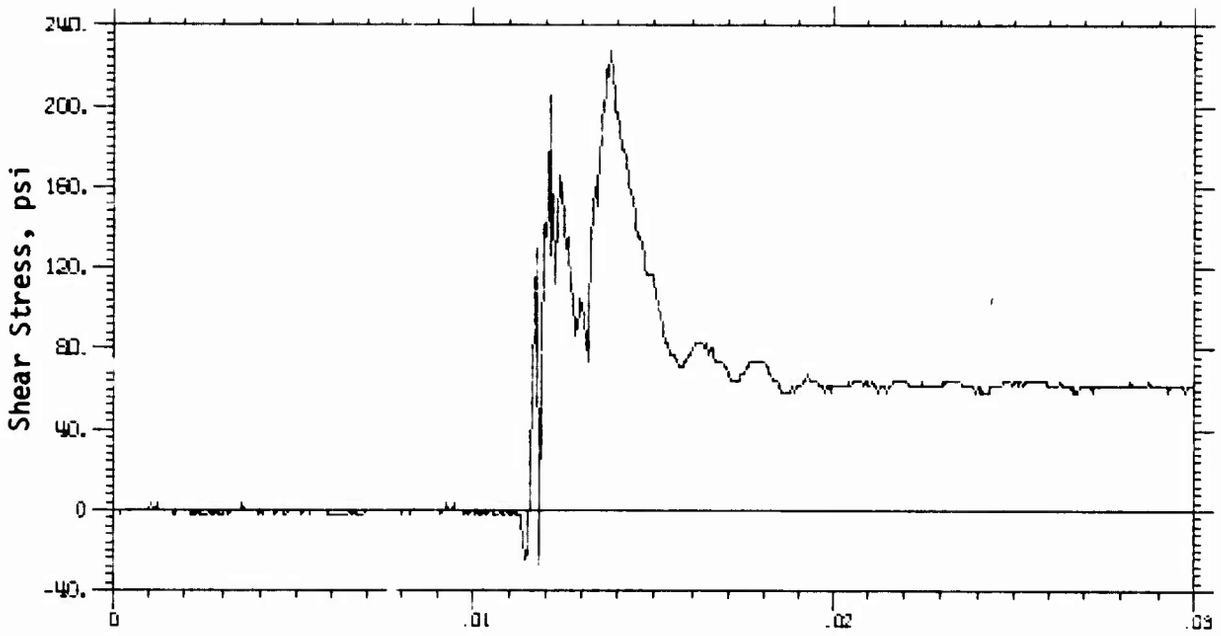

Time, sec

Vertical Shear Stress

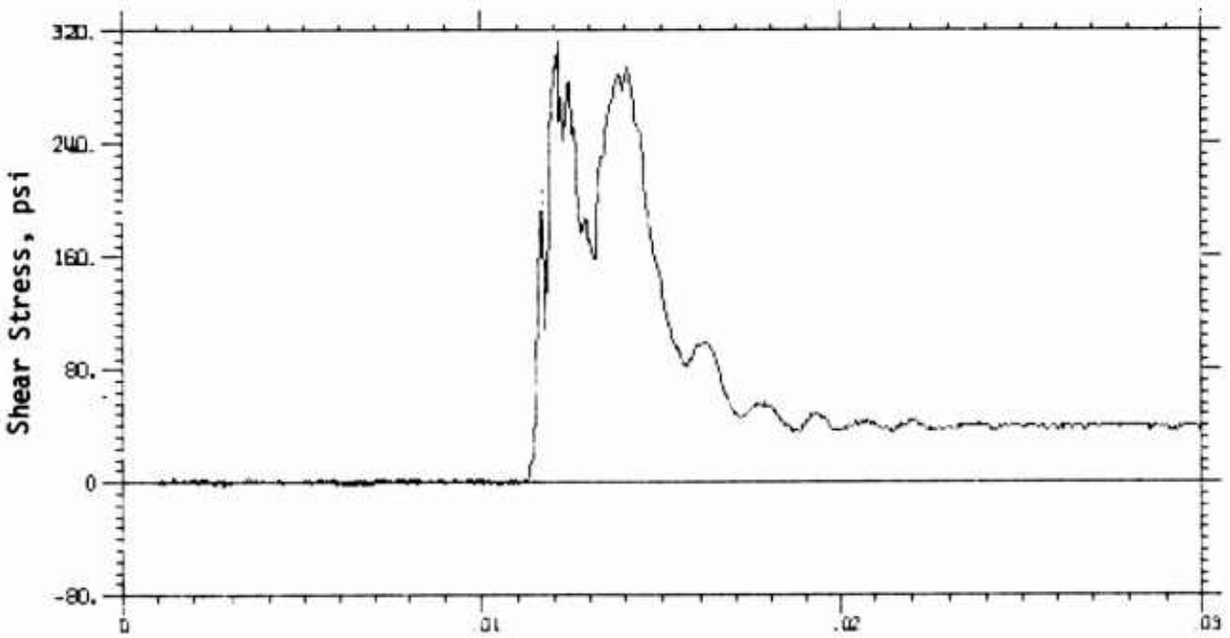

Time, sec

Inferred Vertical Shear Stress

TEST 20 (2 of 3)

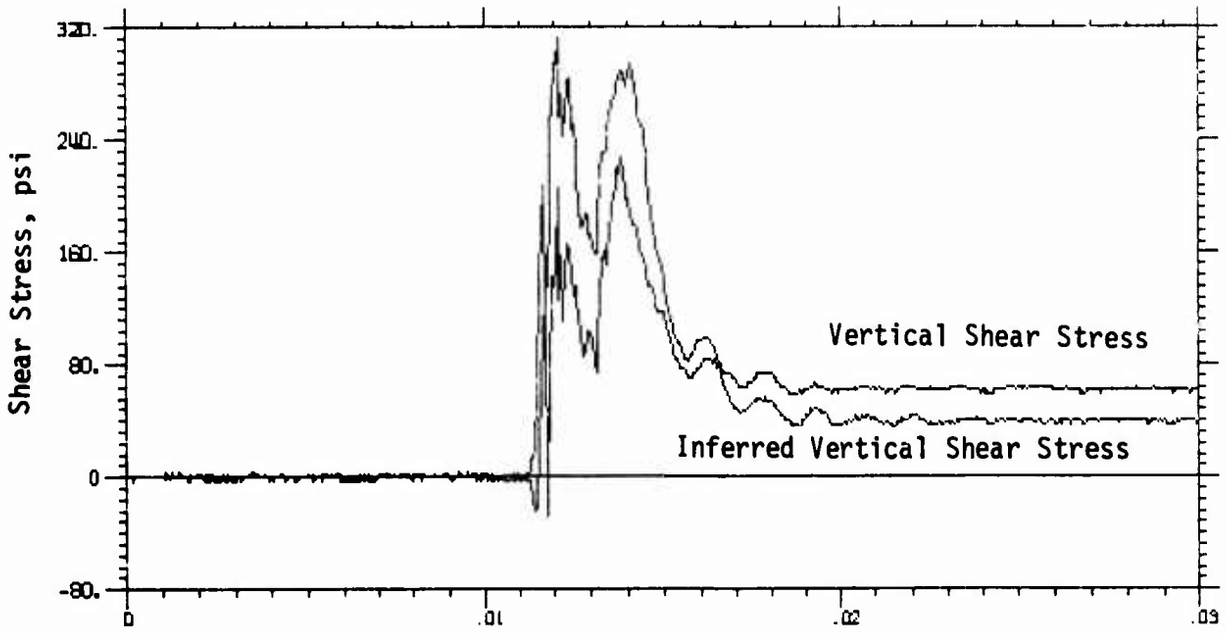

Vertical Shear Stresses (Comparison)

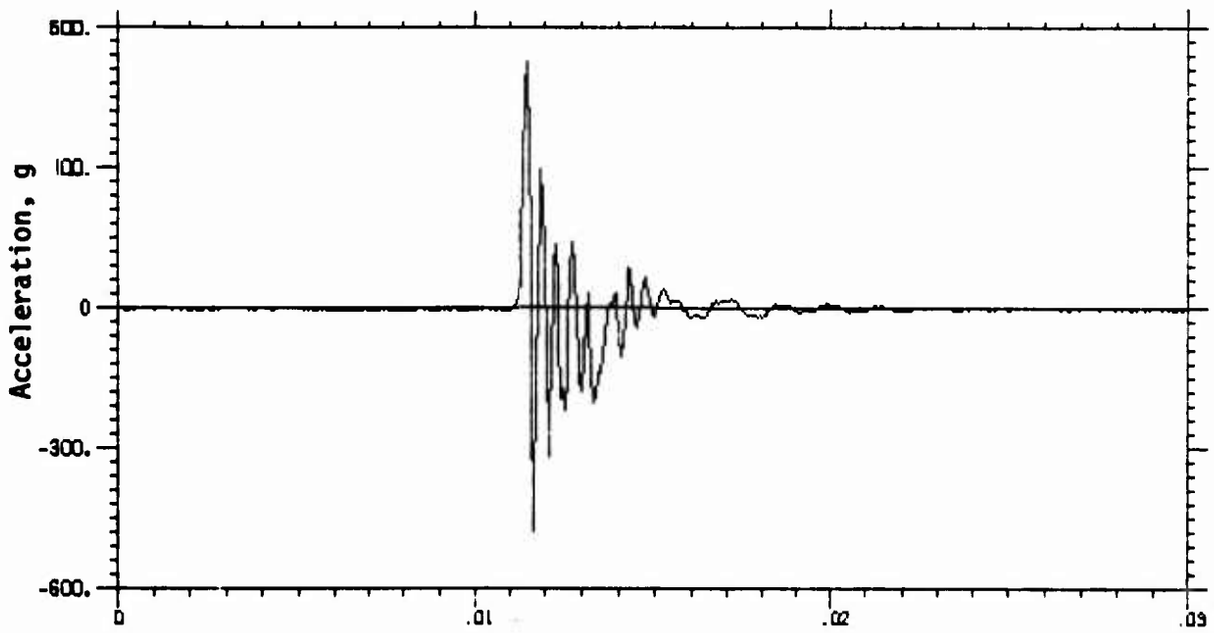

Acceleration

TEST 20 (3 of 3)

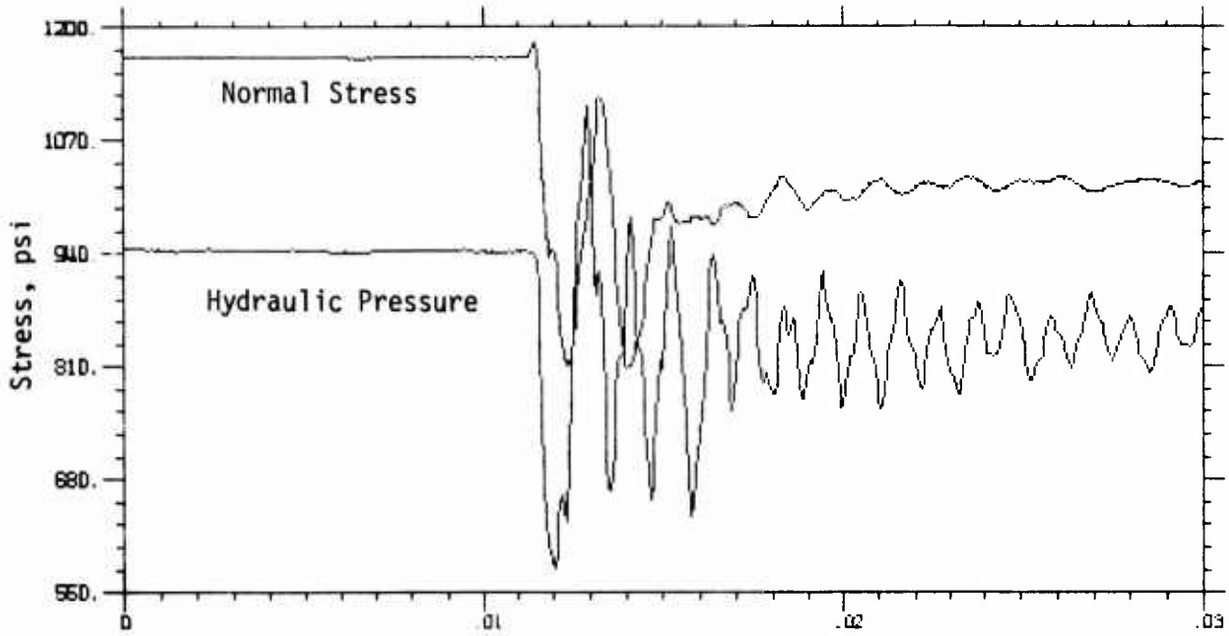

Time, sec

Hydraulic Pressure and Normal Stress

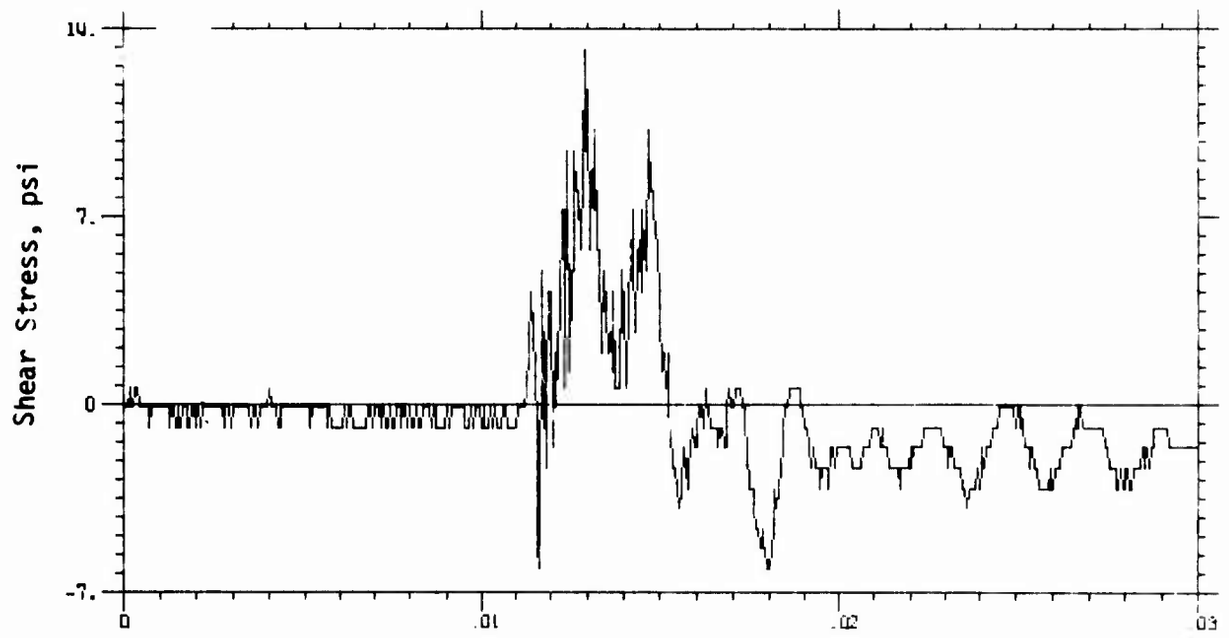

Time, sec

Horizontal Shear Stress

TEST 21 (1 of 3)

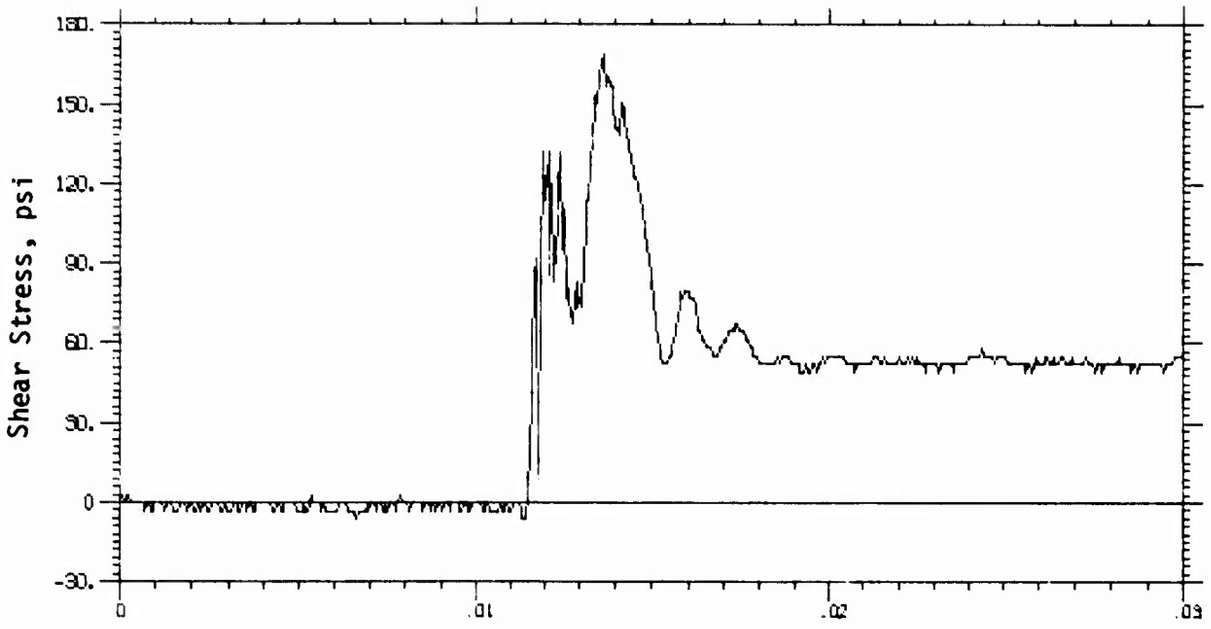

Time, sec

Vertical Shear Stress

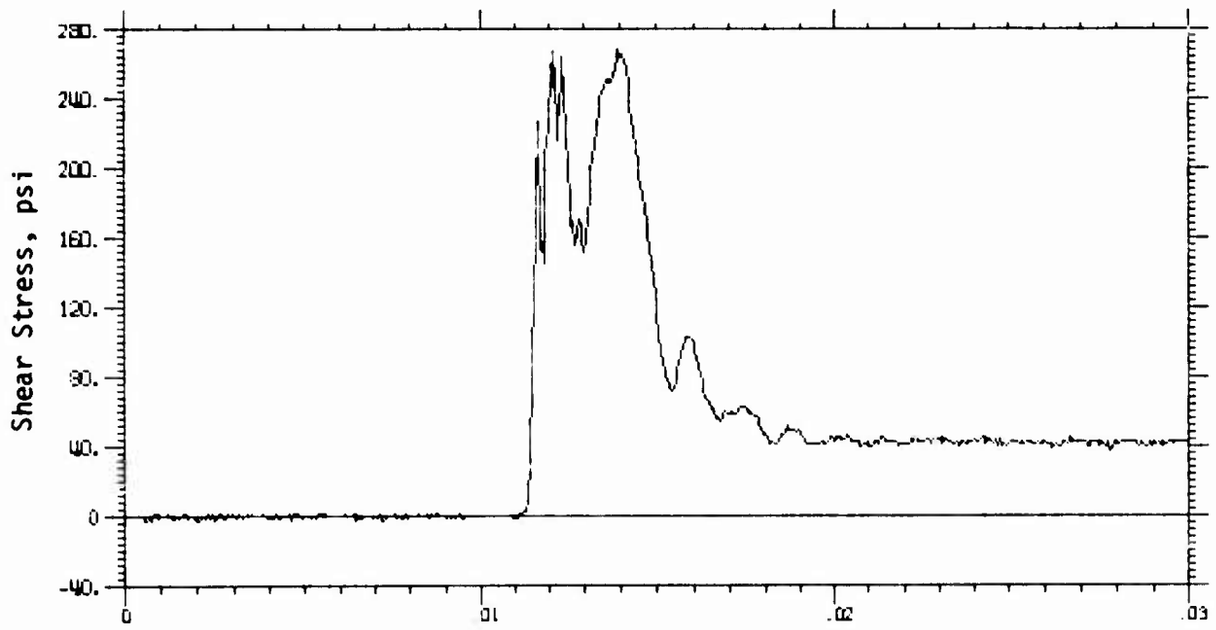

Time, sec

Inferred Vertical Shear Stress

TEST 21 (2 of 3)

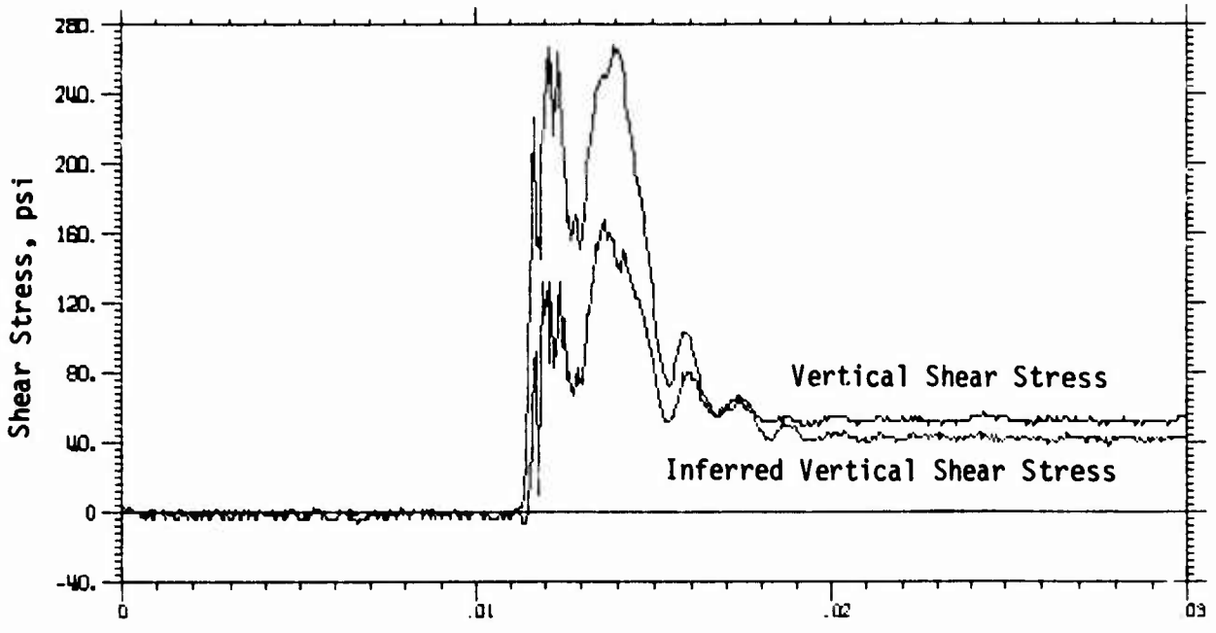

Time, sec

Vertical Shear Stresses (Comparison)

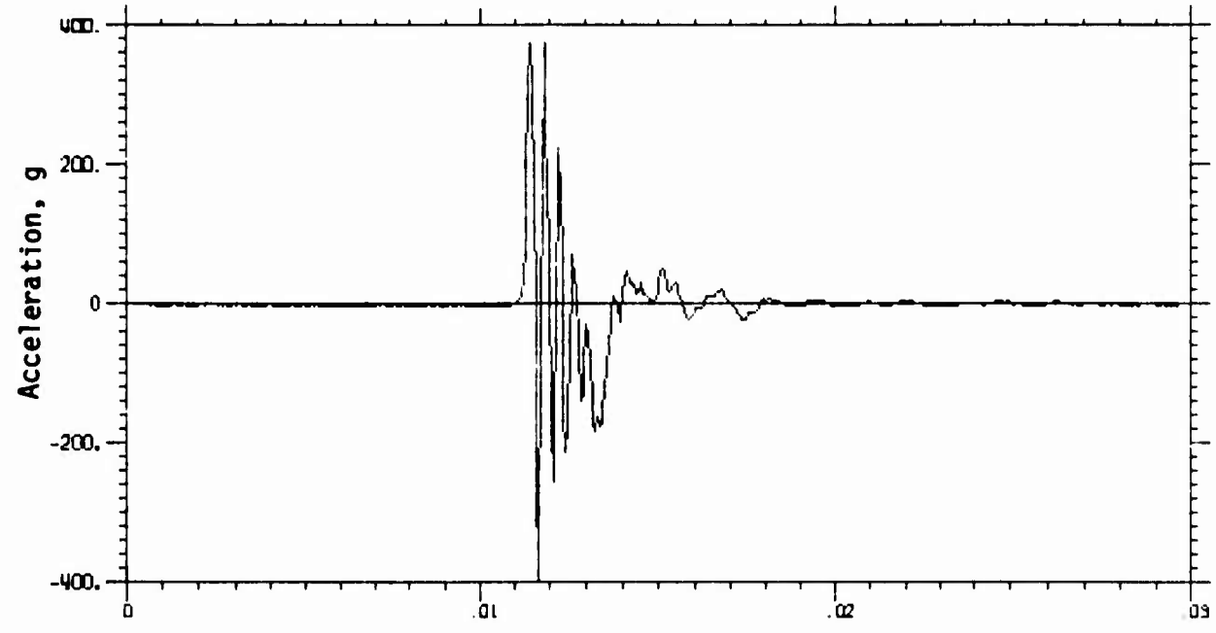

Time, sec

Acceleration

TEST 21 (3 of 3)

LIST OF SYMBOLS

A	effective force-collecting area
E	elastic modulus
E_i	bridge input voltage
E_o	bridge output voltage
E_{oh}	horizontal-axis output voltage
E_{on}	normal-axis output voltage
E_{ov}	vertical-axis output voltage
F_L	lower load-cell force
F_s	total shear force on concrete sample
F_u	upper load-cell force
I	moment of inertia
M_x	bending moment
N	negative type semiconductor material
P	positive type semiconductor material
R	resistance
a	acceleration of sample
a, a'	points of location for active beam upper and lower strain gage, respectively
b, b'	points of location for dummy beam upper and lower strain gage, respectively
c	distance from neutral axis to surface of beam at points a and a'
ℓ	total length of beam
m	mass of sample
x	distance from free end of beam to points a and a'
α	vertical-axis output scale factor with vertical shear input only
α'	horizontal-axis output scale factor with vertical shear input only
α''	normal-axis output scale factor with vertical shear input only
β	vertical-axis output scale factor with horizontal shear input only
β'	horizontal-axis output scale factor with horizontal shear input only
β''	normal-axis output scale factor with horizontal shear input only
γ	vertical-axis output scale factor with normal stress input only
γ'	horizontal-axis output scale factor with normal stress input only
γ''	normal-axis output scale factor with normal stress input only
ζ	strain

σ_n	normal stress
σ_s	shear stress
σ_{sh}	horizontal shear stress
σ_{sv}	vertical shear stress

DISTRIBUTION LIST

DEPARTMENT OF DEFENSE

Director
Defense Advanced Research Project Agency
ATTN: Technical Library
ATTN: STO
ATTN: NMRO
ATTN: PMO

Defense Documentation Center
2 cy ATTN: TC

Director
Defense Nuclear Agency
ATTN: DDST
2 cy ATTN: SPSS
2 cy ATTN: TITL, Tech. Lib.

Commander
Field Command
Defense Nuclear Agency
ATTN: FCTMOF
ATTN: FCPR
ATTN: FCT

DEPARTMENT OF THE ARMY

Chief of Research, Development & Acquisition
ATTN: Technical Library

Commander
Harry Diamond Laboratories
ATTN: DRXDO-NP
ATTN: DRXDO-TI

Director
U. S. Army Ballistic Research Laboratories
ATTN: Tech. Lib., Edward Baicy

Director
U.S. Army Engr. Waterways Experiment Station
ATTN: Leo Ingram
ATTN: Technical Library
ATTN: Francis Hanes
ATTN: J. K. Ingram
ATTN: J. Balsara

Commander
U.S. Army Materiel Dev. & Readiness Command
ATTN: Technical Library

DEPARTMENT OF THE NAVY

Chief of Naval Research
ATTN: Technical Library

Officer-In-Charge
Civil Engineering Laboratory
Naval Construction Battalion Center
ATTN: Technical Library
ATTN: W. Shaw
ATTN: R. J. Odello

Commander
Naval Facilities Engineering Command
ATTN: Technical Library

DEPARTMENT OF THE NAVY (Continued)

Commander
Naval Surface Weapons Center
ATTN: Code 730, Tech. Lib.
ATTN: Code 241, J. Petes
ATTN: Code 1224, Navy Nuc. Prgms. Off.

DEPARTMENT OF THE AIR FORCE

AF Cambridge Research Labs., AFSC
ATTN: SUOL, AFCRL Research Library

AF Institute of Technology, AU
ATTN: Library, AFIT, Bldg. 640, Area B

AF Weapons Laboratory, AFSC
ATTN: SUL
ATTN: DES, M. A. Plamondon
ATTN: DED
ATTN: DED, J. D. Renick
5 cy ATTN: S. J. Ayala

Hq, USAF/IN
ATTN: INATA

DEPARTMENT OF ENERGY

Sandia Laboratories
ATTN: Doc. Control for Tech. Library

Sandia Laboratories
ATTN: Doc. Control for Luke J. Vortman
ATTN: Doc. Control for A. J. Chabai
ATTN: Doc. Control for 3141, Sandia Rpt. Coll.

Department of Energy
Albuquerque Operations Office
ATTN: Doc. Control for Tech. Library

Department of Energy
Division of Headquarters Services
Library Branch, G-043
ATTN: Doc. Con. for Class. Tech. Lib.

Department of Energy
Nevada Operations Office
ATTN: Doc. Con. for Tech. Lib.

University of California
Lawrence Livermore Laboratory
ATTN: Technical Library

DEPARTMENT OF DEFENSE CONTRACTORS

Agbabian Associates
ATTN: M. Agbabian

Artec Associates, Inc.
ATTN: N. Baum

Civil/Nuclear Systems Corp.
ATTN: Robert Crawford

EG&G, Inc.
Albuquerque Division
ATTN: Technical Library

DEPARTMENT OF DEFENSE CONTRACTORS (Continued)

Electromechanical Sys. of New Mexico
ATTN: R. A. Shunk

General Electric Company
TEMPO-Center for Advanced Studies
ATTN: DASIAC

H-Tech. Laboratories
ATTN: Bruce Hartenbaum

Merritt CASES, Inc.
ATTN: J. L. Merritt
ATTN: Technical Library

Kaman Sciences Corporation
ATTN: Don Sachs
ATTN: Library

Nathan M. Newmark
Consulting Engineering Services
ATTN: Nathan M. Newmark

Physics International Company
ATTN: Doc. Con. for Coye Vincent
ATTN: Doc. Con. for Tech. Lib.

DEPARTMENT OF DEFENSE CONTRACTORS (Continued)

R & D Associates
ATTN: Tech. Lib.
ATTN: J. G. Lewis

Stanford Research Institute
ATTN: George R. Abrahamson
ATTN: Burt R. Gasten
ATTN: P. De Carli

Systems, Science and Software, Inc.
ATTN: Tech. Lib.
ATTN: Donald R. Grine

TRW Systems Group
ATTN: Tech. Info. Center, S-1930
ATTN: Paul Lieberman

The Eric H. Wang
Civil Engineering Research Facility
ATTN: Neal Baum
ATTN: Steve Pickett